Renormalization Group Studies of the Interplay between Kondo Effect,Valence Fluctuations and Topological Order

A Thesis

Submitted for the Degree of

DOCTOR OF PHILOSOPHY

in the Faculty of Science

by

Rukhsan Ul Haq

THEORETICAL SCIENCES UNIT
JAWAHARLAL NEHRU CENTRE FOR ADVANCED SCIENTIFIC RESEARCH
Bangalore – 560 064

JULY 2017

To my family

DECLARATION

I hereby declare that the matter embodied in the thesis entitled "**Renormalization Group Studies of the Interplay between Kondo Effect, Valence Fluctuations and Topological order** " is the result of investigations carried out by me at the Theoretical Sciences Unit, Jawaharlal Nehru Centre for Advanced Scientific Research, Bangalore, India under the supervision of Prof. N.S. Vidhyadhiraja and that it has not been submitted elsewhere for the award of any degree or diploma.

In keeping with the general practice in reporting scientific observations, due acknowledgement has been made whenever the work described is based on the findings of other investigators.

Rukhsan Ul Haq

CERTIFICATE

I hereby certify that the matter embodied in this thesis entitled "**Renormalization Group Studies of the Interplay between Kondo effect,Valence Fluctuations and Topological Order**" has been carried out by Mr. Rukhsan Ul Haq at theoretical Sciences Unit, Jawaharlal Nehru Centre for Advanced Scientific Research, Bangalore, India under my supervision and that it has not been submitted elsewhere for the award of any degree or diploma.

Prof. N. S. Vidhyadhiraja
(Research Supervisor)

Acknowledgements

There come situations in life when our words fail us. I am facing such situation now. My journey of PhD has been long and tortuous, and I have had a good share of both exciting days and challenging times. Finally, the day has come to submit PhD thesis. It is NOT due to my efforts alone. This PhD thesis would not have seen the light of the day had I not been immensely fortunate to have all those people in my life who have been working behind the scenes so that I realize my dreams. It is to them that I feel overwhelmingly grateful. Their number is huge, but I won't do justice if their names do not get mentioned at the beginning of this thesis.

The journey of my PhD started with one person who changed my whole life after I had first coffee with him and little did I know at that time, that next many years of my life are going to be spent with him. He is none other than my PhD supervisor, Professor N. S. Vidhyadhiraja who not only supervised my thesis work but has been a source of great strength and wisdom through out all these years. Dear Sir, I owe you a big time, and these words are a just poor substitute. I present you my most sincere wishes and highest regards.

Since I was new to condensed matter physics, so I thank all the professors in JNCASR and IISC and RRI who have helped me to learn the subject. I would like to particularly acknowledge Professor Swapan K. Pati, Professor Umesh Waghmare, Professor Srikanth Sastry, Professor Shobhana Narasimhan, Professor Subir K Das, Professor Santosh Ansumali for offering wonderful courses in JNC.

I would like to thank Professor Joseph Samuel from RRI, Professor Subroto Mukerjee from IISC, Professor Sachin Vaidya from IISC and Dr Subhro Bhattacharjee from ICTS for various enlightening discussions. I acknowledge Professor Diptiman Sen from IISC for many very fruitful discussions about Majorana fermions which were very important for my work on Majorana-Kondo model.

I have been very fortunate to have Professor Louis H. Kauffman as the collaborator on the project on the topological order in Kitaev chain. I sincerely thank Professor Kauffman for being part of my thesis project. I thank Professor Rama from Department of Mathematics, IISER Pune for hosting my visit during which I had exciting and very fruitful meetings with Professor Kauffman.

I acknowledge Professor Mark Jarrell from Louisiana State University for the collaboration on CT-QMC project and for providing access to high performance computing facilities.

I want to acknowledge Professor J*ü*rg Fr*ö*hlich for the hospitality and enlightening discussions while I was visiting him in ETH, Switzerland. I also acknowledge Professor Stefan Kehrein for the discussions and guidance while I visited him in Munich, Germany. I want to acknowledge many discussions with Alexei Kashuba on topological Kondo effect. They were very important for my projects on Majorana-Kondo model. I want to acknowledge Professor Arghya Taraphder for arranging my visit to IIT Kharagpur and for many discussions there. I also thank his whole group for being very nice and hospitable. I particularly thank Swagata and Narayan Mohanta from his group.

I acknowledge JNCASR Bangalore and Department of Science and Technology(DST) for all the funding and resources. I thank all the doctors and other paramedical staff in Dhanvantri for being very supportive and caring. I acknowledge all the JNC security staff for being ever ready to help and guide. I acknowledge Chandraih canteen staff and students mess staff for all the services they have rendered. I particularly thank Sharnappa and Shiva for giving the best coffee whenever it was needed.

It has been a wonderful stay in JNC for all these years during which my career in theoretical physics has been shaped. I have had an amazing time. I have also had my share of difficulties, and it is here that I have been again immensely fortunate to have been surrounded by wonderful friends who have been with me through thick and thin. The list is long, but their names deserve this space. My deepest and sincere thanks go to all of them, and they are: Vijay, Sanjeev, Amrutha, Mighfar, Razdeep Singh, Shahnaz , Chandan Kumar, Negi Singh, Anshul, Ankush, Asahar, Vybhav, Arnab, Arpit, Lakshmi Shaw, Piyush. I would like to especially thank Vijay, Amrutha and Sanjeev for standing with me in difficult times. With Vijay I have had innumerable discussions over the broad range of topics and it has been great learning experience. Razdeep was ever ready to help me in all possible ways. Talking to Vybhav has always been a joy.

JNCASR is like a family, and there are people always ready to help and support. I thank all the Jncians who have supported me all along these years. My best wishes to you all.

I want to thank all my past and present labmates for everything they have done for me. I particularly thank Dasari for lots of discussions both in lab and over coffee and for the collaborative projects, Sudeshna Sen for all the support, Wasim for being helpful and encouraging, Amit for being supportive in the final stages of thesis work, Anirudh for all the discussions and being part of the Majorana projects and Vinayak for making coffee discussions lively. I also thank all the summer students who visited our lab for bringing a lot of enthusiasm and youthful energy to our group and for being a great company. They include: Rajath, Shivam, Keshav and Sachin.

I also want to thank all my TSU batchmates and friends: Priyanka, Sona, Vasu, Sougata, Anjali, Anshul, Bradraj, Ananthu, Meha, for being a great company. Theoretical Sciences Unit is a great place to be part of, and I thank whole TSU community for making TSU such a nice unit.

Bangalore has been a second home for me. I have enjoyed my stay here all along. My Bangalore life was made even more colourful and eventful by friends like Venkat, Suchana and Shalini. They have been a source of immense support, guidance and encouragement. They have been like family for me in Bangalore. My deepest thanks go to you buddies.

I thank Ibrahim, Shafquat, Asif, Inayat and other Kashmiri friends. I particularly thank Ibrahim for being very supportive at the beginning of my stay in Bangalore.I want to specially thank my two buddies Suhail and Mubashir with whom I have had innumerable conversations and they have been source of great support during my Ph.D. years.

I acknowledge all my teachers who have played a pivotal role in shaping my academic career. Notable among them are Syed Noor Sahib, Saleem Sahib, Aziz Shah Sahib, Syed Maqbool Sahib, Lateef Sahib, Syed Shahid Sir, Rouf Rafiqi. Dr Manzoor Malik, from Department of Physics, University of Kashmir, has been a source of constant support and encouragement. I also thank Dr Basharat for various discussions. I want to especially thank Assadullah Sir who came into my life at a crucial stage and since then has been a source of guidance and encouragement.

Last but not least I thank my family without whose support I would not have been able to complete this thesis. I have no words to express my gratefulness for their unconditional love and support and for showing a lot of patience.

Synopsis

Strongly correlated electron systems exhibit a wide panorama of exotic and emergent behaviour which arises due to the quantum entanglement across the whole system which in turn leads to quantum many-body dynamics in these systems. Such dynamics is very intricate and shows strong renormalization effects due to which physics changes at different scales. Strong correlation leads to new energy scales as well. A typical example is the Kondo scale which gets dynamically generated in the strong coupling regime of the Kondo model. Renormalization group methods become natural to deal with such systems. In this thesis, we have used renormalization group methods to study various emergent phenomena in quantum impurity systems which are a special class of strongly correlated electron systems. We have used poor man scaling method and Wegner's flow equation method to do the renormalization studies.

A brief introduction to the strongly correlated electron systems is provided in the first chapter. A detailed description of the renormalization group methods as applied to study the strong correlation physics of the quantum impurity systems follows the introduction in chapter **2**. Our interest has been to explore the interplay between valence fluctuations and Kondo effect in heavy fermion systems and also the interplay between Kondo effect and topological order. For the lattice Hamiltonian, we have used dynamical mean field theory which is a very important method that takes

local quantum fluctuations into consideration while neglecting non-local dynamical spatial fluctuations. We have used continuous time quantum Monte Carlo(CT-QMC) method as the impurity solver for DMFT.

In chapter **3**, we have carried out perturbative renormalization of the extended single impurity Anderson model (e-SIAM), which has a Hubbard repulsion between conduction and impurity electrons in addition to the usual kinetic energy, site-energy, local Coulomb repulsion on the impurity and the hybridization terms. The motivation for this study comes from recent experiments and related theoretical studies which suggest that valence fluctuations could play a crucial role for the quantum criticality in heavy fermion systems. There is also a lot of interest in quantum dots where a rich interplay between spin and charge Kondo effect leads to $SU(4)$ Kondo effect and this interplay has also motivated our study. We have extended Haldane's and Jefferson's scaling approach to our model. We find that renormalization flow of this model is determined by three scaling invariants. Using the scaling invariants, we calculate the Kondo scale in the local moment regime of the model. We find that U_{fc} interaction leads to an increase in the Kondo scale through a renormalization of the prefactor. Enhancement of Kondo scale due to U_{fc} interaction has been found by earlier numerical renormalization calculations as well. We have carried out Schrieffer-Wolff transformation to obtain the effective Hamiltonian corresponding to the strong coupling fixed point of e-SIAM and we find that strong coupling physics of e-SIAM is governed by spin-charge Kondo model which has the interplay between spin and charge Kondo interactions in contrast to the Anderson impurity model where spin fluctuations dominate the strong coupling regime of the model. We also find that valence fluctuations mediated charge Kondo effect co-exists with spin Kondo effect and can lead to $SU(4)$ Kondo effect in quantum dots where as phonon mediated charge Kondo effect can not co-exist with spin Kondo effect and hence can not lead to $SU(4)$ Kondo effect.

In chapter **4** , we study the lattice version of e-SIAM which is called extended Periodic Anderson model. We employed dynamical mean field theory approach which maps e-PAM to an impurity model with self-consistent hybridization. We use, the continuous time quantum Monte Carlo(CT-QMC) as an impurity solver. We find that electron occupation of localized(f) electrons decreases with valence fluctuations and as valence fluctuations become stronger we find abrupt jumps in f electron occupancy which signals a phase transition. We confirm the existence of the phase transition from valence susceptibility which diverges close to transition. Further, valence fluctuations also lead to strong renormalization of the quasiparticle weight which increases with valence fluctuations, hence signifying the renormalization of local Hubbard repulsion of f electrons.

In chapter **5**, we have explored Z_2 topological order in the Kitaev p-wave chain model. In this chapter, we ask the question why there is topological order in Kitaev chain model and not in the Transverse Field Ising model(TFIM) when both these models are related by Jordan-Wigner transformation. We find that there are extra fermionic symmetries in Kitaev chain model. These symmetry operators are actually Majorana mode operators which commute with Hamiltonian and change the parity states. The same symmetry leads to the doubling of the entire spectrum of the Kitaev, chain model. We also explored how the topological order is related to topological entanglement as given by Yang-Baxter equation. We find that Majorana braiding representation arises only in the topological phase of the Kitaev chain. That leads us to propose a new characterization of topological order as an order which gives rise to the solutions of Yang-Baxter equation.

In chapter **6**, we have studied the interplay between Kondo effect and Majorana fermions in a setup where quantum dot is connected to a normal lead on one side and a topological superconductor on another side. The motivation of our study was to find unambiguous ways for the detection of Majorana fermions and find out ex-

perimentally feasible ways of probing the signatures of Majorana fermions. We first write down the Hamiltonian for a setup in which the quantum dot is side-coupled to the topological superconductor and to a normal lead on another side. Projecting this Hamiltonian to its Kondo regime gives us an effective Hamiltonian which has new interactions in addition to the standard Kondo interaction. One of the important signatures of Majorana fermion in this model is the relevance of particle-hole asymmetry for Kondo effect. At the particle-hole symmetric point, Zeeman field and Andreev scattering term vanish at effective Hamiltonian level. We have carried out flow equation renormalization study of Majorana-Kondo model, and we find that flow equations are different for particle-hole symmetric and asymmetric cases. One of our important findings is that even though Zeeman field vanishes at the particle-hole symmetric case, however, it emerges again along the unitary flow of the coupling constants of Majorana-Kondo model and hence making the Kondo physics anisotropic. It also leads to an important observation about the flow equations of the model. These equations have essential instability towards the particle-hole asymmetry, and slightest asymmetry leads to the emergence of Zeeman field and drives the system away from the particle-hole symmetric point. It has physical implications for the realistic experimental situations where asymmetry is generic and particle-hole symmetry being a very special case. Our results suggest that Majorana fermion produces significant renormalization of Kondo couplings even in the particle-hole symmetric case and hence there is no need to detune the gate voltage of the system as had been proposed in earlier studies. Away from particle-hole symmetry, the renormalization effects of Kondo couplings are even stronger due to the contribution of Andreev scattering term to the flow equations. Spin susceptibility is an experimentally accessible quantity, and hence we have calculated this quantity for Majorana-Kondo model, both in particle-hole symmetric and asymmetric cases, to capture the signatures of Majorana fermion in it. Flow equation method gives

access to renormalization of observables as well. We calculated the flow equations for Kondo spin operator, and after solving them numerically, we calculate dynamic spin susceptibility. There are clear signatures of Majorana fermion in this quantity. Our flow equation renormalization studies have confirmed and consolidated the interplay between Majorana fermion and Kondo effect and proposed feasible and unambiguous ways for the detection of Majorana fermion in quantum dots.

List of Figures

Contents

Chapter 1

Strongly Correlated Electron Systems

Contents

1.1 Introduction

Strongly correlated electron systems(SCES) comprise a range of materials which exhibit panorama of exotic and emergent behaviour. These systems include Mott insulators, high T_c superconductors, heavy fermion systems, spin liquids, magnetic materials, fractional quantum Hall fluids. Band theory, based entirely on the quantum theory of solids which have periodic lattice structures, has been a huge success because of the broad range of solid state systems whose transport properties were understood based on this theory. But when it comes to strongly correlated electron systems, band theory fails. The Mott insulating state and Anderson insulators are just two examples which can not be explained on the basis of band theory because there are new physical principles at work. The principles of quantum many-body systems were laid out by many pioneers of this field including Landau, Anderson and Wilson. These principles include adiabatic continuity on which is based Fermi liquid theory, Spontaneous symmetry breaking which is the paradigm for understanding the ordered states of matter, Renormalization group which is the natural framework to study the effects of strong interactions. These principles have been discussed at length in a very beautiful book by Anderson[1]. In this thesis, we have employed renormalization group methods to study the interplay between Kondo effect, valence fluctuations and topological order.

Strong correlation makes the system a quantum many-body system which can not be described by single particle theories. Consequently, the dynamic interplay between the various degrees of freedom leads to a collective behaviour in these systems. Collective behaviour can not occur without interactions, and neither can be described without taking interactions into consideration. P. W. Anderson, one of the pioneers of modern condensed matter physics, has expressed very succinctly in his famous phrase, "More is different" [2]. Emergent behaviour is another term used to express the collective behaviour of strongly correlated systems in which new prop-

erties emerge in the system which are not exhibited by the individual components of which the whole system is made up of. Consequently, in a strongly correlated system, one is not concerned with the constituents themselves, rather with their collective excitations which are the "quasiparticles" of the system. Quasiparticles are not particles in the sense of elementary particles, but they are rather more real because in the presence of interactions, bare particles get dressed or renormalized and the physics is described in terms of quasiparticles rather than the bare particles. This is another feature of strong interactions, which will be discussed in detail in chapter **2** of this thesis, that interactions lead to the renormalization of the bare quantities of the constituents of a system.

Strong correlation leads to quantum many-body dynamics which is very intricate and has the interplay of various energy scales. Strong correlation also dynamically generates new energy scales. Kondo scale being the typical example of such a scale which emerges out of the quantum many-body dynamics of Kondo effect. Standard perturbation theory does not treat all energy scales and consequently leads to logarithmic divergences. One is forced to employ strong coupling expansions like a Schrieffer-Wolff transformation which gives a controlled method to calculate the effective Hamiltonian in the strong coupling regime of the given model. In a strongly correlated electron system, quantum fluctuations are vital for dynamics and need to be taken into consideration. Renormalization group is a well-suited method which takes quantum fluctuations into consideration and hence becomes natural to deal with strong correlation. Kondo effect in which physics is governed by spin fluctuations was finally understood by various renormalization group methods, particularly the numerical renormalization group which was able to capture the Kondo resonance peak in the spectrum of the Kondo model.

Strong correlations also lead to quantum fluctuations, and one needs to go beyond a mean field theory description. The Mott insulating phase is one typical

example where quantum fluctuations become very important, and hence this phase can not be understood based on static mean field theory. In low dimensional systems, quantum fluctuations become even more important and lead to new phases. In one dimensional systems, strong correlation leads to the formation of Luttinger liquid which is entirely different from Fermi liquids which occur in higher dimensions. The effect of quantum fluctuations in one dimensional systems is so strong that there is no order that can take place in one dimensional systems. Rather a very exotic phenomenon happens: spin-charge separation which is basically that charge and spin degrees of freedom behave independently.

In this chapter, we will describe the strong correlation physics based on the quantum many-body Hamiltonians which have been introduced for strongly correlated electron systems. Even though these Hamiltonians are minimal models to capture the physics of SCES, still they have been crucial for the understanding of strong correlation physics. There are two kinds of quantum many-body Hamiltonians: Impurity and Lattice Hamiltonians. We will mainly focus on quantum impurity models. We will also show how in dynamical mean field theory framework, lattice models can be mapped to quantum impurity models which are easier to understand because there is just one quantum impurity in the model which is interacting with conduction electrons which are free fermions. Hence quantum impurity models are of central importance in the field of strongly correlated electron systems.

1.2 Quantum Many-body Hamiltonians

Quantum impurity systems are a special class of strongly correlated electron systems which have been very crucial for the understanding of physics of strongly correlated electron systems. Hence they have been extensively studied. Though they are simple in the sense that there is a single impurity, there is full quantum many-body physics involved because quantum impurity gets coupled to the conduction electrons and

leads to the formation of the quantum many-body ground state. Kondo effect is a prototypical example of such quantum many-body phenomena in which impurity electron forms a Kondo singlet with conduction fermion sea, and it manifests in the spectrum as resonance peak at the Fermi level.

Quantum impurity systems necessitated the need for renormalization group methods in quantum condensed matter physics, and they have been a testing ground for so many different renormalization schemes. Renormalization group is needed because there is the interplay of various energy scales and due to strong correlation emergent scales also also come into play. Also, quantum fluctuations determine the dynamics, and hence renormalization group method becomes natural to study these systems. In fact, Anderson applied renormalization methods to Kondo model[1] before Wilson made renormalization group(RG) well-known by applying it to critical phenomena in statistical physics and Kondo model[3]. There is one important difference in renormalization of quantum impurity systems as compared to the statistical physics models. In quantum impurity models, it is the quantum(temporal) fluctuations which need to be dealt with rather than spatial fluctuations in case of statistical mechanical lattice models. That makes the actual implementation of renormalization different for quantum impurity models.

We will present two very important Hamiltonians of quantum impurity systems, Single impurity Anderson model(SIAM) and Kondo model. Though these models were introduced in different contexts, it was shown using Schrieffer-Wolff transformation[4] that Anderson impurity model gets mapped to Kondo model in its strong coupling regime where valence fluctuations get frozen. To understand the relation between these models, we will also present Schrieffer-Wolff transformation.

1.2.1 Anderson impurity model

Single impurity Anderson model was introduced[5] to understand the fate of local magnetic moment in metals. Blandin and Friedel[6] understood the key aspect of the physics based on scattering theory and they found that there is virtual bound state formation. However, as was customary that time they proposed that there is a ferromagnetic exchange between conduction and impurity electrons. Anderson proposed a Hamiltonian which provided the microscopic understanding of quantum impurity physics. Anderson based on mean field theory was also able to explain the formation of virtual bound state, but he found that the exchange term is of antiferromagnetic nature which was later confirmed based on Schrieffer-Wolff transformation and plays a very important role in Kondo physics.

$$H = \sum_{k\sigma} \epsilon_k c^\dagger_{k\sigma} c_{k\sigma} + \sum_{k\sigma} V_k (c^\dagger_{k\sigma} d_\sigma + h.c.) + \sum_{\sigma} \epsilon_d d^\dagger_\sigma d_\sigma + U n_{d\uparrow} n_{d\downarrow} \tag{1.1}$$

In this model, there are two species of fermions, and hence we can divide the model into two sectors: Impurity sector and conduction electron sector. The new ingredient in this model, introduced by Anderson is the hybridization term which couples the two sectors and this term is important for the formation of virtual bound state. Hybridization term gives the coupling between localized impurity orbital and Bloch wavefunction of conduction electrons. In the absence of the interactions, hybridization leads to the broadening of the impurity state with width given by

$$\Delta = \pi \sum_k (\mid V_k \mid)^2 \delta(\epsilon - \epsilon_k) \tag{1.2}$$

To understand the physics of Anderson model better, it becomes natural to take local picture approach where we start with the atomic picture of the Hamiltonian and then adiabatically turn on the hybridization to the conduction band electrons.

1.2.2 Atomic limit

Hilbert space of impurity electron is four dimensional: $|\ 0\rangle, |\uparrow\rangle, |\downarrow\rangle, |\ 2\rangle$ which corresponds to empty state, singly occupied state with up or down spin and doubly occupied state. For the case of zero hybridization, conduction and impurity sectors get decoupled. The impurity part of the Anderson model for $V = 0$ is the atomic limit of the model and its local Hilbert space is four dimensional as given above.

$$H_{at} = \sum_{\sigma} \epsilon_d d_\sigma^\dagger d_\sigma + U n_{d\uparrow} n_{d\downarrow} \tag{1.3}$$

Energies of the four states are:

$$|\ 2\rangle \quad E = 2\epsilon_d + U \tag{1.4}$$

$$|\ 0\rangle \quad E = 0 \tag{1.5}$$

$$|\uparrow\rangle, |\downarrow\rangle \quad E = \epsilon_d \tag{1.6}$$

When hybridization is switched on, there are transitions between the states determined by the energetics and quantum fluctuations. Since impurity electrons can make transitions to other two states so we can ask under what conditions will local moment be there.

$$E_0 - E_1 = 0 - \epsilon_d > 0 \Rightarrow U/2 > \epsilon_d + U/2 \tag{1.7}$$

$$E_2 - E_1 = 2\epsilon_d + U - \epsilon_d \Rightarrow \epsilon_d + U/2 > -U/2 \tag{1.8}$$

So in atomic limit the condition for the existence of the local moment is

$$U/2 > \epsilon_d + U/2 > -U/2 \tag{1.9}$$

Now the question which Anderson answered using mean field theory is what happens to the local moments when we switch on the hybridization. However, mean field theory can not be trusted when interaction becomes stronger than hybridization strength. Since quantum impurity models are the simplest examples of quantum many-body systems and hence to deal with quantum fluctuations in the presence of interactions one has to resort to renormalization methods. In the case of Anderson model, such a scheme was introduced by Schrieffer and Wolff who used a unitary transformation to integrate out the valence fluctuations and found the effective model for the strong coupling regime of the model. The significance of this transformation is that not only it helped to understand the strong coupling regime of quantum many-body Hamiltonian, but it also provided the connection between two important models which were studied in different contexts. We will come back to Schrieffer-Wolff transformation later in this chapter. Understanding the connection between Anderson model and Kondo model was phenomenal because it showed that the low energy physics of Anderson model is governed by Kondo spin interaction and hence in renormalization sense, the strong coupling physics of the model is governed by Kondo fixed point. This physics was later on confirmed by perturbative RG and finally by Numerical Renormalization group of Wilson. Based on NRG it is known that SIAM has four fixed points which correspond to four parameter regimes of the model. 1. Empty orbital fixed point 2. Local moment fixed point 3. Mixed valent fixed point 4. Kondo fixed point which is the strong coupling fixed point and is very stable to repulsive interactions[7][8].

Though SIAM was introduced to understand the physics of magnetic moments in metals, its significance and applicability have gone beyond this physical context. The same model is used to study the quantum transport in quantum dots where the quantum dot is represented by impurity part of the Hamiltonian; lead electrons are represented by conduction part of the Hamiltonian. This way it became possible

to understand the Kondo effect in quantum dots as well even though the actual situation is more complicated because of other energy scales. This way SIAM has gained interest in quantum transport in quantum dots.

Another reason which made SIAM of central importance in the field of strongly correlated electron systems is that within dynamical mean field theory framework, Hubbard model gets mapped to SIAM in a self-consistent manner. We will come back to this aspect of Anderson impurity model in a later section in this chapter.

1.2.3 Kondo model

Kondo model has been a paradigmatic model of condensed matter physics which exhibits the quantum many-body effects of strong correlation. At Kondo temperature, there is the formation of quantum many-body resonance peak at the Fermi level which is due to the anti-ferromagnetic exchange between the impurity spin and the conduction electrons of the host metal.

$$H = \sum_{k\sigma} \epsilon_k c^\dagger_{k\sigma} c_{k\sigma} + JS.s(0) \tag{1.10}$$

S is the Kondo impurity spin and $s(0) = \sum_{k\sigma} \sum_{k'\sigma'} c^\dagger_{k'\sigma'} \tau_{\sigma\sigma'} c_{k\sigma}$ is the conduction electron spin density at the site of Kondo impurity. Kondo model challenged theorists for many decades but has held immense fascination as well. It is a model for which the theorist's favourite method, perturbation theory broke down and they got pushed to develop renormalization group method. Kondo physics is non-perturbative and is intimately tied to renormalization group methods. It was for this model that Kenneth Wilson developed his Numerical Renormalization group[3] and got the full quantitative understanding of the dynamics and thermodynamics of this model. Before Wilson, Anderson and collaborators had already applied the renormalization group methods to Kondo model and had got some analytical in-

sights into the non-perturbative physics of the model. Anderson's poor man scaling method became standard perturbative renormalization scheme in this field but due to its perturbative nature could not access the regime below Kondo scale. Renormalization group methods brought out the scaling properties of the Kondo model. The logarithmic divergences in perturbation theory are usually symptoms of scale invariance of the model. Renormalization group method introduces a scale/cut-off such that physics does not depend on the cut-off, but this procedure helps to construct the new model which has same physics but is supposed to be tractable as compared to the original model. It was found that Kondo coupling constant grows under this renormalization flow of Kondo model and at a particular scale when Kondo singlet is formed, local moment gets completely quenched. This scenario is similar to asymptotic freedom in quantum chromodynamics. Renormalization group methods were instrumental in the exploration of Kondo physics. However, there were other methods and approaches which also played very important role to understand other aspects of rich physics of Kondo model. Phil Noziéries' local Fermi liquid theory approach also helped to have an intuitive understanding of the Kondo physics. He used familiar methods from scattering theory and Landaus Fermi liquid theory to show the information about the Kondo singlet formation is in phase shifts.

1.3 Methods for Calculating the Effective Hamiltonians

In this section, we will present two important methods to calculate the effective Hamiltonians for strongly correlated electron systems: Schrieffer-Wolff transformation and Projection operator method. In Schrieffer-Wolff transformation, effective Hamiltonian is calculated by projecting out the high energy excitations using a unitary transformation while as in projection operator method, effective Hamiltonian is obtained by projecting the Hamiltonian into the desired subspace of the full Hilbert space.

1.3.1 Schrieffer-Wolff transformation

Schrieffer-Wolff transformation(SWT) was introduced in[4] to relate Anderson impurity model and Kondo model. Since then this transformation has been used very extensively in condensed matter physics to calculate the effective Hamiltonians. SWT is a version of degenerate perturbation theory[9], but here we would like to emphasize its connection to renormalization group[10]. The reason being that, in the case of strongly correlated electron systems there are emergent scales and SWT is used to obtain the effective Hamiltonian which results out of the renormalization process and is associated with new energy scale. SWT integrates out the high energy excitations by decoupling the high energy and low energy subspaces. Due to the decoupling, there is renormalization of the low energy sector of the model. SWT is a generic method for calculating the effective Hamiltonians of quantum many-body systems, so we will give a detailed discussion of this transformation. SWT will be later on used to calculate the effective Hamiltonians for the systems of our interest. Schrieffer-Wolff transformation being very important transformation has been generalized in various ways. One very important generalization was done by Wegner[11] and Glazek and Wilson[12] independently. The new method has been called Flow equation method by Wegner and Similarity Renormalization by Glazek and Wilson. In flow equation method the unitary transformation is once again used, but it is done in a continuous fashion because the generator depends on the flow parameter. The relation between SW transformation and flow equation method has been worked out in [13]. SWT has been applied to dissipative systems[14], periodically driven systems[15]and has also been given a path integral formulation[16]. In [9] the authors have given a mathematically rigorous treatment of the transformation and have applied SWT to quantum spin systems.

1.3.2 SWT as unitary transformation

Unitary transformation is the standard method for diagonalization in quantum mechanics and condensed matter physics[17]. By the unitary transformation, one changes to the basis in which the given Hamiltonian becomes diagonal and one achieves diagonalization in a one step process. However, this is not possible for all Hamiltonians. So in latter case, one tries to diagonalize the Hamiltonian in a perturbative manner. One can still use unitary transformation to achieve this goal. Schrieffer-Wolff transformation is such a method. It has been used extensively in different areas of physics under different names[9]. In relativistic Quantum Mechanics, it is called Foldy-Wutheysen transformation[18], in Semiconductor physics, it is called k.p perturbation theory[19] and in condensed matter physics it has been used as Frohlich transformation for electron-phonon problem[20]. Schrieffer-Wolff transformation not only diagonalizes the Hamiltonian in a perturbative manner in which case it is unitary perturbation theory but it also renormalizes the parameters in the Hamiltonian and hence is a kind of renormalization procedure. SW transformation in the latter sense is used to get the effective Hamiltonian of the given quantum many-body Hamiltonian[4].

Schrieffer-Wolff transformation is a unitary transformation. So one chooses the proper unitary operator which can either fully diagonalize the Hamiltonian or to some desired order.

$$H' = U^{\dagger} H U \tag{1.11}$$

$$H' = e^{S} H e^{-S} \tag{1.12}$$

where S is the generator of this transformation and is an anti-hermitian operator. Usually one requires of this transformation to cancel the off-diagonal terms to the

first order so that following condition is satisfied.

$$[S, H_0] = -H_v \tag{1.13}$$

Expanding the operator exponential using Baker-Campbell-Haussdorff(BCH) formula one gets series expansion for the transformed Hamiltonian H'

$$H' = H_0 + \frac{1}{2}[S, H_v] + \frac{1}{3}[S, [S, H_v]] + ... \tag{1.14}$$

where H_0 and H_v are diagonal and off-diagonal parts of the Hamiltonian H. Since the off-diagonal term gets cancelled to the first order so the effective Hamiltonian to the second order is given by

$$H_{eff} = H_0 + \frac{1}{2}[S, H_v] \tag{1.15}$$

1.3.3 How to get the generator?

The most crucial step in doing SW transformation is to get the generator of the transformation. Once the generator is calculated the rest of the calculation is quite straightforward. So having an explicit method for calculating the generator is of immense value. In this section we will present a systematic method to calculate the generator of Schrieffer-Wolff transformation for a general Hamiltonian and then will apply this method to Anderson impurity model.

Let H be our full Hamiltonian and H_0 be the diagonal part and H_v be the off-diagonal part of the full Hamiltonian. To obtain the generator, we will proceed in two steps. In the first step, we will find the commutator $[H_0, H_v]$ and call it η. In the second step, we will impose the condition of removing the off-diagonal part till first order on η. To do that we will have to keep the coefficients undetermined and they will be determined by the above condition. So η has to statisfy $[\eta, H_0] = -H_v$

in order to be the generator of the transformation. The latter condition determines the coefficients and we get the generator for SW transformation of the given Hamiltonian. In the next section we will calculate the generator of SW transformation for Single Impurity Anderson Model for which the transformation was carried out in the original paper[4].

1.3.4 Generator for Anderson Impurity Model

We will first write down the single impurity Anderson Hamiltonian in second quantized notation:

$$H = \sum_{k\sigma} \epsilon_k c^\dagger_{k\sigma} c_{k\sigma} + \sum_{\sigma} \epsilon_d d^\dagger_\sigma d_\sigma + \sum_{k\sigma} V_k (c^\dagger_{k\sigma} d_\sigma + d^\dagger_\sigma c_{k\sigma}) + U n_{d\uparrow} n_{d\downarrow} \tag{1.16}$$

The Hamiltonian has one off-diagonal term which we call as H_v and diagonal terms which together we call H_0.

$$H_0 = \sum_{k\sigma} \epsilon_k c^\dagger_{k\sigma} c_{k\sigma} + \sum_{\sigma} \epsilon_d d^\dagger_\sigma d_\sigma + U n_{d\uparrow} n_{d\downarrow} \tag{1.17}$$

$$H_v = \sum_{k\sigma} V_k (c^\dagger_{k\sigma} d_\sigma + d^\dagger_\sigma c_{k\sigma}) \tag{1.18}$$

Now the first step is to calculate η which is basically commutator of diagonal part with off-diagonal part of the Hamiltonian.

$$\eta = [H_0, H_v] \tag{1.19}$$

$$\eta = \left[\sum_{k\sigma} \epsilon_k c^\dagger_{k\sigma} c_{k\sigma} + \sum_{\sigma} \epsilon_d d^\dagger_\sigma d_\sigma + U n_{d\uparrow} n_{d\downarrow}, \sum_{k\sigma} V_k (c^\dagger_{k\sigma} d_\sigma + d^\dagger_\sigma c_{k\sigma}) \right] \tag{1.20}$$

$$\eta = \sum_{k\sigma} (\epsilon_k - \epsilon_d - U n_{d\bar{\sigma}}) V_k (c^\dagger_{k\sigma} d_\sigma - d^\dagger_\sigma c_{k\sigma}) \tag{1.21}$$

In the second step we will impose the condition of removing the off-diagonal term to the first order. To do that we will keep the coefficients undetermined and actually

they will get determined automatically once η satisfies the condition. We will label it with S to emphasize that it is not actually η which is the generator rather it is S with correct coefficients. What η has similar to S is the form of the operators.

$$S = \sum_{k\sigma}(A_k - B_k n_{d\bar{\sigma}})V_k(c^\dagger_{k\sigma}d_\sigma - d^\dagger_\sigma c_{k\sigma}) \tag{1.22}$$

Now we will impose the condition on S to determine A_k and B_k

$$[S, H_0] = -H_v \tag{1.23}$$

$$\Rightarrow \left[\sum_{k\sigma} A_k(\epsilon_d - \epsilon_k) + \sum_{k\sigma}(A_k U - B_k(\epsilon_d - \epsilon_k + U)n_{d\bar{\sigma}})\right](V_k(c^\dagger_{k\sigma}d_\sigma + d^\dagger_\sigma c_{k\sigma}) \tag{1.24}$$

$$= -\sum_{k\sigma} V_k(c^\dagger_{k\sigma}d_\sigma + d_\sigma c^\dagger_{k\sigma}) \tag{1.25}$$

$$\Rightarrow A_k(\epsilon_d - \epsilon_k) + (A_k U + B_k(\epsilon_d - \epsilon_k + U)n_{d\bar{\sigma}} = -1 \tag{1.26}$$

Solving for A_k and B_k we obtain:

$$A_k = \frac{1}{\epsilon_k - \epsilon_d} \tag{1.27}$$

$$B_k = \frac{1}{\epsilon_k - \epsilon_d - U} - \frac{1}{\epsilon_k - \epsilon_d} \tag{1.28}$$

In this way we have calculated the generator of SW transformation for Single Impurity Anderson Model. We can write the generator in the same form as was written in[4] by using extra index α which takes two values.

$$\mathrm{S} = \sum_{k\sigma\alpha} \frac{V_k}{\epsilon_k - \epsilon_\alpha} n^\alpha_{d,\bar{\sigma}} c^\dagger_{k\sigma} d_\sigma - h.c. \tag{1.29}$$

$$n^{\alpha}_{d\bar{\sigma}} = n_{d\bar{\sigma}} \qquad \epsilon_\alpha = \epsilon_d + U \quad \alpha = + \tag{1.30}$$

$$= 1 - n_{d\bar{\sigma}} \qquad \epsilon_\alpha = \epsilon_d \quad \alpha = - \tag{1.31}$$

Summing over α we get S in the same form as we have calculated.

$$\mathrm{S} = \sum_{k\sigma} \big[\frac{V_k}{\epsilon_k - \epsilon_d - U} n_{d\bar{\sigma}} c^\dagger_{k\sigma} d_\sigma + \frac{V_k}{\epsilon_k - \epsilon_d}(1 - n_{d\bar{\sigma}}) c^\dagger_{k\sigma} d_\sigma \big] - h.c. \tag{1.32}$$

1.3.5 SW Transformation of SIAM

To carry out SWT we will have to calculate the following commutator:

$$[S, H_v] \tag{1.33}$$
$$= \left[\sum_{k\sigma} (A_k + B_k n_{d\bar{\sigma}}) V_k (c^\dagger_{k\sigma} d_\sigma - d^\dagger_\sigma c_{k\sigma}), \sum_{k'\sigma'} V_{k'} \left(c^\dagger_{k'\sigma'} d_{\sigma'} + d^\dagger_{\sigma'} c_{k'\sigma'} \right) \right]$$

$$\begin{aligned}
&[S, H_v] \\
&= \sum_{kk'\sigma} A_k V_k V_{k'} (c^\dagger_{k\sigma} c_{k'\sigma} + h.c) - \sum_{k\sigma} A_k V_k^2 (d^\dagger_\sigma d_\sigma + h.c.) - \\
&\sum_{k\sigma} B_k V_k^2 (n_{d\bar{\sigma}} d^\dagger_\sigma d_\sigma + h.c.) + \sum_{kk'\sigma} B_k V_k V_{k'} (d^\dagger_{\bar{\sigma}} c_{k'\bar{\sigma}} c^\dagger_{k\sigma} d_\sigma + h.c) - \\
&\sum_{kk'\sigma} B_k V_k V_{k'} (c^\dagger_{k'\bar{\sigma}} d_{\bar{\sigma}} c^\dagger_{k\sigma} d_\sigma + h.c.) + \sum_{kk'\sigma} B_k V_k V_{k'} (c^\dagger_{k\sigma} c_{k'\sigma} n_{d\bar{\sigma}} + h.c.)
\end{aligned} \tag{1.34}$$

Switching to Nambu Spinor representation:

$$\Psi^\dagger_k = \begin{pmatrix} c^\dagger_{k\uparrow} \\ c^\dagger_{k\downarrow} \end{pmatrix} \qquad \Psi_k = \begin{pmatrix} c_{k\uparrow} \\ c_{k\downarrow} \end{pmatrix} \qquad \Psi^\dagger_d = \begin{pmatrix} d^\dagger_{\uparrow} \\ d^\dagger_{\downarrow} \end{pmatrix} \qquad \Psi_d = \begin{pmatrix} d_{\uparrow} \\ d_{\downarrow} \end{pmatrix} \tag{1.35}$$

We get the Kondo exchange term

$$= \sum_{kk'} J_{kk'} \left(\Psi_k^\dagger S \Psi_{k'} \right) \left(\Psi_d^\dagger S \Psi_d \right) \tag{1.36}$$

where exchange constant is given by

$$J_{kk'} = V_k V_{k'} \left(\frac{1}{\epsilon_d - \epsilon_k + U} + \frac{1}{\epsilon_d - \epsilon_{k'} + U} - \frac{1}{\epsilon_d - \epsilon_k} - \frac{1}{\epsilon_d - \epsilon_{k'}} \right) \tag{1.37}$$

In addition to the Kondo exchange term the commutator $[S, H_v]$ also has following terms which correspond to other scattering processes:

$$H_{dir} = \sum_{kk'\sigma} \left(A_k V_k V_{k'} + B_k V_k V_{k'} \frac{n_{d\sigma} + n_{d\bar{\sigma}}}{2} \right) c_{k\sigma}^\dagger c_{k'\sigma} + h.c. \tag{1.38}$$

$$H_{hop} = -\sum_{k\sigma} V_k^2 \left(A_k + B_k n_{d\bar{\sigma}} \right) n_{d\sigma} + h.c. \tag{1.39}$$

$$H_{ch} = \sum_{kk'\sigma} B_k V_k V_{k'} \left(c_{k\bar{\sigma}}^\dagger d_{\bar{\sigma}} c_{k'\sigma}^\dagger d_\sigma \right) + h.c. \tag{1.40}$$

1.3.6 Projection Operator Method

In this section we will calculate the low energy effective model of e-SIAM using projection operator method as given in[21]. The Hilbert space of the impurity consists of empty state, singly occupied state and doubly occupied state which can be written $|0\rangle, |\uparrow\rangle, |\downarrow\rangle, |\uparrow\downarrow\rangle$. To get the low energy effective Hamiltonian we will project out excitations to empty and doubly occupied subspaces and restrict the dynamics to singly occupied subspace which corresponds to the Kondo regime. The

corresponding projection operators are:

$$P_0 = |0\rangle\langle 0| = (1 - n_{d\uparrow})(1 - n_{d\downarrow}) \tag{1.41}$$

$$P_\uparrow = |\uparrow\rangle\langle\uparrow| = (n_{d\uparrow})(1 - n_{d\downarrow}) \tag{1.42}$$

$$P_\downarrow = |\downarrow\rangle\langle\downarrow| = (n_{d\downarrow})(1 - n_{d\uparrow}) \tag{1.43}$$

$$P_d = |\uparrow\downarrow\rangle\langle\uparrow\downarrow| = n_{d\uparrow} n_{d\downarrow} \tag{1.44}$$

Completeness of the local Hilbert space is given by$P_{j0} + P_{j\uparrow} + P_{j\downarrow} + P_{jd} = 1$

Schrodinger equation for the impurity electron can be written as

$$H\Psi = E\Psi \tag{1.45}$$

$$\sum_{m=0}^{2} H_{nm}\Psi_m = E\Psi_n \quad \text{where} \quad H_{nm} = P_n H P_m \tag{1.46}$$

$$H_{00}\Psi_0 + H_{01}\Psi_1 + H_{02}\Psi_2 = E\Psi_0 \tag{1.47}$$

$$H_{10}\Psi_0 + H_{11}\Psi_1 + H_{12}\Psi_2 = E\Psi_1 \tag{1.48}$$

$$H_{20}\Psi_0 + H_{21}\Psi_1 + H_{22}\Psi_2 = E\Psi_2 \tag{1.49}$$

Since there is no term in the Hamiltonian which connects empty and doubly occupied sub-spaces therefore we get $H_{02} = H_{20} = 0$.

Schrodinger equation in $|0\rangle$ subspace is

$$H_{00}\Psi_0 + H_{01}\Psi_1 = E\Psi_0 \tag{1.50}$$

$$(H_{00} - E)\Psi_0 = -H_{01}\Psi_1 \tag{1.51}$$

$$\Rightarrow \Psi_0 = (E - H_{00})^{-1} H_{01}\Psi_1 \tag{1.52}$$

Schrodinger equation in $|2\rangle$ subspace is given by

$$H_{21}\Psi_1 + H_{22}\Psi_2 = E\Psi_2 \tag{1.53}$$

$$(E - H_{22})\Psi_2 = H_{21}\Psi_1 \tag{1.54}$$

$$\Rightarrow \Psi_2 = (E - H_{22})^{-1} H_{21}\Psi_1 \tag{1.55}$$

Schrodinger equation in the $|1\rangle$ subspace is given by

$$H_{10}\Psi_0 + H_{11}\Psi_1 + H_{12}\Psi_2 = E\Psi_1 \tag{1.56}$$

Substituting for Ψ_0 and Ψ_2 in equation 1.48 we obtain:

$$\left[H_{10}\frac{1}{E - H_{00}}H_{01} + H_{11} + H_{12}\frac{1}{E - H_{22}}H_{21}\right]|\Psi_1\rangle = E \mid \Psi_1\rangle \tag{1.57}$$

The projected terms of the Hamiltonian are :

$$H_{00} = P_0 H P_0 = \sum_{k\sigma} \epsilon_k c^\dagger_{k\sigma} c_{k\sigma} \tag{1.58}$$

$$H_{11} = P_1 H P_1 = \sum_{k\sigma} \epsilon_k n_{k\sigma} + \epsilon_d \tag{1.59}$$

$$H_{22} = P_2 H P_2 = \sum_{k\sigma} \epsilon_k n_{k\sigma} + 2\epsilon_d + U \tag{1.60}$$

$$H_{12} = P_1 H P_2 = \sum_{k} V_k c^\dagger_{k\sigma} d_\sigma n_{d\bar{\sigma}} \qquad H_{21} = H^\dagger_{12} \tag{1.61}$$

$$H_{01} = P_0 H P_1 = \sum_{k} V_k c^\dagger_{k\sigma} d_\sigma (1 - n_{d\bar{\sigma}}) \qquad H_{10} = H^\dagger_{01} \tag{1.62}$$

To evaluate the effective Hamiltonian we need following commutators:

$$[H_{12}, H_{22}] = \left[\sum_{k\sigma} V_k c^\dagger_{k\sigma} d_\sigma n_{d\bar{\sigma}}, \sum_{k'\sigma'} \epsilon_{k'} n_{k'\sigma'} + 2\epsilon_d + U\right] \tag{1.63}$$

$$= -\sum_{k\sigma} V_k(\epsilon_k) c^\dagger_{k\sigma} d_\sigma n_{d\bar{\sigma}} \tag{1.64}$$

$$[H_{10}, H_{00}] = \left[\sum_{k'\sigma'} V_{k'} d^\dagger_{\sigma'} c_{k'\sigma'} \left(1 - n_{d_{\bar{\sigma'}}}\right), \sum_{k\sigma} \epsilon_k c^\dagger_{k\sigma} c_{k\sigma}\right] \tag{1.65}$$

$$= \sum_{k\sigma} \epsilon_k (V_k d^\dagger_\sigma c_{k\sigma}(1 - n_{d_{\bar{\sigma}}})) \tag{1.66}$$

$$H_{12} \frac{1}{E - H_{22}} H_{12} \tag{1.67}$$

$$= \sum_{k\sigma}\sum_{k'\sigma'} V_{k'} c^\dagger_{k'\sigma'} d_\sigma n_{d_{\bar{\sigma'}}} \frac{1}{E - H_{00} - 2\epsilon_d - U} V_k d^\dagger_\sigma c_{k\sigma} n_{d_{\bar{\sigma}}} \tag{1.68}$$

$$= \sum_{k'\sigma'}\sum_{k\sigma} \frac{-V_{k'}V_k}{U + \epsilon_d - \epsilon_{k'}} (1 - \frac{E - H_{00} - \epsilon_d}{U + \epsilon_d - \epsilon_{k'}})^{-1} c^\dagger_{k'\sigma'} d_{\sigma'} n_{d_{\bar{\sigma'}}} d^\dagger_\sigma c_{k\sigma} n_{d\bar{\sigma}} \tag{1.69}$$

$$= -\sum_{k\sigma}\sum_{k\sigma} \frac{V_{k'}V_k}{U + \epsilon_d - \epsilon_{k'}} c^\dagger_{k'\sigma'} d_{\sigma'} n_{d_{\bar{\sigma'}}} d^\dagger_\sigma c_{k\sigma} n_{d\bar{\sigma}} \tag{1.70}$$

$$= -\sum_{k'k}\sum_{\sigma'\sigma} \frac{V_k V_{k'}}{U + \epsilon_d - \epsilon_{k'}} \left(1/2 \sum_\sigma c^\dagger_{k\sigma} c_{k'\sigma} - \sum_{\sigma\sigma'} S.c^\dagger_{k\sigma}(\sigma)_{\sigma\sigma'} c_{k'\sigma'}\right) \tag{1.71}$$

Similarly first term in equation 1.57 can be calculated. It incorporates the excitations between empty state and singly occupied state. The contribution of this term is given by:

$$H_{10} \frac{1}{E - H_{00}} H_{01} \tag{1.72}$$

$$= \sum_{k\sigma}\sum_{k'\sigma'} V_{k'} V_k (E - H_{00} - \epsilon_{k'})^{-1} d^\dagger_{\sigma'} c_{k'\sigma'} c^\dagger_{k\sigma} d_\sigma (1 - n_{d_{\bar{\sigma'}}})(1 - n_{d_{\bar{\sigma}}}) \tag{1.73}$$

From this term one gets contribution to Kondo exchange term and potential scattering term. Potential scattering term will be dropped down from the effective Hamiltonian. Putting all the terms together one gets the following effective Hamil-

tonian.

$$H = \sum_{k\sigma} \sum_{k\sigma'} \epsilon_k c^\dagger_{k\sigma} c_{k\sigma} + J_{kk'} S.c^\dagger_{k\sigma}(\sigma)_{\sigma\sigma'} c_{k'\sigma'} \tag{1.74}$$

where the coupling constant given by

$$J_{kk'} = V_k V_{k'} \left(\frac{1}{U + \epsilon_d - \epsilon_{k'}} + \frac{1}{\epsilon_k - \epsilon_d} \right) \tag{1.75}$$

Using the projection operator method we obtain only Kondo exchange term and potential scattering term in the effective Hamiltonian which is because we have restricted the Hamiltonian to the singly occupied subspace. In contrast, the effective Hamiltonian which we have obtained via Schrieffer-Wolff transformation has other terms in addition to Kondo exchange term. However, both methods yield Kondo exchange interaction which determies the strong coupling physics of Anderson impurity model.

In previous sections we have introduced two important quantum impurity models and then using Schrieffer-Wolff transformation and projection operator method, shown how Kondo model arises as an effective Hamiltonian in the strong coupling regime of Anderson impurity model. Now we turn to lattice models and present a paradigmatic model for strongly correlated electron systems.

1.4 Hubbard model and Dynamical Mean Field theory

Hubbard model is the simplest lattice model which was introduced for strongly correlated electron systems[22].

$$H = -\sum_{\langle ij \rangle, \sigma} t_{ij} (c^\dagger_{i\sigma} c_{j\sigma} + c^\dagger_{j\sigma} c_{i\sigma}) + U \sum_i n_{i\uparrow} n_{i\downarrow} - \mu \sum_i c^\dagger_{i\sigma} c_{i\sigma} \tag{1.76}$$

t_{ij} is the hopping amplitude and U is the local Hubbard interaction and μ is the chemical potential.

However, the Hubbard model is exactly solvable only in one dimension[23]. For higher dimensions, we need to rely on different methods which can not capture the full phase diagram of the model. Hence it came as a great breakthrough when it was shown by Metzner and Vollhardt[24] that in infinite dimensions, self-energy and vertex function for the Hubbard model become local. Later on it was shown that Hubbard model can be mapped to single impurity Anderson with self-consistent hybridization[25]. This formalism of mapping lattice models to impurity Anderson model with self-consistency has been very successful to study the various lattice models of SCES and has particularly helped to understand interaction driven Mott transition. This formalism is called dynamical mean field theory(DMFT) because it treats spatial fluctuations in mean field way but takes into consideration local quantum fluctuations which lead to the phenomena like Mott transition. There are many ways to derive and understand this mapping of lattice models to quantum impurity models, we will follow cavity method[25].

1.4.1 DMFT Mapping and Self-Consistency Conditions

In this section we derive the effective action of Anderson impurity model from the Hubbard model and in that way we map the lattice model to a quantum impurity model. Important in this derivation is the infinite dimensional limit which makes the dynamic quantities like Green's functions and self-energies local. Since we are not taking into consideration the momentum dependence and hence spatial fluctuations can not be treated and DMFT becomes an approximation which takes only local dynamical fluctuations into account.

$$S = \int_0^\beta d\tau \sum_{i\sigma} c^*_{i\sigma}(\tau) \left(\frac{\partial}{\partial \tau} - \mu \right) c_{i\sigma} - \sum_{ij\sigma} t_{ij} c^*_{i\sigma}(\tau) c_{j\sigma}(\tau) + \sum_i U c^*_{i\uparrow}(\tau) c_{i\uparrow}(\tau) c^*_{i\downarrow}(\tau) c_{i\downarrow}(\tau) \tag{1.77}$$

$c^*_{i\sigma}$ and $c_{i\sigma}$ are Grassmann variables. The action for Hubbard model can be divided into three parts.

$$S = S_0 + \Delta S + S^0 \tag{1.78}$$

$$S_0 = \int_0^\beta \sum_\sigma c^*_{0\sigma}(\tau)\left(\frac{\partial}{\partial\tau} - \mu\right) c_{0\sigma}(\tau) + U c^*_{0\uparrow}(\tau)c_{0\uparrow}(\tau)c^*_{0\downarrow}(\tau)c_{0\downarrow}(\tau) \tag{1.79}$$

$$\Delta S = -\int_0^\beta d\tau \sum_{i\sigma}(t_{i0}c^*_{i\sigma}(\tau)c_{0\sigma}(\tau) + t_{0i}c^*_{0\sigma}(\tau)c_{i\sigma}(\tau)) \tag{1.80}$$

$$S^0 = \int_0^\beta d\tau \sum_{i\neq 0,\sigma} c^*_{i\sigma}(\tau)\left(\frac{\partial}{\partial\tau} - \mu\right) c_{i\sigma}(\tau) - \sum_{ij} c^*_{i\sigma}(\tau)c_{j\sigma}(\tau) +$$

$$U c^*_{i\uparrow}(\tau)c_{i\uparrow}(\tau)c^*_{i\downarrow}(\tau)c_{i\downarrow}(\tau) \tag{1.81}$$

$\eta \equiv t_{i0}c_{0\sigma}$ plays the role of the source field which is coupled to $c^\dagger_{i\sigma}$. After integrating out the fermions at all the sites except for cavity site ,we obtain the effective action:

$$S_{eff} = \sum_{n=1}^{\infty}\sum_{i_1\ldots j_n}\int \eta^\dagger_{i_i}(\tau_{i_1})\ldots\eta^\dagger_{i_n}(\tau_{i_n})n_{j_1}(\tau_{j_1})\ldots\eta_{j_n}(\tau_{j_n})G^0_{i_1\ldots j_n}(\tau_{i_1}..\tau_{i_n},\tau_{j_1}..\tau_{j_n}) +$$

$$S_0 + \text{const.} \tag{1.82}$$

In this form this result is not useful because we still need to calculate the full cavity Green's function. However something very interesting happens when we take the limit of infinite co-ordination number. In this limit the hopping amplitude needs to be rescaled as $t_{ij} \propto \frac{1}{\sqrt{d^{|i-j|}}}$. This scaling of t_{ij} ensures that Greens functions scales as $G^0 \propto (\frac{1}{\sqrt{d}})^{|i-j|}$ and hence the leading term is of the order unity and all other higher order terms have $\frac{1}{d}$ decay. So in the infinite dimensions limit only the leading order terms survive and the effective action simplifies to:

$$S_{eff} = \int d\tau d\tau' c^*_{0\sigma}\left(-\partial_\tau + \mu - \sum_{ij} t_{0i}t_{0j}G^0\right) c_{0\sigma} + \int d\tau U n_{0\uparrow}n_{0\downarrow}(\tau) \tag{1.83}$$

Here we introduce important quantity in DMFT: Weiss field which is related to the Greens's function of the Hubbard model *with one site removed*.

$$\mathcal{G}^0(i\omega_n) = i\omega_n + \mu - \sum_{ij} t_{0i} t_{0j} G^0_{ij}(i\omega) \tag{1.84}$$

However we still have to calculate G^0 and the full lattice Green's function for the Hubbard model. For a general lattice the relation between the cavity and full Green's functions is given by:

$$G^{(0)}_{ij} = G_{ij} - \frac{G_{i0} G_{0j}}{G_{00}} \tag{1.85}$$

Substituting for cavity Green's function in equation 1.84, we relate Weiss field with lattice Green's function.

$$\mathcal{G}^0(i\omega_n)^{-1} = i\omega_n + \mu - \sum_{ij} t_{0i} t_{0j} (G_{ij} - \frac{G_{i0} G_{0j}}{G_{00}}) \tag{1.86}$$

Taking the Fourier transform of hopping amplitude and Green's function we arrive at:

$$G(k, i\omega_n) = \frac{1}{i\omega_n + \mu - \epsilon_k - \Sigma_{i\omega_n}} \tag{1.87}$$

Where we have used the local self-energy $\Sigma(i\omega_n) = \Sigma(k, i\omega_n)$. Using the Dyson equation

$$\Sigma(i\omega_n) = \mathcal{G}^0(i\omega_n)^{-1} - G(i\omega)^{-1} \tag{1.88}$$

we arrive at the full lattice Green's function

$$G(i\omega_n) = \int_{-\infty}^{\infty} d\epsilon \frac{D(\epsilon)}{i\omega_n + \mu - \epsilon - \Sigma(i\omega_n}) \tag{1.89}$$

$D(\epsilon)$ is the density of states and depends on the choice of the lattice. The set of equations we have derived constitute the self-consistent equations of DMFT and lead to what is called DMFT self-consistency loop. The main step in the DMFT loop is to solve the quantum impurity model which has been obtained after DMFT mapping.

DMFT loop can be written as an algorithm which consists of following steps and can be written as flow diagram as shown in Figure 1.1.

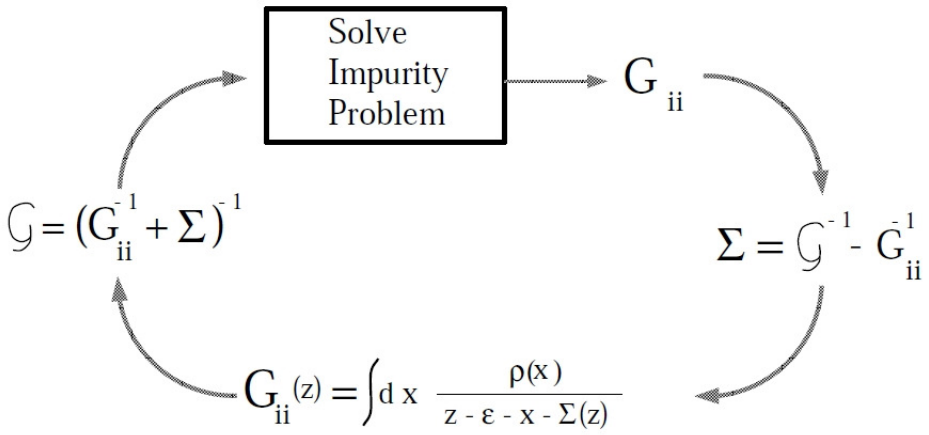

Figure 1.1: DMFT self-consistency loop.(Figure adapted from Phd thesis of N. S. Vidhyadhiraja)

Step 1: Start with non-interacting Green's function for the quantum impurity model.

Step 2: Using impurity solver calculate the full Green's function for impurity model.

Step 3: Using the Dyson equation calculate the self-energy.

Step 4: Using Hilbert transform to calculate the local Green's function of the lattice model. (In this step DMFT approximation is used which equates impurity self-energy with Lattice model self-energy).

Step 5: Using Dyson equation calculate the bath Green's function for the next iteration.

Step 6: Run the DMFT loop iteration until convergence is reached.

We have written this algorithm in terms of Green's function, but it can also be done in terms of hybridization function. The main step in DMFT computations is to solve the quantum impurity model. There are many impurity solvers which have been used within DMFT. Notable among them are numerical renormalization group method(NRG), Exact diagonalization method(ED), quantum Monte Carlo method(QMC), density matrix renormalization group (DMRG)method.

1.5 Summary

In this chapter, we have given a brief introduction to strongly correlated electron systems and how strong correlation physics leads to new emergent phenomena which need new methods for their exploration. To show the concrete examples of strongly correlated systems we have discussed three important Hamiltonians for strongly correlated electron systems, namely Anderson impurity model, Kondo model and Hubbard model. We have presented two methods for the calculation of effective Hamiltonians and based on them showed how Anderson impurity model is related to Kondo model. We have also discussed how within the dynamical mean field theory framework, Hubbard model(lattice model) gets mapped to Single impurity Anderson model in a self-consistent manner. This mapping is very important because quantum impurity models are well-understood models and within DMFT one can use quantum impurity models to understand lattice models.

Bibliography

[1] P. W. Anderson, *Basic notions of Condensed matter physics*, The Benjamin-Cummings Publishing Company, Inc. (1984).

[2] P. W. Anderson, Science, Vol **177**, Issue 4047, pp 393-396 (1972).

[3] Kenneth G. Wilson, Rev. Mod. Phys. **47**, 4 (1975).

[4] J. R. Schrieffer and P. A. Wolff, Phys. Rev. **149**, 2 (1966).

[5] P. W. Anderson, Phys. Rev. **124**, 41, (1961).

[6] A. Blandin and J. Friedel, J. Phys. Radium **19**, 573 (1958).

[7] H. R. Krishnamurthy, J. W. Wilkins and K. G. Wilson, Phys. Rev. B., **21**, 3,1003 (1980).

[8] H. R. Krishnamurthy, J. W. Wilkins and K. G. Wilson, Phys. Rev. B., **21**, 3,1044 (1980).

[9] Sergey Bravyi, David P. DiVincenzo and Daniel Loss, Annals of Physics **326**, 2793 (2011).

[10] Piers Coleman, *Local Moment Physics in Heavy Electron Systems*(Lectures on the Physics of Highly Correlated Electron Systems VI, Editor F. Mancini, American Institute of Physics, New York (2002), p 79 - 160.

[11] F. Wegner, Ann. Phys. (Leipzig) **3**, 77 (1994).

[12] S. D. Glazek and K.G. Wilson, Phys. Rev. D **48**, 5863 (1993).

[13] S. K. Kehrein and A. Mielke, Annals of Physics **252**, 1-32 (1996).

[14] E. M. Kessler, Phys. Rev. A **86**, 012126 (2012).

[15] Marin Bukov, Michael Kolodrubetz and Anatoli Polkovnikov, Phys. Rev. Lett. ,**116**, 125301 (2016).

[16] Farzaneh Zamani, Pedro Riberio and Stefan Kirchner, New Journal of Physics, **18** 063024 (2016).

[17] Max Wagner, *Unitary Transformations in Solid State Physics*(North-Holland Physics Publishing House, (1986).

[18] L. L. Foldy and S. A. Wouthuysen, Phys. Rev. **78**, 29-36 (1950).

[19] R. Winkler, *Spin-Orbit Coupling Effects in Two-Dimensional Electron and Hole Systems*(Springer Tracts in Modern Physics) , Vol.**191**, Springer-Verlag, Berlin (2010).

[20] H. Frohlich, Proc. Roy. Soc. A, **215**, 291 (1952).

[21] A. C. Hewson, *The Kondo Problem to Heavy Fermions*, Cambridge University Press (2003).

[22] J. Hubbard, Proceedings of the Royal Society of London, **276**, 1365, 238257 (1963).

[23] F. H. L. Essler, H. Frahm, F. Ghmann, A. Klmper,V. E. Korepin, *The One-Dimensional Hubbard Model*, Cambridge University Press (2005).

[24] W. Metzner and D. Vollhardt, Phys. Rev. Lett. **62**,324 (1989).

[25] A. Georges, G. Kotliar, W. Krauth and M. J. Rozenberg, Rev. Mod. Phys **68** 13 (1996).

Chapter 2

Renormalization Group Methods for Quantum Many-body Hamiltonians

Contents

2.1 Introduction

Strong correlation leads to the renormalization of the bare quantities of the electrons in real systems. Landau's Fermi liquid theory, which has been a corner stone of condensed matter physics, is based on the renormalization of the free fermions due to weak correlation. The effective description of Fermi liquid theory is in terms of "quasiparticles" which have got dressed due to renormalization effects. Similarly, all the bare properties of free electrons like mass, charge and lifetime also get renormalized, and it is these renormalized quantities which are physical rather than the bare quantities. At the level of quantum many-body Hamiltonian, the model parameters get renormalized, and as the energy scales of the model are changed, the parameters undergo renormalization flows. In the field of strongly correlated electron systems, renormalization group methods were first applied by Anderson[1][2] to get an understanding of Kondo model for which perturbation methods had given divergent results. Hence renormalization method played a very important role in understanding the quantum many-body physics of Kondo effect. Later on Wilson[3] came up with an even more robust method of renormalization called Numerical renormalization group(NRG) which helped eventually to solve what had been called "Kondo problem".

Renormalization methods become natural when we deal with many-body systems where there is an interplay between various degrees of freedom at different scales present in the system. The logarithmic divergence in the perturbation theory is a

symptom of the many energy scales. The divergent integral takes the form $\int \frac{dE}{E}$ and as the energy scale goes to the infrared limit, there is a divergence. Another feature of these systems where renormalization group becomes important is the lack of an energy scale or in other words scale invariance. Critical phenomena are the prime examples where there is no energy scale (hence scale invariance) and that is why understanding phase transitions necessitated scaling and renormalization group methods[4][5][6]. In strongly correlated electron systems, Kondo physics was the first such phenomenon which exhibited scale invariance and hence the universality[2][8]. Renormalization group methods capture these scale invariant aspects of the systems by calculating the scaling equations and the scaling invariants of the quantum many-body system.

Renormalization group method finds extensive application in quantum field theory, statistical physics, condensed matter physics, non-linear dynamics[12]. By now, there are many different methods to do the renormalization group study in condensed matter physics which include, most importantly poor man scaling [8][7], flow equation method [13], functional renormalization group [14], numerical renormalization group [15] and density matrix renormalization group [16]. However, the underlying philosophy in all the methods is similar. One identifies high energy(ultraviolet) and low energy scales in the system. Then the high energy states are integrated out iteratively. This leads to a series of effective Hamiltonians which scale towards a fixed point where the scaling flow stops. However, a fixed point can be stable, unstable or marginal depending on what happens to the scaling flow under a perturbation. This gives the fixed point structure of the Hamiltonian and determines the scaling behaviour. A Hamiltonian flows towards stable fixed point. The scaling flow of a given Hamiltonian can be written as a differential equation, often called beta function which can be solved to calculate the scaling invariants for the given model.

In this chapter, we will discuss renormalization methods for the quantum impurity models which were introduced in the previous chapter. In quantum impurity models, renormalization group methods have played a very important role. In quantum impurity models, there are two main energy scales associated with charge and spin fluctuations. The energy scale associated with the charge fluctuations is higher as compared to that of spin fluctuations which survive down to the low energy scales. As seen in the last chapter, Schrieffer-Wolff transformation projects out the high energy real charge excitations and generates an effective Hamiltonian which has spin fluctuations alone. The scaling procedure can be continued on the effective Hamiltonian. That we will do for Kondo model by applying Anderson's poor man scaling method of perturbative renormalization. We will extract the Kondo scale from the beta function of Kondo model. Then we will carry out scaling analysis of Anderson impurity model directly without integrating out the charge excitations.

Next, we will introduce another renormalization method which is an extension of Poor man scaling method. This method is called flow equation renormalization method. We will apply this method to Kondo model and show how we capture aspects of scaling behaviour of Kondo model which do not get captured in poor man scaling method. We will especially solve the flow equations for the Kondo spin operator and from them calculate dynamic spin susceptibility for Kondo model.

2.2 Renormalization group methods for quantum impurity systems

Perturbation theory of quantum impurity Hamiltonians leads to logarithmic divergences. This logarithmic dependence comes from the scaling properties of these models. The low energy physics, which is also the strong coupling regime of these models, does not depend on the bare parameters only. Strong coupling physics de-

pends on renormalized parameters which have the renormalization effects of high energy states as well. These renormalized quantities which determine the low energy physics are the scaling invariants of the Hamiltonian. In the process of scaling, though the parameters of the Hamiltonian get renormalized, however, physics remains same. The scaling transformations not only renormalize the bare parameters of the model but also produce retardation effects and generate new terms as well. So the scaling transformation is an iterative map which starting with a given Hamiltonian generates a series of effective Hamiltonians as the high energy states are projected out, and the parameters of the effective Hamiltonians keep getting renormalized. All these effective Hamiltonians lie on scaling trajectories which are determined by scaling invariants of the Hamiltonian. The iterative scaling transformations can be written as differential equations for the coupling constants of the model. Kondo model is one of the celebrated models which shows this kind of scaling behaviour. For Kondo model, Anderson based on his poor man's scaling analysis calculated the flow equation for Kondo coupling.

$$\frac{dg}{dlnD} = -g^2 \tag{2.1}$$

where J is Kondo coupling constant, $g = J\rho_0$ is dimensionless Kondo coupling constant and ρ_0 is the density of states at Fermi level. Though this differential equation looks very common and simple, its solution is very interesting and gave very important physical insights into Kondo physics.

$$g(D) = \frac{g_0}{1 - g_0 \ln(\frac{D_0}{D})} \tag{2.2}$$

Here D is the running band-width and D_0 is the initial band-width. The solution shows that as the band width is decreased and hence the high energy states are projected out, Kondo coupling constant grows and in fact it diverges logarithmically

as the band-width approaches zero. This is the well- known Kondo divergence which plagues perturbative expansions and is symptomatic of the the formation of Kondo singlet. Later on, it was confirmed that Kondo coupling actually diverges when Kondo effect takes place and consequently Kondo singlet is formed. We can define Kondo scale as the energy scale at which flow of coupling enters strong coupling regime. So Kondo scale is the energy scale at which coupling constant diverges, and perturbation expansion breaks down. Kondo scale itself is a scaling invariant and hence does not depend on band-width.

2.3 Poor Man's Scaling of Kondo model

In this section, we will carry out the poor man's scaling analysis of Kondo model[1]. In literature, this method has been called Poor man's scaling and poor man scaling method, so we will use these names interchangeably. Poor man scaling method being very important method has been discussed by many authors including[7–11]. Particularly the last two authors have done a critical study of this method. We will mainly follow [8] and [9] in this section. First, we will show how Anderson arrived at renormalized interaction using the T matrix and projection operator algebra. Then we will calculate the scaling equation for the Kondo couplings by considering the renormalization effects on various spin scattering processes.

Since Kondo effect involves spin scattering, so one introduces the T matrix which incorporates the scattering effects due to interactions.

$$T(\omega) = V_{int} + V_{int} G_0(\omega) T(\omega) \tag{2.3}$$

$G_0(\omega) = \frac{1}{\omega - H_0}$ is the resolvent operator corresponding to $H_0 = \sum_{k\sigma} \epsilon_k c^\dagger_{k\sigma} c_{k\sigma}$ for

the conduction electrons. For the Kondo model V_{int} is given by:

$$V_{int} = \frac{J_{\pm}}{2}(S^{+}s^{-} + S^{-}s^{+}) + J_z S^z s^z \tag{2.4}$$

To project out the high energy states from the conduction band we need to introduce a projection operator $P_{\delta D}$ which projects onto the states which have at least one particle in the range(D-δD,D) or one hole in the range(-D,-D+δD). $(1 - P_{\delta D})$ is the projection operator for orthogonal subspace. Using the properties of the projection operators, T matrix can be written as:

$$T = V_{int} + V_{int}(1 - P_{\delta D})G_0 T + V_{int}P_{\delta D}G_0 T \tag{2.5}$$

Substituting for T matrix in third term we get:

$$\begin{aligned} T = {} & V_{int} + V_{int}(1 - P_{\delta D})G_0 T + V_{int}P_{\delta D}G_0 V_{int} \\ & + V_{int}P_{\delta D}G_0 V_{int}(1 - P_{\delta D})G_0 T + V_{int}P_{\delta D}G_0 V_{int}P_{\delta D}G_0 T \end{aligned} \tag{2.6}$$

Re-arranging the terms, T matrix can be written as:

$$\begin{aligned} T = {} & V_{int} + V_{int}P_{\delta D}G_0 V_{int} + (V_{int} + V_{int}P_{\delta D}G_0 V_{int})(1 - P_{\delta D})G_0 T \\ & + V_{int}P_{\delta D}G_0 V_{int}P_{\delta D}G_0 T \end{aligned} \tag{2.7}$$

We can define $V'_{int} = V_{int} + V_{int}P_{\delta D}G_0 V_{int}$ as the renormalized interaction and after neglecting the last term, T matrix takes the form.

$$T = V'_{int} + V'_{int}(1 - P_{\delta D})G_0 T \tag{2.8}$$

T matrix is of the same form as in equation 2.3, however the interaction has got renormalized. Projecting out the high energy states renormalizes the interaction

while keeping the form of T matrix same. $\Delta V_{int} = V'_{int} - V_{int}$ gives the renormalized interaction: $\Delta V_{int} = V_{int} P_{\delta D} G_0 V_{int}$

$$\Delta V_{int} = \sum_{k_2\sigma_2} \sum_{k_1\sigma_1} \sum_{k\sigma} c^{\dagger}_{k_2\sigma_2}(\tau)_{\sigma_2\sigma} c_{k\sigma} . s_d \frac{P_{\delta D}}{\omega - H_0} c^{\dagger}_{k\sigma}(\tau)_{\sigma\sigma_1} c_{k_1\sigma_1} \tag{2.9}$$

We have used the Abrikosov's pseudofermion representation for conduction electrons.

$$S^z = \frac{1}{2}(c^{\dagger}_{k\uparrow} c_{k\uparrow} - c^{\dagger}_{k\downarrow} c_{k\downarrow}) \quad S^+ = c^{\dagger}_{k\uparrow} c_{k\downarrow} \quad S^- = c^{\dagger}_{k\downarrow} c_{k\uparrow} \tag{2.10}$$

This is how renormalized interaction was derived by Anderson [1]. Though Anderson arrived at the renormalized interation using T matrix and the fact that it should remain invariant under scaling transformation, we can obtain the renormalized interaction using effective Hamiltonion theory[8][19]. This method was later on used by Haldane[17] and Jefferson[18] to do the scaling analysis of asymmetric Anderson impurity model and by Kuramoto[19] for the renormalization of multi-channel Kondo models. The details of this method can be found in [8][9]. In this chapter and chapter **3**, we will apply the effective Hamiltonian way of doing the poor man scaling analysis of quantum impurity models. The effective Hamiltonian formulation of poor man scaling is an iterative way of generating effective Hamiltonians in which using the projection operators, the high energy states are being projected out and the resulting effective Hamiltonian acts on smaller Hilbert space. The renormalization effects of the projected out states gets incorporated in the coupling constants. So unlike Anderson's original formulation in terms of T matrix, where the original problem is being mapped to a simpler problem keeping the physics(T matrix) invariant, in the effective Hamiltonian method, one maps the original Hamiltonian to low energy effective Hamiltonian which has smaller Hilbert space and is simpler than the original Hamiltonian, the physics is kept invariant by incorporating the effects of the high energy states on the coupling constants of the low energy effective

Hamiltonian. The effective Hamiltonian can be calculated as[18][19]:

$$H_{eff}(\tilde{D}) = (1-P_{\delta D})H(1-P_{\delta D}) + (1-P_{\delta D})HP_{\delta D} + (1-P_{\delta D})HP_{\delta D}\frac{1}{E-P_{\delta D}HP_{\delta D}}P_{\delta D}H(1-P_{\delta D}) \tag{2.11}$$

The renormalized interaction is given by the third term. When we substitute Kondo interaction for H_V in above equation, we arrive at the renormalized interaction calculated using T matrix approach. To carry out the poor man scaling analysis of Kondo model, we need to consider the renormalization effects of all the spin scattering processes. Spin conserving scattering processes will renormalize longitudinal Kondo coupling while as the transverse Kondo coupling will get renormalized due to spin flip(transverse) scattering processes.

2.3.1 Renormalization of J_z

In this case only those scattering processes will contribute which are spin conserving and hence involve two spin flip scattering.

$$J_+J_-\sum_q S^-c^\dagger_{k'\uparrow}c_{q\downarrow}\frac{1}{\omega-H_0}\sum_{q'}S^+c^\dagger_{q'\downarrow}c_{k\uparrow} \tag{2.12}$$

The sum on q over the intermediate states is restricted within δD from the top of the band. Because the band edge states are originally unoccupied, we get $c_q c^\dagger_{q'} = \delta_{qq'}$ Using the commutator $[H_0, c^\dagger_{q'\downarrow}c_{k\uparrow}] = (\epsilon_{q'}-\epsilon_k)c^\dagger_{q'\downarrow}c_{k\uparrow}$, Equation 2.12 simplifies to

$$J_+J_-\delta D\rho_0 S^-S^+c^\dagger_{k'\uparrow}c_{k\uparrow}(E-\epsilon_q-\epsilon_k-H_0)^{-1} \tag{2.13}$$

Setting $\epsilon_q = D$ and using the relation $S^-S^+ = \frac{h^2}{2} - hS^z$, we arrive at

$$J_+J_-\delta D\rho_0 h^2(\frac{1}{2}-\frac{S^z}{h})c^\dagger_{k'\uparrow}c_{k\uparrow}(E-D+\epsilon_k)^{-1} \tag{2.14}$$

Similar contribution when the holes are involved in scattering is given below.

$$J_+J_-\delta D\rho_0 h^2(\frac{1}{2}+\frac{S^z}{h})c_{k\uparrow}c^\dagger_{k'\uparrow}(E-D-\epsilon_{k'})^{-1} \tag{2.15}$$

Here we have set $\epsilon_q = -D$ and $S^+S^- = \frac{h^2}{2} + hS^z$.

Similar contribution from the down spin electrons and holes are:

$$J_+J_-\delta D\rho_0 h^2(\frac{1}{2}+\frac{S^z}{h})c^\dagger_{k'\downarrow}c_{k\downarrow}\frac{1}{E-D+\epsilon_k} \tag{2.16}$$

$$J_+J_-\delta D\rho_0 h^2(\frac{1}{2}-\frac{S^z}{h})c_{k\downarrow}c^\dagger_{k'\downarrow}\frac{1}{E-D-\epsilon_{k'}} \tag{2.17}$$

Summing the contributions from all these terms and comparing with the original Hamiltonian we obtain the renormalized longitudinal coupling.

$$\delta J_z = -J_-J_+\rho_0\delta D\left(\frac{1}{E-D}+\frac{1}{E-D}\right) \tag{2.18}$$

Renormalized transverse Kondo coupling can be obtained in a similar manner by considering all spin-flip scattering processes.

$$\delta J_\pm = \frac{1}{2}J_\pm J_z\rho_0\delta D\left(\frac{1}{E-D}+\frac{1}{E-D}\right) \tag{2.19}$$

The renormalized Kondo couplings are energy dependent which shows that the renormalization leads to retardation of effective interaction. For low energy excitations close to Fermi level, E dependence can be neglected compared to D and $\epsilon_k, \epsilon_{k'}$ can be set to zero. In this case the the scaling equations for anisotropic Kondo model become:

$$\frac{dJ_z}{dlnD} = -2J_+J_- \tag{2.20}$$

$$\frac{dJ_\pm}{dlnD} = -2\rho_0 J_z J_\pm \tag{2.21}$$

Dividing these two scaling equations and integrating gives the scaling trajectories which are hyberbolic curves.

$$J_z^2 - J_\pm^2 = \kappa \tag{2.22}$$

J_z always increases as the band-width is decreased. In case of ferromagnetic models, $J_z < 0$ and $|J_z| > J_\pm$, the above equation shows that $J_\pm$ vanishes along the scaling flow. While as for antiferromagnetic case, Kondo coupling grows and leads to divergence for the perturbative renormalization methods. For the antiferromagnetic case, scaling equation can be solved for $J_\pm = J_z$

$$\frac{dJ}{dlnD} = -J^2\rho_0 \tag{2.23}$$

$$J(D) = \frac{J(D_0)}{1 + \rho_0 J(D_0) \ln\left(\frac{D}{D_0}\right)} \tag{2.24}$$

Scaling trajectories are characterised by a scaling invariant which also defines the Kondo scale T_k.

$$De^{\frac{-1}{2J\rho_0}} = \tilde{D}e^{\frac{-1}{2\tilde{J}\rho_0}} = k_B T_k \tag{2.25}$$

Kondo temperature is the only energy scale present in the Kondo regime, and thermodynamic quantities depend only on this scale and hence show universality.

2.4 Scaling analysis of Anderson model

In this section, we will extend perturbative renormalization to Anderson impurity model where valence fluctuations are also present in addition to spin fluctuations. The local Hilbert space of this model is larger, and it also has bigger parameter space as compared to the Kondo model. Consequently, this model has richer fixed

point structure. There are other fixed points and hence parameter regimes apart from the Kondo regime which corresponds to the strong coupling fixed point of Anderson impurity model. As we have seen in previous chapter that Kondo model is related to Anderson impurity model via Schrieffer-Wolff transformation. Poor man scaling analysis of SIAM was first done by Haldane[17] and Jefferson[18]. Though both papers had a similar motivation of understanding the mixed valence regime of asymmetric SIAM, in [17] the scaling invariants and scaling trajectories of the model parameters have been calculated. Perturbative renormalization was done till second order where hybridization was not found to get renormalized. Renormalization of impurity energy levels was also calculated. In [18] third order perturbative renormalization of the model was done, and scaling equation was also obtained for hybridization.

In this section, we will apply poor man scaling method to study the scaling behaviour of Anderson impurity model following[8][17]. We will calculate the scaling equations for the model parameters and also the renormalization of impurity energy levels. We begin with a calculation of the renormalization of the impurity energy levels. This will allow us to extract the scaling equations for the orbital energy, ϵ_d and the Hubbard U. As mentioned in the previous section, projecting out the high lying conduction band states yields an effective interaction as follows:

$$H_v(\tilde{D}) = (1 - P_{\delta D}) H_v P_{\delta D} \frac{1}{E - P_{\delta D} H_c P_{\delta D} - H_{loc}} P_{\delta D} H_v (1 - P_{\delta D}) \tag{2.26}$$

where H_c is the Hamiltonian for conduction electrons and H_{loc} is the the Hamiltonian for the impurity. Since there are real charge fluctuations involved in this model, the natural choice for representing impurity operators is through Hubbard operators. These are generalized projection operators and satisfy the following superalgebra:

$$[X^{pq}, X^{lm}] = \delta_{ql} X^{pm} - \delta_{mp} X^{lq} \tag{2.27}$$

The usual fermionic operators can also be represented in X operator representation as:

$$d_\sigma^\dagger = X^{\sigma:0} + \eta X^{2:\bar{\sigma}} \tag{2.28}$$

Where $\eta = \mp$ for for down and up spin respectively. In the new representation, the hybridization term becomes:

$$H_v = \sum_{k\sigma} \left(V_k c_{k\sigma}^\dagger (X^{0:\sigma} + \eta X^{\sigma:2}) \right) + V_k^* \left(X^{\sigma:0} + \eta X^{2:\bar{\sigma}}) c_{k\sigma}) \right) \tag{2.29}$$

This implies that

$$H_{01} = \sum_{k\sigma} V_k c_{k\sigma}^\dagger X^{0:\sigma} \tag{2.30}$$

$$H_{21} = \sum_{k\sigma} V_k \eta X^{2:\bar{\sigma}} c_{k\sigma} \tag{2.31}$$

Similarly the local part of the Hamiltonian can be written in Hubbard operator representation:

$$H_{loc} = \sum_\sigma \epsilon_d n_{d\sigma} + U n_{d\uparrow} n_{d\downarrow} \tag{2.32}$$

$$= E_0 X^{00} + \sum_\sigma E_1 X^{\sigma\sigma} + E_2 X^{22} \tag{2.33}$$

where E_1, E_2, E_3 are the energies of empty, singly occupied and doubly occupied enegy impurity states.

The contribution from the term $H_{10}\frac{1}{E-QH_0Q}H_{01}$ is

$$\begin{aligned}
&\sum_q V_q(X^{\sigma:0}+\eta X^{2:\bar{\sigma}})c_{q\sigma}\frac{1}{E-P_{\delta D}H_cP_{\delta D}-H_{loc}}\sum_q V_q^*c_{q\sigma}^\dagger(X^{0:\sigma}+\eta X^{\bar{\sigma}:2})\\
&=\sum_q V_qV_q^*(X^{\sigma:0}X^{0:\sigma}\frac{1}{E-P_{\delta D}H_cP_{\delta D}+\epsilon_d-\epsilon_q})\\
&+\sum_q V_qV_q^*(X^{2:\bar{\sigma}}X^{\bar{\sigma}:2}\frac{1}{E-P_{\delta D}H_cP_{\delta D}+\epsilon_d+U-\epsilon_q}) \qquad (2.34)\\
&=\sum_q V_qV_q^*\frac{1}{E-\epsilon_q+\epsilon_d}X^{\sigma:\sigma}+\sum_q V_qV_q^*\frac{1}{E-\epsilon_q+\epsilon_d+U}X^{2:2}\\
&=\sum_q V_qV_q^*\left(\frac{1}{-D+\epsilon_d}X^{\sigma:\sigma}+\frac{1}{-D+\epsilon_d+U}X^{2:2}\right) \qquad (2.35)
\end{aligned}$$

The contribution from the term $H_{12}\frac{1}{E-QH_0Q}H_{21}$

$$\begin{aligned}
&\sum_q V_qc_{q\sigma}(X^{\sigma:0}+\eta X^{2:\sigma})\frac{1}{E-P_{\delta D}H_cP_{\delta D}-H_{loc}}\sum_q V_q^*c_{q\sigma}^\dagger(X^{0:\sigma}+\eta X^{\sigma:2})\\
&=\sum_q V_qV_q^*X^{\sigma:0}X^{0:\sigma}\frac{1}{E-P_{\delta D}H_cP_{\delta D}-\epsilon_d-U-\epsilon_q}\\
&+\sum_q V_qV_q^*X^{2:\sigma}X^{\sigma:2}\frac{1}{E-P_{\delta D}H_cP_{\delta D}-\epsilon_d-U+\epsilon_q}\\
&=\sum_q V_qV_q^*\left(\frac{1}{-D-\epsilon_d-U}X^{\sigma:\sigma}+\frac{1}{-D+\epsilon_d+U}X^{2:2}\right) \qquad (2.36)
\end{aligned}$$

The contribution of the term $H_{12}\frac{1}{E-QH_0Q}H_{01}$

$$\begin{aligned}
&\sum_q V_q^*c_{q\sigma}^\dagger(X^{0:\sigma}+\eta X^{\sigma:2})\frac{1}{E-P_{\delta D}H_cP_{\delta D}}\sum_q V_q(X^{\sigma:0}+\eta X^{2:\bar{\sigma}})c_{q\sigma})\\
&=\sum_q V_q^*V_qX^{0:\sigma}X^{\sigma:0}\frac{1}{-\epsilon_q-\epsilon_d}+X^{\bar{\sigma}:2}X^{2:\bar{\sigma}}\frac{1}{-\epsilon_q-\epsilon_d-U} \qquad (2.37)\\
&=\sum_q V_qV_q^*(X^{0:0}\frac{1}{-\epsilon_q-\epsilon_d}+\sum_q \mid V_q\mid^2 X^{\bar{\sigma}:\bar{\sigma}}\frac{1}{-\epsilon_q-\epsilon_d-U}\\
&=\sum_q V_qV_q^*\left(X^{0:0}\frac{1}{-D-\epsilon_d}+X^{\bar{\sigma}:\bar{\sigma}}\frac{1}{-D-\epsilon_d-U}\right) \qquad (2.38)
\end{aligned}$$

Summing up all the contributions from all the terms and comparing them with the local Hamiltonian given in equation 2.33, we get the following equations for the renormalization of the quantum impurity energy levels:

$$E_0' = E_0 - \frac{2\triangle}{\pi}\frac{\mid \delta D \mid}{D + \epsilon_d} \tag{2.39}$$

$$E_1' = E_1 - \frac{\triangle \mid \delta D \mid}{\pi}\Big(\frac{1}{D - \epsilon_d} + \frac{1}{D + \epsilon_d + U}\Big) \tag{2.40}$$

$$E_2' = E_2 - \frac{2\triangle \mid \delta D \mid}{\pi}\Big(\frac{1}{D - \epsilon_d - U}\Big) \tag{2.41}$$

where E_0, E_1, E_2 are the energies of empty, singly occupied and doubly occupied impurity electron states. Given these renormalized energies, the scaling equations for the interaction strength and the orbital energy, may be obtained through $\epsilon_d = E_1' - E_0'$ and $U = E_2' - 2E_1' + E_0'$ [8] as:

$$\frac{dU}{dD} = -\frac{2\Delta}{\pi}\left(\frac{1}{D - \epsilon_d} + \frac{1}{D + \epsilon_d + U} - \frac{1}{D - \epsilon_d - U} - \frac{1}{D + \epsilon_d}\right) \tag{2.42}$$

$$\frac{d\epsilon_d}{dD} = -\frac{\Delta}{\pi}\left(\frac{2}{D + \epsilon_d} - \frac{1}{D - \epsilon_d} + \frac{1}{D + \epsilon_d + U}\right) \tag{2.43}$$

In chapter **3** we will come back to these equations and they will be solved numerically. There we will also extend the scaling analysis done here to an extended version of Anderson impurity model.

2.5 Flow Equation Renormalization Method

In the previous sections we have used poor man scaling method, which is a perturbative renormalization scheme to understand the scaling behaviour of quantum impurity models. The perturbative renormalization methods are very important in getting analytical insights into renormalization of quantum many-body Hamiltonians. However due to their perturbative nature they break down in the strong coupling regime. So it becomes natural to ask whether there are methods which can be

used to study the renormalization flows of the models which exhibit strong coupling physics. In this section we will introduce one such method which has recently found extensive applications in quantum many-body physics. This method is called flow equation renormalization group (FERG) method or flow equation method (FEM) for short[13]. We will present the formalism of this method and apply it to study the renormalization flow of Kondo model which exhibits strong coupling physics.

This method is an extension of poor man scaling method as it can be applied to situations where perturbative methods either fail or need to be modified. One very important example where flow equation method describes the physics in a natural manner is non-equilibrium quantum many-body dynamics [13][23][24][25]. Perturbative methods fail here by their very construction as they depend on projecting out the high energy states which can not be done in the non-equilibrium situation. Flow equation renormalization method is a non-perturbative method and hence is able to capture the strong coupling regime of Kondo model[22] and other models like Sine-Gordon model[13]. Hence FEM captures the full crossover from weak-coupling to strong coupling fixed points. While poor man scaling is applicable only in weak coupling and breaks down precisely at the strong coupling fixed point where the coupling constant diverges.

Flow equation method also integrates very well with bosonization. In fact, FERG is similar to bosonization in the sense that it is a non-perturbative method to calculate effective Hamiltonians of quantum many-body systems. So mathematically it gives us a quadratic form for a fermionic system whose Hamiltonian also has quartic interaction terms. Bosonization uses Kac-Moody algebras(current algebras)[26] to write down the Hamiltonian, and when we do the same procedure in FERG, we end up having closed form solutions to flow equations. The flow equations for the Kondo model written in bosonized form, have closed form solutions and Kondo coupling constant flows to Toulouse point which turns out to be the strong coupling fixed

point.

In flow equation method we can also study the renormalization of observables and calculate correlation and response functions. This is one of the distinct advantages of flow equation method over perturbative methods like poor man scaling in which we can only study the renormalization flows of the coupling constants. In flow equation method, there is an expansion of observables which is very similar to operator product expansion(OPE). However, this expansion of observables has to satisfy mathematical consistency and physical plausibility conditions. The expansion has to conserve canonical commutation(bosons)or anti-commutation(fermions) relations. Similarly, the expansion has to respect the sum rules as applicable to correlation and response functions. Since flow equation method is more general method than poor man scaling so the scaling equations of latter can be recovered in a limit called infrared parametrization in which case momentum/energy is restricted close to Fermi level.

Recently there have been many new applications and developments of flow equation method. It has been used to calculate the entanglement entropy for quantum many-body systems, and hence a new direction called "flow equation holography" [27] has opened up which looks very promising for bringing holographic methods to quantum many-body systems. In a similar vein, flow equation method has been integrated with tensor network renormalization methods[28] and the corresponding scheme has been called "Entanglement Continuous unitary transformation"(e-CUT for short). Since flow equation method brings the quantum many-body Hamiltonian in the diagonal or block-diagonal form, so it was used[29] with density matrix renormalization group and there have been many applications of this FEM-DMRG scheme in quantum chemistry[30].

2.5.1 Formalism

Flow equation method is Hamiltonian renormalization method which was introduced by Wegner[20] and Glazek and Wilson[21]. It uses unitary transformations to bring the Hamiltonian in a diagonal or band diagonal form. It does not integrate out the states as in Wilsonian RG. Rather it removes the interaction matrix elements and hence attains the diagonalization.

$$H(l) = U(l)H(0)U^{\dagger}(l) \tag{2.44}$$

where l is the continous parameter. $H(0)$ is the original Hamiltonian for $l = 0$

$$\frac{dH}{dl} = [\eta(l), H(l)] \tag{2.45}$$

where $\eta(l) = \frac{dU(l)}{dl}U^{\dagger}$. One can see that $\eta(l)$ is an anti-hermitian operator.

$$\eta^{\dagger}(l) = U(l)\frac{dU^{\dagger}(l)}{dl} = -\frac{dU}{dl}U^{\dagger}(l) = -\eta(l) \tag{2.46}$$

Here comes the important contribution of Franz Wegner[20] who gave the method to calculate the canonical generator. Wegner's generator η is given by the commutator of diagonal and off-diagonal terms of the Hamiltonian.

$$\eta(l) = [H_0(l), H_v(l)] \tag{2.47}$$

Wegner's generator removes the off-diagonal matrix elements and hence in the limit $l \longrightarrow \infty$, Hamiltonian is either diagonal or band-diagonal.

$$\frac{dH(l)}{dl} = [\eta(l), H(l)] \tag{2.48}$$

$$\left(\frac{dH}{dl}\right)_{ij} = (\eta H)_{ij} - (H\eta)_{ij} \tag{2.49}$$

$$= \sum_k (\epsilon_i - \epsilon_k) h_{ik} h_{kj} - (\epsilon_k - \epsilon_j) h_{kj} h_{ik} \tag{2.50}$$

$$= \sum_k (\epsilon_i + \epsilon_j - 2\epsilon_k) h_{ik} h_{kj} \tag{2.51}$$

So the evolution of matrix elements is given by:

$$\frac{dh_{ij}}{dl} = \sum_k (\epsilon_i + \epsilon_j - 2\epsilon_k) h_{ik} h_{kj} \tag{2.52}$$

From this equation we can write down the flow of diagonal and off-diagonal elements:

$$\frac{d\epsilon_i}{dl} = \sum_k 2(\epsilon_i - \epsilon_k) h_{ik} h_{ki} \qquad \frac{dV_{ij}}{dl} = \sum_k (\epsilon_i + \epsilon_j - 2\epsilon_k) h_{ik} h_{kj} \tag{2.53}$$

One of the very important properties of Wegner's generator is that it leads to the decay of the off-diagonal elements. That can bee shown by using the invariance of trace under unitary transformations.

$$Tr(H^2) = \sum_{ik} h_{ik} h_{ki} = \sum_k \epsilon_k^2 + \sum_{ik, i \neq k} h_{ik} h_{ki} \tag{2.54}$$

$$\frac{d}{dl} Tr(H^2) = \sum_{ik} \frac{d}{dl} (h_{ik} h_{ki}) = 0 \tag{2.55}$$

Invariance of trace under the unitary flow leads to following relation between the flow and diagonal and off-diagonal elements in Equation 2.53.

$$\sum_k \frac{d}{dl}\epsilon_k^2 = -\sum_{ik,k\neq i} \frac{d}{dl}(h_{ik}h_{ki}) \tag{2.56}$$

$$\sum_k \frac{d\epsilon_k^2}{dl} = \sum_k 2\epsilon_k \frac{d\epsilon_k}{dl} \tag{2.57}$$

$$\frac{d}{dl}\sum_k \epsilon_k^2 = 2\sum_{i,k}(\epsilon_i - \epsilon_k)^2 \mid v_{ik} \mid^2 \geq 0 \tag{2.58}$$

One can see from the last equation that the off-diagonal elements decrease proportional to the energy differences between the two levels. The interaction elements with largest energy differences vanish first and this process continues until only diagonal elements remain. Thus, Wegner's choice of the generator is appropriate to calculate the flow equations of Hamiltonians. There are other choices of the generator for flow equations like as the one by Glazek and Wilson[21], in this thesis, we will always use Wegner's choice of generator.

2.5.2 Flow Equation Method treatment of Kondo Model

In this section we will carry out flow equation renormalization of Kondo model following [13]. We write Kondo model as:

$$H(l) = H_0 + H_{int}(l) \tag{2.59}$$

where

$$H_0 = \sum_{t,\alpha} \epsilon_t c_{t\alpha}^\dagger c_{t\alpha} \tag{2.60}$$

$$H_{int}(l) = \sum_{t't} J_{t't}(l) : S.s_{t't} : \tag{2.61}$$

Here t and t' are general indices which in this case represent momenta. One should note that normal ordering prescription which is used for quantum many-body systems has been incorporated. The conduction electron spin desnity is given by:

$$s_{t't} = \sum_{\alpha,\beta} c^{\dagger}_{t'\alpha} \frac{\sigma_{\alpha\beta}}{2} c_{t\beta} \tag{2.62}$$

2.5.3 1-loop calculation

First we calculate the generator for flow equations of Kondo model.

$$\eta^1(l) = [H_0, H_{int}(l)] \tag{2.63}$$

$$\eta^1(l) = \sum_{t't} \eta^1_{t't}(:S.s_{t't}:) \tag{2.64}$$

where $\eta^1_{t't}(l) = (\epsilon_{t'} - \epsilon_t) J_{t't}(l)$. The commutator of generator with the diagonal part of the Hamiltonian is

$$[\eta^1(l), H_0] = -\sum_{t't} (\epsilon_{t'} - \epsilon_t)^2 J_{t't}(l) : S.s_{t't} : \tag{2.65}$$

To calculate the commutator of the generator with the interaction term needs working out some algebra which has been done in following.

$$C^1 = [\eta^1(l), H_{int}(l)] \tag{2.66}$$

$$= [\eta^1(l) : S.s_{t't} :, \sum_{u'u} J_{u'u}(l) : S.s_{u'u} :] \tag{2.67}$$

We need to work out the following commutator:

$$
\begin{aligned}
B^1 &= [: S.s_{t't} :, : S.s_{u'u} :] \\
&= \frac{i}{8} \sum_{ijk} \epsilon_{ijk} \sigma^i_{\alpha\beta} \sigma^j_{\mu\nu} S^k (: c^\dagger_{t'\alpha} c_{t\beta} :: c^\dagger_{u'\mu} c_{u\nu} : + : c^\dagger_{u'\mu} c_{u\nu} :: c^\dagger_{t'\alpha} c_{t\beta} :) \\
&+ \frac{3}{16} \sum_{\alpha} (\delta_{tu'} : c^\dagger_{t'\alpha} c_{u\alpha} : - \delta_{t'u} : c^\dagger_{u'\alpha} c_{t\alpha} :) \\
&+ \frac{3}{8} \delta_{tu'} \delta_{t'u} (n(t') - n(t))
\end{aligned} \tag{2.68}
$$

After doing the normal ordering one gets

$$
\begin{aligned}
B^1 &= i : S.(s_{t't} \times s_{u'u}) : \\
&+ : S.s_{t'u} : \delta_{tu'} (n(t) - 1/2) - : S.s_{u't} : \delta_{t'u} (n(t') - 1/2) \\
&+ \frac{3}{16} \sum_{\alpha} (\delta_{tu'} : c^\dagger_{t'\alpha} c_{u\alpha} : - \delta_{t'u} : c^\dagger_{u'\alpha} c_{t\alpha} :) \\
&+ \frac{3}{8} \delta_{tu'} \delta_{t'u} (n(t') - n(t))
\end{aligned} \tag{2.69}
$$

Fermi functions arise due to the normal ordering prescription which is used in flow equation method. Plugging in the expression of B^1 in the the commutator C^1 we obtain:

$$
\begin{aligned}
C^1 &= i \sum_{t,t',u,u'} (\epsilon_{t'} - \epsilon_t) J_{t't} J_{u'u} : S.(s_{t't} \times s_{u'u}) : \\
&+ \sum_{t',t,v} (\epsilon_{t'} + \epsilon_t - 2\epsilon_v) J_{t'v} J_{vt} (n(v) - 1/2) : S.s_{t't} : \\
&+ \frac{3}{16} \sum_{t',t,v,\alpha} (\epsilon_{t'} + \epsilon_t - 2\epsilon_v) J_{t'v} J_{vt} : c^\dagger_{t'\alpha} c_{t\alpha} : \\
&+ 2 \times \frac{3}{16} \sum_{t,v} (2\epsilon_t - 2\epsilon_v) J_{tv} J_{vt} n(t)
\end{aligned} \tag{2.70}
$$

The flow equation for Kondo coupling till first loop is:

$$\frac{dJ_{t't}}{dl} = -(\epsilon_{t'} - \epsilon_t)^2 J_{t't} + \sum_v (\epsilon_{t'} + \epsilon_t - 2\epsilon_v) J_{t'v} J_{vt} (n(v) - 1/2) \tag{2.71}$$

Unlike poor man scaling where Kondo coupling is momentum independent and hence there is only one scaling equation for isotropic Kondo model, the flow equation given above is actually a system of equations corresponding to different momenta. The set of equations in non-linear and coupled. Hence analytical solution is not possible except in some special cases. Infrared limit is one such special case and we will now discuss that in next section.

2.5.4 Infrared parametrization

To get the scaling behaviour of the coupling constant at energies close to Fermi level(infrared limit) we will use infrared parametrization and calculate the beta function to the leading order. We will extract the Kondo scale from the flow equation which we obtain after infrared parametrization.

$$J_{t't}(l) = \frac{J_{IR}}{N}(l) e^{-l(\epsilon_{t'} - \epsilon_t)^2} \tag{2.72}$$

where J_{IR} is the Kondo coupling close to Fermi level($t = t' = 0$). Substituting it in the flow equation one gets:

$$\frac{dJ_{IR}}{dl} = -2J_{IR}^2 \frac{1}{N} \sum_\nu \epsilon_\nu e^{-2l\epsilon_\nu^2} (n(\epsilon_\nu) - \frac{1}{2}) \tag{2.73}$$

$$= -2J_{IR}^2 \int d\epsilon \rho(\epsilon) \epsilon e^{-2l\epsilon^2} (n(\epsilon) - \frac{1}{2}) \tag{2.74}$$

To proceed further, we need to specify density of states. We take the constant density of states with conduction band width 2D ($\epsilon \in [-D, D]$) and set the temperature to

be zero. That makes electron occupation function a step function.

$$\frac{dg}{dl} = \frac{g^2}{2l}(1 - e^{-2lD^2}) \tag{2.75}$$

Where $g = \rho J_{IR}$ is dimensionless Kondo coupling. For $l \leq D^{-2}$ flow is negligible.

$$\frac{dg}{dl} = \frac{g^2}{2l} \tag{2.76}$$

We can obtain the poor man scaling equation by noting that RG scale Λ is related to flow parameter as $\Lambda = l^{-\frac{1}{2}}$ and $dl = -2ldln\Lambda$

$$\frac{dg}{dln\Lambda} = -g^2 \tag{2.77}$$

This is one-loop scaling equation for isotropic Kondo model. This is the scaling equation which we obtained from poor man scaling analysis of isotropic Kondo model.

2.5.5 Extraction of Kondo Scale

Flow equation can be solved for running coupling constant.

$$\begin{aligned} \int_{g_0}^{g} \frac{dg}{g^2} &= \int_{D_0^{-2}}^{D^{-2}} \frac{dl}{2l} \\ \frac{1}{g} - \frac{1}{g_0} &= ln(\frac{D}{D_0}) \\ g &= \frac{1}{\frac{1}{g_0} - ln(\frac{D_0}{D})} \end{aligned} \tag{2.78}$$

Energy scale can not be continuously decreased, and there is special energy scale at which coupling constant diverges. This scale is called Kondo scale T_k and physically

corresponds to the Kondo singlet formation.

$$T_k \sim D_0 e^{-\frac{1}{g_0}} \tag{2.79}$$

We have seen that in infrared limit, flow equations recover poor man scaling equations. Infrared parametrization of flow equations is important for another reason as well. As shown above we can extract Kondo scale from flow equations in this limit by using the definition of Kondo scale as the scale at which flow equations diverge in infrared limit, as used in poor man scaling. Based on this idea, we have come up with a numerical procedure for extraction of Kondo scale from the numerical solution of flow equations as well. We will describe the details of this numerical procedure in next section.

2.5.6 Numerical Solution of Flow equations of Kondo Model

Flow equations are coupled non-linear differential equations. They generally can not be solved analytically except in some special limits e.g. in the infrared limit when the momentum of the coupling constants is restricted to be close to Fermi level. In this case, flow equations reproduce the results of the conventional scaling methods like poor man scaling. Flow equations can be solved by numerical methods like as Runga-Kutta methods. The number of flow equations to be solved scales as $O(N^2)$ where N is the number of energy states of the conduction band in case of Kondo model. Since flow equations are renormalization flows and hence they meet many different energy scales during the unitary flow and hence become stiff also. In this section, we solve the flow equations of Kondo model numerically. We have used DOPRI5 Fortran subroutine as the solver. DOPRI5 is based on fifth order Runga-Kutta method. As we have seen above that in the infrared limit, flow equations recover poor man scaling equation of Kondo model. Kondo coupling grows logarithmically and finally diverges at Kondo scale. Numerical solution of flow equations gives access

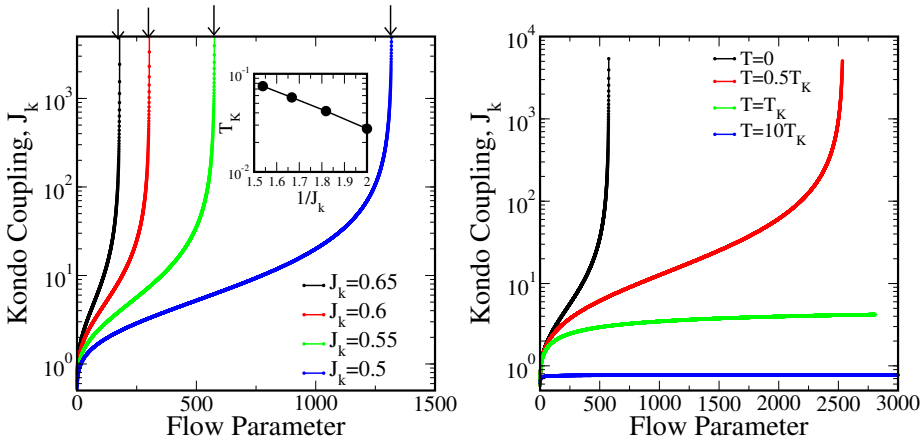

Figure 2.1: Kondo coupling has been plotted versus flow parameter. In the left panel, the effect of increasing initial value of Kondo coupling can be seen. In right panel, temperature T has been varied.

to all the Kondo couplings for different momenta. However to see the divergence of the Kondo coupling we did infrared parametrization numerically by restricting momenta to Fermi level($\epsilon_k = 0 = \epsilon_{k'}$). And as shown in the Figure 2.1, we find the divergence as expected. In the left panel of this figure, we find that as we increase the Kondo coupling, Kondo divergence becomes steeper and also occurs at different flow parameter value which is because Kondo scale also changes with Kondo coupling. The arrows point to the values of flow parameter l_c where Kondo divergence occurs.

However, the main significance of our numerical procedure is that we can extract Kondo scale from the numerical solution of flow equations. From the solution of flow equation in infrared limit as given in Equation 2.78, we find that $T_k = \frac{1}{\sqrt{l_c}}$ where l_c is the flow parameter value where Kondo coupling diverges. In the inset is plotted the Kondo scale which we have extracted from our procedure, versus inverse Kondo coupling and as can be seen that it a straight line. We also found that slope of this straight line is 2(within numerical error) as expected from the expression $\ln T_k = \ln D - 2\frac{1}{J_{IR}}$. Our procedure can be used to extract Kondo scale for the cases where poor man scaling can not be applied. In chapter 6, we have applied this procedure to extract Kondo scale for Majorana-Kondo model.

In right panel of Figure 2.1, we see that as temperature is increased, there is softening of Kondo divergence which is because of going away from Kondo temperature and also there are incoherent thermal fluctuations which dominate over Kondo spin fluctuations.

2.5.7 Flow equation for Observables

In the flow equation method, we can calculate the renormalization flows of observables as well. The way observables and their time evolution is calculated in FEM is quite different than that of conventional many-body methods. Solving the Heisenberg equations of motion for observables is easier in the flow equation method. The reason for that is the in FEM Hamiltonian is brought in diagonal(or block-diagonal) form and then evaluating the dynamics with quadratic Hamiltonian becomes easier. While as to evaluate the dynamics with the original Hamiltonian is very difficult. In this section, we will present the formalism for calculating the renormalization flows of the observables. And then we will apply this formalism to calculate the dynamical spin susceptibility of Kondo model.

Zero Temperature expectation value of observable O is given by:

$$\langle O\rangle_{GS} = \langle \Psi_{GS}|O|\Psi_{GS}\rangle \tag{2.80}$$

$|\Psi_{GS}\rangle$ is the ground state of the full interacting Hamiltonian.

$$H|\Psi_{GS}\rangle = E_{GS}|\Psi_{GS}\rangle \tag{2.81}$$

Since flow equation method basically diagonalizes the Hamiltonian so we can write

$$\tilde{H}|\tilde{\Psi}_{GS}\rangle = E_{GS}\tilde{\Psi}_{GS} \tag{2.82}$$

where $|\tilde{\Psi_{GS}}\rangle = U^{\dagger}(l)|\Psi_{GS}\rangle$ Now comes the important idea: *In FEM the observables also get transformed under the unitary flow.* So to calculate the expectation value of the observable we use the transformed basis.

$$\langle O_{GS}\rangle = \langle\tilde{\Psi}_{GS}|\tilde{O}|\tilde{\Psi}_{GS}\rangle \tag{2.83}$$

$$\tilde{O} = U(l\to\infty)OU^{\dagger}(l\to\infty) \tag{2.84}$$

The observable O satisfies the flow equation

$$\frac{dO(l)}{dl} = [\eta(l), O(l)] \tag{2.85}$$

So under the unitary flow the observable O becomes a linear combination of infinitely many operators denoted by T_a.

$$O(l\to\infty) = \sum_a t_a(O)T_a \tag{2.86}$$

The coefficients t_a depend on the observable. Since $\tilde{H}$ is in the diagonal form we get

$$\left[\tilde{H}, T_a\right] = \Omega_a T_a \tag{2.87}$$

So we can write the expectation value as:

$$\langle O\rangle_{GS} = \sum_a t_a(O)\langle\tilde{\Psi}_{GS}|T_a|\tilde{\Psi}_{GS}\rangle \tag{2.88}$$

$$C(t_1,t_2) = \langle O_1(t_1)O_2(t_2)\rangle \tag{2.89}$$

The operators are in the Heisenberg representation

$$O(t_i) = e^{iHt_i}Oe^{-iHt_i} \tag{2.90}$$

Transforming to the diagonal basis:

$$C(t_1,t_2) = \langle\tilde{\Psi}_{GS}|\tilde{O}_1(t_1)\tilde{O}_2(t_2)|\tilde{\Psi}_{GS}\rangle \tag{2.91}$$

$$= \langle\tilde{\Psi}_{GS}|e^{i\tilde{H}t_1}\tilde{O}_1 e^{-i\tilde{H}(t_1-t_2)}\tilde{O}_2 e^{-i\tilde{H}t_2}|\tilde{\Psi}_{GS}\rangle \tag{2.92}$$

$$= \langle\tilde{\Psi}_{GS}|\tilde{O}_1 e^{i(\tilde{H}-E_{GS})(t_2-t_1)}\tilde{O}_2|\tilde{\Psi}_{GS}\rangle \tag{2.93}$$

Employing the expansion for transformed observables:

$$C(t_1,t_2) = \langle\tilde{\Psi}_{GS}|\sum_{a_1} t_{a_1}T_{a_1}e^{i(\tilde{H}-E_{GS})(t_2-t_1)}\sum_{a_2} t_{a_2}T_{a_2}|\tilde{\Psi}_{GS}\rangle \tag{2.94}$$

$$= \sum_{a_1} t_{a_1}\sum_{a_2} t_{a_2}e^{-i\Omega_{a_2}(t_1-t_2)}\langle\tilde{\Psi}_{GS}|T_{a_1}T_{a_2}|\tilde{\Psi}_{GS}\rangle \tag{2.95}$$

Similarly one can also write down the (retarded) Greens function.

$$G_{kk'}(\tau) = -i\Theta(\tau)\sum_{a_1a_2} t_{a_1}t_{a_2}\langle\tilde{\Psi}_{GS}|\{T_{a_1},T^{\dagger}_{a_2}\}|\tilde{\Psi}_{GS}\rangle \tag{2.96}$$

Taking the Fourier transform one gets

$$G_{kk'}(\omega) = \sum_{a_1a_2} t_{a_1}(k)t^{*}_{a_2}(k')\frac{\langle\tilde{\Psi}_{GS}|\{T_{a_1},T^{\dagger}_{a_2}\}|\tilde{\Psi}_{GS}\rangle}{\omega-\Omega_{a_2}+i\epsilon} \tag{2.97}$$

2.5.8 Finite Temperature Formalism

In this section we will extend the formalism of previous section for non-zero temperature. The expectation value of observable O at finite temperature is given by:

$$\langle O\rangle = Tr(\rho O) = \frac{1}{Z}\sum_n \langle n|e^{-\beta H}O|n\rangle \tag{2.98}$$

where ρ is the density matrix and Z is the partition function of the system. Using the fact that trace is invariant under cyclic permutation we insert the unitary

transformation and get:

$$\frac{1}{Z}\sum_{n}\langle n|e^{-\beta\tilde{H}}\tilde{O}|n\rangle \tag{2.99}$$

Using the expansion for the observable we get the final expression for the expectation value of the observable at finite temperature.

$$\langle O\rangle = \frac{1}{\tilde{Z}}\sum_{a} t_a(O)\sum_{n} e^{-\beta\epsilon_n}\langle n|T_a|n\rangle \tag{2.100}$$

Here $\tilde{Z}$ is the partition function with transformed Hamiltonian. Similarly the equations for correlation functions can also be generalized to finite temperature.

$$C(t_1,t_2) = \frac{1}{Z}Tr(\rho O_1(t_1)O_2(t_2)) \tag{2.101}$$

Using the operator expansion one gets

$$C(t_1,t_2) = \frac{1}{\tilde{Z}}\sum_{n}\sum_{a_1a_2} t_{a_1}(O_1)t_{a_2}(O_2)e^{-\beta E_n - i\Omega_{a_2}(t_1-t_2)}\langle n|T_{a_1}T_{a_2}|n\rangle \tag{2.102}$$

2.5.9 Spin Dynamics

In this section we will calculate the flow equation for Kondo impurity spin operator and then calculate the dynamic spin susceptibility from the numerical solution of the flow equations.

$$\frac{dS^a(l)}{dl} = [\eta_l, S^a(l)] \tag{2.103}$$

We will use the one loop generator, given in equation 2.64 to evaluate the above commutator. We use the following ansatz for spin operator:

$$S^a(l) = h(l)S^a + i\sum_{u'u}\gamma_{u'u}(l) : (S\times s_{u'u})^a : \tag{2.104}$$

The flow equations for the coefficients are

$$\frac{dh}{dl} = \sum_{t't}(\epsilon_{t'} - \epsilon_t)J_{t't}\gamma_{tt'}n(t')(1 - n(t)) \tag{2.105}$$

$$\frac{d\gamma_{t't}}{dl} = h(\epsilon_{t'} - \epsilon_t)J_{t't} - \frac{1}{4}\sum_{u}((\epsilon_{u'} - \epsilon_u)J_{t'u}\gamma_{t'u})(1 - 2n(u))) \tag{2.106}$$

Using the above formalism we can calculate spin-spin correlation function.

$$C(t) = \frac{1}{2}\langle S^z(0), S^z(t)\rangle \tag{2.107}$$

Plugging the ansatz of spin operator in equation 2.102 and Fourier transforming to frequency domain, we obtain:

$$\begin{aligned} C(\omega) = -\frac{\pi}{Z(\beta)}\sum_n e^{-\beta E_n}\sum_{tt'}\sum_{uu'}\gamma_{tt'}(l\to\infty)\gamma_{u'u}(l\to\infty) \\ \times \langle n| : (S \times s_{t't})^z :: (S \times s_{u'u})^z : |n\rangle \\ \times (\delta(\omega - \epsilon_{u'} + \epsilon_u) + \delta(\omega + \epsilon_{u'} - \epsilon_u)) \end{aligned} \tag{2.108}$$

$$C(\omega) = \frac{\pi}{4}\sum_u \gamma^2_{\epsilon_u+\omega,\epsilon_u}(l\to\infty) \times (n(\epsilon_u)(1 - n(\epsilon_u + \omega)(1 - n(\epsilon_u) \tag{2.109}$$

The quantity which we are interested in and which we have calculated is imaginary part of the dynamic spin susceptibility $\chi(\omega)$. Fluctuation-dissipation theorm relates $\chi(\omega)$ to the spin-spin correlation function $C(\omega)$ calculated above.

$$\chi(\omega) = tanh\left(\frac{\omega}{2T}\right)C(\omega) \tag{2.110}$$

Spin susceptibility is plotted in Figure 2.2. As we decrease Kondo coupling and hence Kondo effect becomes weaker, spin susceptibility gets enhanced. We want to

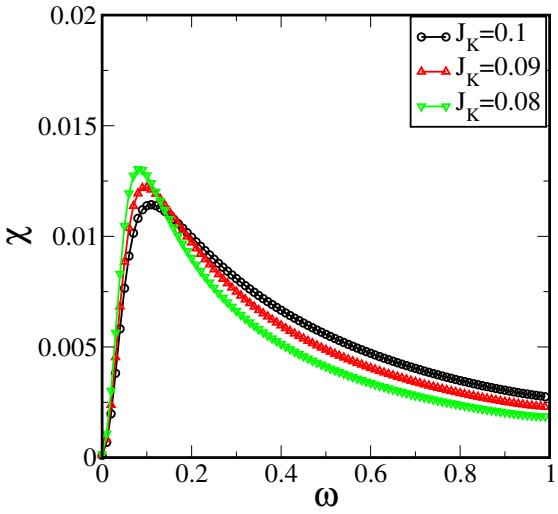

Figure 2.2: Spin susceptibility of isotropic Kondo model is plotted as function of frequency. Kondo coupling J_k is increasing from top to bottom. $\beta = \frac{1}{T} = 78.0$ has been used .

point out that we obtained these curves with out any broadening which has been done in[13][22].

2.6 Summary

In this chapter we have given discussion about the renormalization group methods which have been used in this thesis. Anderson's poor man scaling method has been discussed and then applied to calculate the scaling equations for Kondo coupling. Solving the scaling equation we have calculated Kondo scale. We have also carried out scaling analysis of Anderson impurity model. Then we have discussed about flow equation renormalization method and shown how it is an extension of poor man scaling method. After presenting the formalism of this method we have done the flow equation renormalization of Kondo model and showed how in infrared limit, we recover poor man scaling results. We also presented our numerical procedure to extract Kondo scale from the numerical solutions of flow equations of Kondo model. Our numerical procedure can be applied to extract Kondo scale for cases where poor

man scaling can not be applied. One distinct advantage of FERG is that we can also study the renormalization behaviour of observables and hence calculate correlation and response functions. For the Kondo model, we have calculated the flow equation for spin observable and then solving those equations numerically, we obtain dynamic spin susceptibility. Within flow equation method we can calculate flow equations at finite temperature as well and they give reliable behaviour for temperatures above Kondo scale.

Bibliography

[1] P. W. Anderson, J. Phys. C **3**, 2436 (1970).

[2] P. W. Anderson, *Basic notions of Condensed matter physics*, The Benjamin-Cummings Publishing Company, Inc. (1984).

[3] Kenneth G. Wilson, Rev. Mod. Phys. **47**, 4(1975).

[4] Leo P. Kadanoff, *Statistical Physics*, World Scientific, Singapore (2000).

[5] John Cardy, *Scaling and Renormalization*, Cambridge University Press (1996).

[6] Jean Zinn-Justin, *Phase transitions and Renormalization Group*, Oxford University Press (2007).

[7] Piers Coleman, *Local Moment Physics in Heavy Electron Systems*(Lectures on the Physics of Highly Correlated Electron Systems VI, Editor F. Mancini, American Institute of Physics, New York (2002), p 79 - 160.

[8] A. C. Hewson, *The Kondo Problem to Heavy Fermions*, Cambridge University Press, (2003).

[9] Philip Phillips, *Advanced Solid State Physics*,WestView Press, (2003)

[10] J. Solyom and A. Zawadowski, J. Phys. F: Metal Phys. **4**, 80 (1974).

[11] P. Nozieres, Journal de Physique, **39**, 10 (1978)

[12] W. D. McComb, *Renormalization Methods: A guide for Beginners*, Oxford University Press (2004).

[13] Stefan Kehrein, *The Flow Equation Approach to Many Particle Systems*. Springer,Berlin (2006).

[14] P. Kopietz, L. Bartosch and F. Schutz *Introduction to the Functional Renormalization Group*, Springer-Verlag, Berlin (2010).

[15] Ralf Bulla, Theo Costi and Thomas Pruschke, Rev. Mod. Phys. **80**, 2, (2008).

[16] U. Schollwock, Rev. Mod. Phys. **77**, 1 (2005).

[17] F. D. M. Haldane, Phys. Rev. Lett, **40**, 6 (1978).

[18] J. H. Jefferson, J. Phys. C **10** (1977).

[19] Y. Kuramoto, Eur. Phys. J. B **5**, 457 (1998).

[20] F. Wegner, Ann. Phys. (Leipzig) **3**, 77 (1994).

[21] S.D. Glazek and K.G. Wilson, Phys. Rev. D **48**, 5863 (1993).

[22] W. Hofstetter and S. Kehrein, Phys. Rev. B **63**,140402 (2001).

[23] S. Kehrein, Phys. Rev. Lett. **95**, 056602 (2005).

[24] P. Fritsch and S. Kehrein, Ann. Phys.**324**,1105 (2009).

[25] P. Fritsch and S. Kehrein, Phys. Rev. B **81**, 035113 (2010).

[26] A. O. Gogolin, A. A. Nersesyan and A. M. Tsvelik *Bosonization and Strongly Correlated Systems*, Cambridge University Press (2001).

[27] Stefan Kehrein, Flow Equation Holography, arxiv:1703.03925 (2017).

[28] Serkan Sahin, Kai Schmidt and Roman Orus, EPL **117**, 20002 (2017).

[29] Steven R. White, The Journal of Chemical Physics, **117**, 7472 (2002).

[30] Takeshi Yanai and Garnet Kin-Lic Chan, The Journal of Chemical Physics,**124**, 194106 (2006).

Chapter 3

Scaling Analysis of extended Anderson Impurity Model

Contents

3.1 Introduction

The Doniach phase diagram provides a natural framework to understand the physics of heavy fermion systems[1, 2], where spin fluctuations govern the low energy Kondo physics[3]. Though one can understand a broad range of phenomenology in rare-earths in terms of spin fluctuations alone, there are many experimental observations such as first order valence transition, unconventional superconductivity in $CeCu_2Se_2$ and quantum criticality in $YbRh_2Si_2$, $\beta - YbAlB_4$ and $CeIrIn_5$ [4, 5], that require incorporating valence fluctuations on an equal footing. Historically the Falicov-Kimball(FK) model was introduced to investigate valence fluctuations. But, the FK model has spinless electrons; hence to get a realistic description, the Anderson model is a more appropriate choice. The latter exhibits a mixed valent phase in which valence fluctuations are dominant. However, they do not lead to any phase transition. To capture stronger effects of valence fluctuations, the Anderson Hamiltonian has been extended by including a Hubbard repulsion between localized f and itinerant c electrons in the Anderson model[6, 7]. In the literature, this term is called the Falicov-Kimball(FK) term or the U_{fc} term. We will change these terms interchangeably.

Several theoretical studies of the extended single-impurity Anderson model (e-SIAM) have been carried out. In Ref [7], the authors have carried out a numerical renormalization group(NRG) study of the e-SIAM, and they found that the U_{fc} term does not lead to significant effect on spectral and thermodynamic properties. They could fit their results to the Anderson impurity model with renormalized parameters. In Ref [8], the authors have used renormalized perturbation theory (RPT) to study the effect of U_{fc} term and they found that there is no change in the low energy fixed point of the Anderson model due to this term and all it does is the renormalization of the parameters of Anderson impurity model. However, in Ref [9] a scaling analysis of SIAM with FK interaction showed that hybridization and hence the Kondo

scale gets heavily renormalized. Later on, a complete study of the asymmetric SIAM using NRG[10] found that the FK interaction affects thermodynamic properties like specific heat. The authors have suggested that due to the FK interaction, there are excitonic excitations which lead to this renormalization. Thus, the role of the U_{fc} term and the ensuing valence fluctuations in the extended SIAM is still debatable. We have addressed this debate by using a complementary set of methods which include perturbative renormalization methods as given in Refs [12–14] and the Schrieffer-Wolff transformation [15, 16].

Though the standard model for heavy fermions is the periodic Anderson model(PAM), we have considered the single impurity version of this model. There are many motivations to do so. One important reason is that in dynamical mean field theory (DMFT), which is one of the most important methods to study lattice models, the PAM is mapped to impurity Anderson model, so it becomes very important to understand the latter. There is yet another interesting reason to study the SIAM which comes from a recent study of Ref[17]. The authors in the latter show that a charge Kondo effect can arise due to pair hopping mechanism. They have considered an extended Anderson impurity along with pair hopping terms. In the isospin representation, the U_{fc} term is the longitudinal component of the charge Kondo interaction which is $I_c^z I_d^z = (n_{k\sigma} - 1)(n_{d\sigma} - 1)$ where I_c and I_d are isospin operators of conduction electrons and impurity respectively. Since charge (valence) fluctuations play a significant role in quantum transport, the effect of U_{fc} interaction has been studied in this context [18–21]. Quantum criticality has also been found in impurity Anderson models with particular forms of the density of states [22]. This gives an added motivation for this work.

In this chapter, we have employed perturbative renormalization methods of Refs. [13, 14] to study the scaling behaviour of e-SIAM, with a focus on the differences introduced by the U_{fc} interaction term. Scaling trajectories of any Hamil-

tonian are governed by the scaling invariants of that model and hence to explore the effect of valence fluctuations in e-SIAM, we have calculated its scaling invariants. We find that they differ from those of SIAM. Since the strong coupling regime of the SIAM is governed by Kondo physics, we have explored the renormalization of the Kondo scale due to valence fluctuations and one of the very important findings of this work is that Kondo scale of e-SIAM gets enhanced due to valence fluctuations. The Kondo scale has been extracted from the scaling invariants of e-SIAM rather than from the corresponding Kondo model. The motivation for this is as follows: to explore the effect of valence fluctuations on Kondo scale, we have to incorporate valence fluctuations, which is not the case when we use the Kondo model which is obtained via Schrieffer-Wolff transformation that projects out first order valence fluctuations. It is known for the case of SIAM, that the hybridization does not get renormalized at second order level[13][15] and that is what we found for e-SIAM as well. Nevertheless, we wanted to explore the renormalization effects of U_{fc} on hybridization so using Jefferson's method[14] we did a third order scaling analysis of e-SIAM and calculated a scaling equation for the hybridization as well. Our perturbative renormalization calculations show that the U_{fc} interaction does have strong renormalization effects on the model parameters of e-SIAM, and hence the Kondo scale also gets renormalized.

To explore these renormalization effects at an effective Hamiltonian level, we employed Schrieffer-Wolff transformation and found that the strong coupling physics of e-SIAM is not governed by Kondo model rather it is the *spin-charge Kondo model* which has an interplay of spin and charge Kondo effects which govern the strong coupling physics of this model. We also found that if one uses only projection operator method, what one gets is the standard Kondo model with renormalized Kondo coupling which does not capture the full effect of U_{fc} interaction because projection operator method projects the Hamiltonian to the singly occupied subspace. That

is why we had to calculate the effective Hamiltonian using unitary transformation. Based on all these methods, we have done a detailed perturbative renormalization study of e-SIAM and explored the role of the valence fluctuations in this model.

The rest of this chapter is being organized as follows: First we introduce the model we have studied. Then based on projection operator method, we have calculated the Kondo model and the Kondo scale. Next, we have carried out Schrieffer-Wolff transformation of the model. Then we have done the perturbative renormalization of the model and calculated the scaling equations and the scaling invariants of the model. Using Hubbard operator representation we have also found the renormalization of impurity energy levels. Finally, we have summarized our results and given the discussion about them.

3.2 Hamiltonian and the Methods

The Hamiltonian we have studied is the extended single impurity Anderson impurity (e-SIAM) model in which a U_{fc} term is added to the usual(standard) Anderson model to capture the effect of valence fluctuations. In second quantized notation, the Hamiltonian is written below:

$$H = \sum_{k\sigma} \epsilon_k c^\dagger_{k\sigma} c_{k\sigma} + \sum_{\sigma} \epsilon_d d^\dagger_\sigma d_\sigma + \sum_{k\sigma} V_k (c^\dagger_{k\sigma} d_\sigma + d^\dagger_\sigma c_{k\sigma}) + U n_{d\uparrow} n_{d\downarrow} + \sum_{k\sigma\sigma'} U_{fc} n_{k\sigma} n_{d\sigma'} \tag{3.1}$$

The extended SIAM captures the dynamics of a local impurity hybridising with a sea of free fermions which have dispersion but no interactions. These itinerant electrons are written as c electrons, and the first term corresponds to them. The impurity which is a localized d electron has no dispersion, but there is on-site Hubbard interaction between d electrons.The local impurity is represented by second and fourth terms. The hybridization between itinerant and localized electrons is written as

the third term. The last term is the U_{fc} term which captures the Hubbard repulsion between itinerant and localized electrons. The standard SIAM($U_{fc} = 0$) has three main regimes called Kondo regime, the mixed valent regime and local moment regime which is connected by smooth crossovers.

3.3 Effective Hamiltonian through a Schrieffer-Wolf transformation

The Schrieffer-Wolff transformation(SWT) is a method which gives the low energy effective Hamiltonian of a given quantum many-body Hamiltonian by projecting out the high energy excitations. In case of SIAM this transformation maps the model to Kondo model which lies at strong coupling fixed point of SIAM. To understand the strong coupling regime of e-SIAM we have used SWT and calculated the corresponding Kondo model and found out how does the valence fluctuations renormalize the Kondo exchange coupling. There are at least two different ways of doing SWT: 1)One can use unitary transformation method as used in[16] or 2) One can use projection operator method[15]. We have used both of these methods. To map e-SIAM to the corresponding Kondo model we used projection operator method and to map e-SIAM with assisted hopping we have used unitary transformation method. In SIAM Kondo scale is the low energy scale which is an emergent scale and gets dynamically generated by the interplay of local Hubbard interaction at the impurity site and hybridization of local moments with the free conduction electrons. Kondo scale is the most prominent signature of many-body dynamics in this model. Kondo scale signals the formation of Kondo singlet as manifested in Kondo resonance in the spectral function of the model. At the Kondo scale the system goes from the local moment regime to the localized Fermi liquid regime. Anderson's poor man scaling[12](which is a perturbative renormalization method) gives the scaling equa-

tion of the coupling constant from which Kondo scale can be extracted. However we have directly done perturbative renormalization of the e-SIAM and calculated the Kondo scale. So we have studied the effect of valence fluctuations on Kondo scale both in Kondo regime as well in mixed valent regime. We have also found out the scaling invariants of e-SIAM.

In this section we carry out Schrieffer-Wolff transformation of e-SIAM. The details of this method are given in chapter **2**. We have calculated the generator of SW transformation for the extended SIAM.

$$S = \sum_{k\sigma} (A_k + B_k n_{d\bar{\sigma}}) V_k (c^\dagger_{k\sigma} d_\sigma - d^\dagger_\sigma c_{k\sigma}) \tag{3.2}$$

where A_k and B_k are given below:

$$A_k = \frac{1}{\epsilon_k - \epsilon_d} \tag{3.3}$$

$$B_k = \frac{1}{\epsilon_k - \epsilon_d + U_{fc} - U} - \frac{1}{\epsilon_k - \epsilon_d} \tag{3.4}$$

To carry out the transformation we need to evaluate the commutator,$[S, H_v]$ as is done below:

$$\begin{aligned}
[S, H_v] = &\sum_{kk'\sigma} A_k V_k V_{k'} (c^\dagger_{k\sigma} c_{k'\sigma} + h.c) - \sum_{k\sigma} A_k V_k^2 (d^\dagger_\sigma d_\sigma + h.c.) \\
&- \sum_{k\sigma} B_k V_k^2 (n_{d\bar{\sigma}} d^\dagger_\sigma d_\sigma + h.c.) - \sum_{kk'\sigma} B_k V_k V_{k'} (c^\dagger_{k'\bar{\sigma}} d_{\bar{\sigma}} c^\dagger_{k\sigma} d_\sigma + h.c.) + \\
&+ \sum_{kk'\sigma} B_k V_k V_{k'} (d^\dagger_{\bar{\sigma}} c_{k'\bar{\sigma}} c^\dagger_{k\sigma} d_\sigma + h.c) + \sum_{kk'\sigma} B_k V_k V_{k'} (c^\dagger_{k\sigma} c_{k'\sigma} n_{d\bar{\sigma}} + h.c.)
\end{aligned} \tag{3.5}$$

As shown in the previous chapter, we need to use Nambu Spinor notation to write the Kondo exchange term in terms of Spin operators. There are other terms also present in $[S, H_v]$ commutator. Combining all of them we have the following terms

in the effective Hamiltonian:

$$H_{eff} = H_0 + H_{ex} + H_{pot} + H_{dir} + H_{char} \tag{3.6}$$

$$H_0 = \sum_{k\sigma} \epsilon_k c^\dagger_{k\sigma} c_{k\sigma} \tag{3.7}$$

$$H_{ex} = \sum_{kk'\sigma} J_{kk'} \left(\Psi^\dagger_k S \Psi_{k'}\right) \left(\Psi^\dagger_d S \Psi_d\right) \tag{3.8}$$

$$H_{dir} = \sum_{kk'\sigma} \left(W_{kk'} + \frac{1}{2} J_{kk'} n_{d\bar{\sigma}}\right) c^\dagger_{k\sigma} c_{k'\sigma} + h.c. \tag{3.9}$$

$$H_{hop} = -\sum_{k\sigma} \left(W_{kk} + \frac{1}{2} J_{kk} n_{d\bar{\sigma}}\right) n_{d\sigma} \tag{3.10}$$

$$H_{char} = \frac{1}{2} \sum_{kk'\sigma} J_{kk'} \left(c^\dagger_{k\bar{\sigma}} d_{\bar{\sigma}} c^\dagger_{k'\sigma} d_\sigma\right) + h.c. \tag{3.11}$$

where $J_{kk'}$ and $W_{kk'}$ are given by:

$$J_{kk'} = V_k V_{k'} \left(\frac{1}{\epsilon_k - \epsilon_d + U_{fc} - U} + \frac{1}{\epsilon_{k'} - \epsilon_d + U_{fc} - U} - \frac{1}{\epsilon_k - \epsilon_d} - \frac{1}{\epsilon_{k'} - \epsilon_d}\right) \tag{3.12}$$

$$W_{kk'} = V_k V_{k'} \left(\frac{1}{\epsilon_k - \epsilon_d} + \frac{1}{\epsilon_{k'} - \epsilon_d}\right) \tag{3.13}$$

Choosing $k = k'$ Kondo coupling constant becomes

$$J_k = 2V_k^2 \left(\frac{1}{\epsilon_k - \epsilon_d + U_{fc} - U} - \frac{1}{\epsilon_k - \epsilon_d}\right) \tag{3.14}$$

What needs to be immediately noted that as compared to SWT of SIAM we have charge Kondo interaction term also in the effective Hamiltonian(in H_0) which when combined with H_{ch} gives the full charge Kondo interaction. It is usually ignored by arguing that spin Kondo model lives in $n_d = 1$ subspace of Anderson Hamiltonian. However as noted in [25] in a system with valence fluctuations both Kondo interactions are significant. From symmetry point of view charge Kondo interaction has $su(2)_c$ symmetry which commutes with symmetry of spin Kondo interaction[26].

Charge Kondo interaction interacts with isopsin(pairing) part of the conduction bath and gives rise to Kondo effect[24]. So we have obtained the spin-charge Kondo model in which spin and charge Kondo effects co-exist as was been already found in NRG calculations[17]. Our results show that spin-charge Kondo model can arise in a system with repulsive interactions alone and there is no need for phononic mechanisms to have attractive interaction.

3.3.1 Effective Hamiltonian through projection operator method

A minor point that we would like to emphasise is that the elimination of charge fluctuations can be done in multiple ways, and there are subtle differences between the methods. For example, the projection operator method, introduced in chapter-2 does yield the Kondo model, when applied to the conventional SIAM. However, since the projection to the $n_d = 1$ subspace is built into the method, the charge Kondo terms automatically vanish. This is in contrast to the SWT, which is a unitary transformation and until a projection to the singly occupied subspace is carried out, all the quartic operators remain. This implies that the projection operator method, yields only a renormalized Kondo model (ignoring potential scattering),

$$H = \sum_{k\sigma}\sum_{k\sigma'}(\epsilon_k c^\dagger_{k\sigma}c_{k\sigma} + J_{kk'}S.c^\dagger_{k\sigma}(\sigma)_{\sigma\sigma'}c_{k'\sigma'} \tag{3.15}$$

where the coupling constant is given by

$$J_{kk'} = -V_k V_{k'}\left(\frac{1}{U+\epsilon_d-\epsilon_{k'}-2U_{fc}} + \frac{1}{\epsilon_k-\epsilon_d}\right) \tag{3.16}$$

and not the full spin-charge Kondo model given by the SWT.

3.4 Perturbative scaling of the E-SIAM: Finite U

In the last chapter we discussed the methods for perturbative renormalization of the Kondo model and the Anderson impurity model. In this section, we will apply the same method to the e-SIAM. Our focus will be on the changes in the scaling equations and the corresponding scaling invariants due to the U_{fc} interaction. We begin with a calculation of the renormalization of the impurity energy levels. This will allow us to extract the scaling equations for the orbital energy, ϵ_d and the Hubbard U. Following the same procedure of poor man scaling for e-SIAM as done for Anderson impurity model in previous chapter, we obtain the renormalized impurity energy levels:

$$E_0' = E_0 - \frac{2\triangle}{\pi}\frac{\mid \delta D \mid}{D+\epsilon_d} \tag{3.17}$$

$$E_1' = E_1 - \frac{\triangle \mid \delta D \mid}{\pi}\Big(\frac{1}{D+U_{fc}-\epsilon_d} + \frac{1}{D+2U_{fc}+\epsilon_d+U}\Big) \tag{3.18}$$

$$E_2' = E_2 - \frac{2\triangle \mid \delta D \mid}{\pi}\Big(\frac{1}{D+2U_{fc}-\epsilon_d-U}\Big) \tag{3.19}$$

where E_0,E_1,E_2 are the energies of empty, singly occupied and doubly occupied impurity electron states and $\triangle = \frac{\rho_0}{\pi} \mid V^2 \mid$ where ρ_0 is the density of the states at the Fermi level. Given these renormalized energies, the scaling equations for the interaction strength and the orbital energy, may be obtained through $\epsilon_d = E_1' - E_0'$ and $U = E_2' - 2E_1' + E_0'$ [15] as:

$$\frac{dU}{dD} = -\frac{2\Delta}{\pi}\left(\frac{1}{D+U_{fc}-\epsilon_d} + \frac{1}{D+2U_{fc}+\epsilon_d+U} - \frac{1}{D+2U_{fc}-\epsilon_d-U} - \frac{1}{D+\epsilon_d}\right) \tag{3.20}$$

$$\frac{d\epsilon_d}{dD} = -\frac{\Delta}{\pi}\left(\frac{2}{D+\epsilon_d} - \frac{1}{D+U_{fc}-\epsilon_d} + \frac{1}{D+2U_{fc}+\epsilon_d+U}\right) \tag{3.21}$$

These equations may be solved easily using the Euler's discretization, and the results are presented below.

3.4.1 Particle-hole symmetric case

For the particle-hole (ph) symmetric case, $\epsilon_d = -U/2$ is maintained even during the flow, hence we can focus only on the interaction strength. With $U_{fc} = 0$, the flow should be the same as that of the conventional Anderson model. Figure 3.1 shows the flow of U with decreasing bandwidth for various initial D values. We see that if the orbital energy is within the initial band, the interaction strength flows to lower values and eventually vanishes, implying a flow to a non-interacting system and hence the strong coupling fixed point. While if the initial bandwidth, D is smaller than $|\epsilon_d|$, the interaction strength flows to higher values, and this may be interpreted as a flow to the local moment fixed point. Hence the separatrix is $D = -\epsilon_d$. It is well known (e.g from NRG calculations) that a separatrix is absent in the SIAM, and for all initial values in the ph-symmetric case, the system flows to the strong coupling fixed point. The flow to the LM fixed point seen in figure 3.1 is an artefact of the perturbative renormalization employed here. Next, we investigate the effect of U_{fc} on the scaling trajectories. For $U_{fc} = 0$, we have seen from figure 3.1 that for $D < -\epsilon_d$, the flow is always towards the LM fixed point, since the U increases monotonically with decreasing bandwidth. The Falicov-Kimball interactions changes the flow as shown below. The left panel of figure 3.2 shows that for the same parameter regime ($D = 2.5$, such that $D < -\epsilon_d$), a new separatrix is introduced at a finite value of U_{fc}, which separates the upward renormalization from the downward flow. However, a difference with the $U_{fc} = 0$ case is that the $D \to 0$ value of U is finite instead of vanishing as in figure 3.1. Nevertheless, as U_{fc} increases, the system always flows towards lower interaction strengths, implying an increase in valence fluctuations. This observation is reiterated in the right panel of figure 3.2 ($D = 3.1$ such that

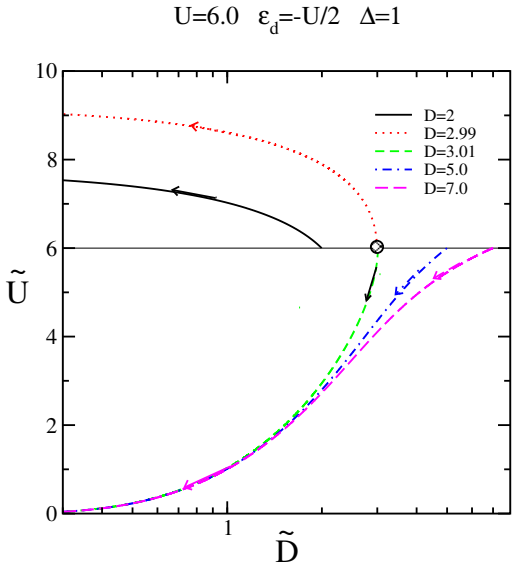

Figure 3.1: Scaling flow of U for the particle-hole symmetric case with $U = 6, \epsilon_d = -U/2$ for $U_{fc} = 0$.

$D > -\epsilon_d$), where increasing U_{fc} leads to uniformly downward renormalization and progressively smaller values of the interaction strength as $D \to 0$.

3.4.2 Particle-hole asymmetric case

In the p-h symmetric case, the d-occupancy is 1, and the asymmetry, defined as $\eta = 1 + 2\epsilon_d/U$ vanishes. In the asymmetric case, $\epsilon_d \neq -U/2$, hence $\eta \neq 0$ and the occupancy n_d deviates from unity, becoming either electron doped ($n_d > 1$) or hole doped ($n_d < 1$). Before we investigate the effects of U_{fc} for $\eta \neq 0$, the behaviour of the scaling equations for $U_{fc} = 0$ should be understood. We show the scaling flow of U and ϵ_d for decreasing bandwidth in the top and bottom panels respectively of figure 3.3. In contrast to the symmetric case, the flows here are seen to be quite non-monotonic and interesting. Although $D = -\epsilon_d$ is still a separatrix, the $D << |\epsilon_d|$ flows show initial downward renormalization, but as $D \to 0$, the interaction strength grows and saturates at a finite value higher than the initial value. For all $D > |\epsilon_d|$ however, the $\tilde{U}$ eventually vanishes. So, qualitatively, the infrared flows are exactly

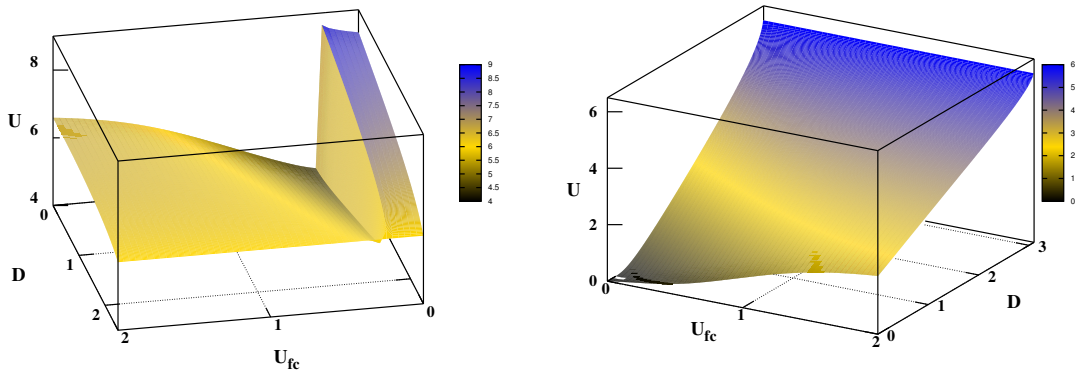

Figure 3.2: Scaling flow of U with decreasing bandwidth, for various U_{fc} values in the ph-symmetric case. The initial bandwidth in the left panel is $D = 2.5$, such that $D < -\epsilon_d$ and in the right panel, $D = 3.1$, such that $D > -\epsilon_d$.

the same for the symmetric and the asymmetric case. The lower panel of figure 3.3 showing $\tilde{\epsilon}_d$ mirrors the flows seen for the symmetric case. For an initial impurity energy within the band, the flow is towards $\tilde{\epsilon}_d \to 0$, while for initial ϵ_d below the band, the renormalization is towards the LM fixed point. Next we turn on U_{fc}. The effect of U_{fc} is expected to be far more significant in the p-h asymmetric case, since valence fluctuations are much more favourable when $n_d \neq 1$. Figure 3.4 shows the flow of U with decreasing bandwidth for $U = 10.0$, and $\eta = 0.58$, which implies $\epsilon_d = -2.1$. The left panel shows results for $D < -\epsilon_d$, such that the d-level lies below the conduction band. In the absence of U_{fc}, the system flows to the LM fixed point, but with increasing U_{fc}, a separatrix is introduced at $U_{fc} \sim 2.9$ in parallel to the p-h symmetric case. Since the U flows downward beyond this separatrix, we can interpret this as U_{fc} driven increase in valence fluctuations. For, $D > -\epsilon_d$, such that the d-level lies within the conduction band, the flow in the absence of U_{fc} (as seen in the right panel of figure 3.4) is non-monotonic. The U decreases initially, bu as the bandwidth reduces, the interaction strength goes through a shallow dip and increases steeply as $D \to 0$. Again this behaviour changes qualitatively with increasing U_{fc}. Although there is no separatrix, the U decreases monotonically for

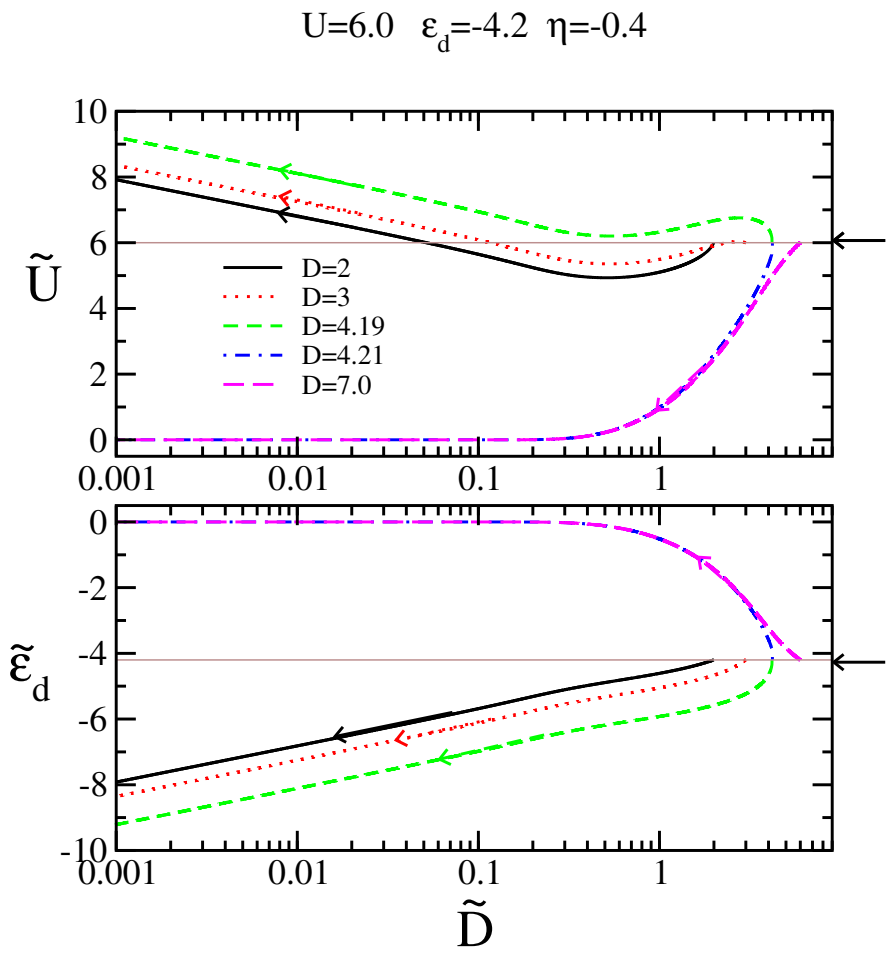

Figure 3.3: Scaling flow of U and ϵ_d for asymmetric case with $U_{fc} = 0$.

larger U_{fc} again leading to the interpretation that valence fluctuations are enhanced.

In the next section, we will consider the $U \to \infty$ limit so that we will study the effect of valence fluctuations between the empty and singly occupied states only.

3.5 Perturbative scaling of the E-SIAM: Infinite U limit

We consider the $U \to \infty$ limit due to which doubly occupied states get decoupled so the renormalization of Hubbard repulsion is not a consideration in the following. In this section, we will first get the scaling equation for ϵ_d, and subsequently investigate the renormalization of hybridization.

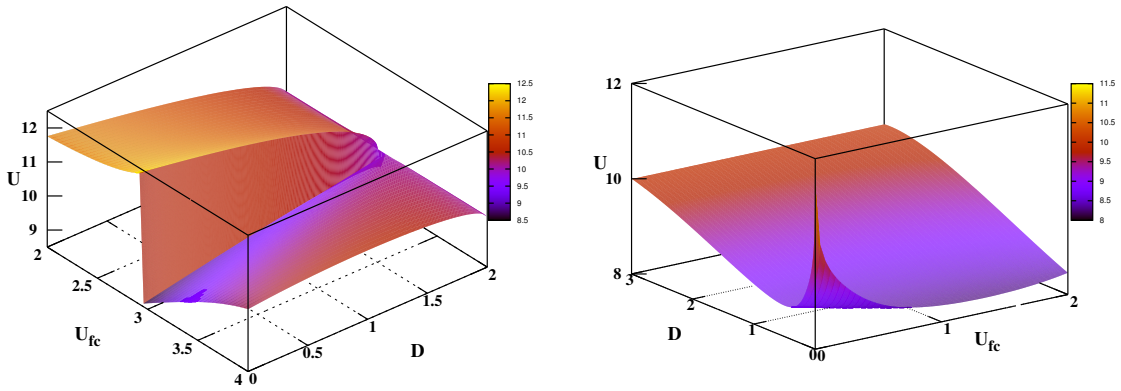

Figure 3.4: Scaling flow of U with decreasing bandwidth for various U_{fc} values in the ph-asymmetric case with initial asymmetry of 0.58. The initial bandwidth in the left panel is $D = 2.0$ such that $D < -\epsilon_d$ and in the right panel, $D = 3.0$, such that $D > -\epsilon_d$. The initial interaction strength is $U = 10.0$.

3.5.1 Scaling flow of ϵ_d

Following Jefferson[14] we will calculate the scaling equation for ϵ_d by calculating the effective Hamiltonian till second order and comparing with the bare Hamiltonian given in Equation 3.1.

$$H^2_{eff} = Q_{\delta D} H_v \sum_{\alpha} G_\alpha H_v Q_{\delta D} \tag{3.22}$$

$$= \sum_{q\sigma} \sum_{q'\sigma'} Q_{\delta D} d^\dagger_\sigma c_{q'\sigma'} G c^\dagger_{q\sigma} d_\sigma Q_{\delta D} + Q_{\delta D} c^\dagger_{q'\sigma'} d_{\sigma'} G d_\sigma c_{q\sigma} Q_{\delta D} \tag{3.23}$$

$$= \sum_{q\sigma} \sum_{q'\sigma'} \left(d^\dagger_{\sigma'} c_{q'\sigma'} c^\dagger_{q\sigma} d_\sigma \frac{1}{-\epsilon_q - U_{fc} + \epsilon_d} + c^\dagger_{q'\sigma'} d_{\sigma'} d^\dagger_\sigma c_{q\sigma} \frac{1}{-\epsilon_q - \epsilon_d} \right) \tag{3.24}$$

where $G_\alpha = \frac{P_{\delta D}}{E_\alpha - H_0}$. Uisng the fact that there are no particles/holes in the high energy states and after summing over the intermediate states, the above effective Hamiltonian gives us the renormalized Hamiltonian written below:

$$H(\tilde{D}) = \sum_{k\sigma} \epsilon_k c^\dagger_{k\sigma} c_{k\sigma} + \sum_{k\sigma\sigma'} U_{fc} n_{k\sigma} n_{d\sigma'} + \sum_k V^0_k (c^\dagger_{k\sigma} d_\sigma + h.c.) + \tag{3.25}$$

$$\sum_\sigma (\epsilon^0_d + \frac{\rho_0 V^2 \delta D}{-D - U_{fc} + \epsilon_d} - \frac{2\rho_0 V^2 \delta D}{-D - \epsilon_d}) n_{d\sigma}\,, \tag{3.26}$$

where V^0_k and ϵ^0_d are bare values of hybridization and impurity orbital energy and k is restricted to model space. It is easy to see that the impurity energy has got renormalized. After comparing with the bare Hamiltonian(Equation 3.1) we can write down the effect due to renormalization.

$$\delta\epsilon_d = \rho_0 V^2 \delta D (\frac{2}{D + \epsilon_d} - \frac{1}{D + U_{fc} - \epsilon_d}) \tag{3.27}$$

This equation is identical to the one obtained before 3.21 in the limit of $U \to \infty$. We have solved this equation numerically and the results are presented in Figure 3.5. As is shown in figure 3.5, the effect of U_{fc} is stronger in the mixed valent regime ($D > -\epsilon_d$, top panel) while for the local moment regime ($D < -\epsilon_d$, bottom panel), where the impurity energy level lies deeper below the band, the effect of U_{fc} is insignificant. A few analytical forms may be obtained in a limiting case, namely $D \gg |\epsilon_d|$. The scaling equation for ϵ_d becomes in this case:

$$\frac{d\epsilon_d}{dD} = -\frac{\Delta}{\pi} \left(\frac{2}{D} - \frac{1}{D + U_{fc}} \right)\,, \tag{3.28}$$

where $\Delta = \pi\rho_0 V^2$. A scaling invariant can be obtained through this equation.

$$\epsilon_d + \frac{\Delta}{\pi} \left[ln \frac{D}{D_0} + ln \left(\frac{D}{D_0} \frac{D_0 + U_{fc}}{D + U_{fc}} \right) \right] = const \tag{3.29}$$

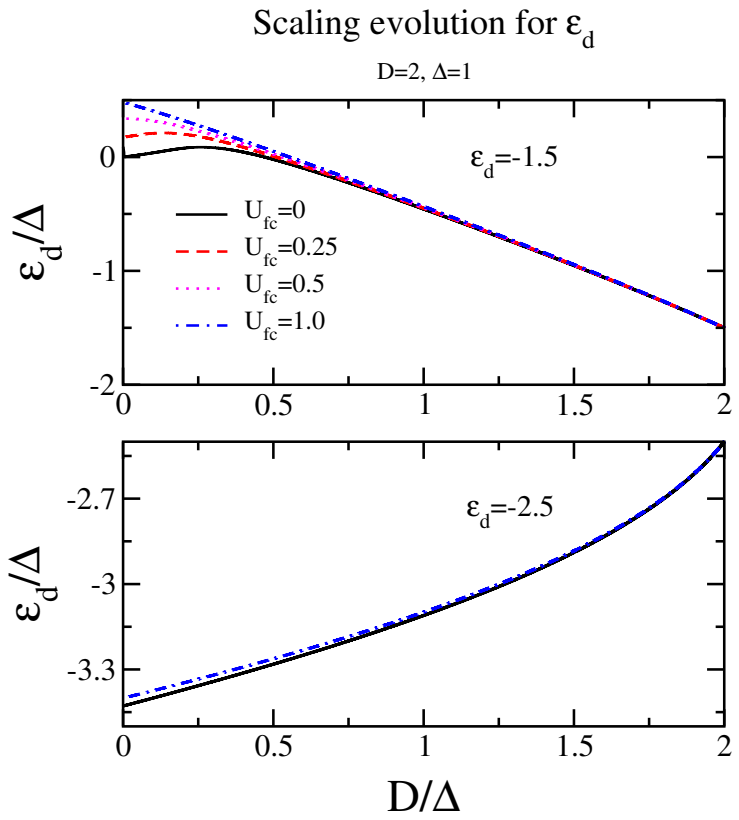

Figure 3.5: Scaling flow of ϵ_d for mixed valent regime($D > -\epsilon_d$, top panel) and local moment regime ($D > -\epsilon_d$, bottom panel).

Using the fact that U_{fc} is small as compared to bandwidth D which is the largest enery scale of the model, we can further simplify this expression of scaling invariant.

$$\epsilon_d^* = \epsilon_d + \frac{\Delta}{\pi} ln \frac{D}{D_0} - \frac{\Delta}{\pi} \frac{U_{fc}}{D} \tag{3.30}$$

The scaling invariant of e-SIAM has been written in this form to see its relation with the corresponding scaling invariant for SIAM where $U_{fc} = 0$. The first two terms constitute the scaling invariant for SIAM and third term gives the contribution of U_{fc} term. From the scaling analysis of SIAM[13][14][15], it is known that ϵ_d increases with scaling and the impurity energy level moves closer to the Fermi level and hence inreasing the valence fluctuations. From the above equation we can see that the effect

of U_{fc} term is to further enhance the increase in ϵ_d and hence U_{fc} term enhances the valence fluctuations even further.

We have already calculated first *scaling invariant* for our model. At second order, there is no renormalization of hybridization so Δ is another scaling invariant. In our model, we have third scaling invariant as well which is U_{fc} interaction itself. So the renormalization flow of e-SIAM is characterized by three scaling invariants. Later on, we will see the hybridization gets renormalized and we will find out the scaling behaviour of hybridization at the third order level.

3.5.2 Renormalization of Hybridization

The hybridization does not get renormalized at the second order level and hence is taken as a scaling invariant for the Anderson impurity model[13]. In the e-SIAM also, we did not get any renormalization of hybridization at the second order of perturbative renormalization and hence hybridization is once again a scaling invariant of this model. However at third order, hybridization does get renormalized and for the conventional Anderson impurity model, Jefferson has calculated the corresponding scaling equations[14]. In this section we will calculate the scaling equations for hybridization in the e-SIAM. Here also we will continue to keep doubly occupied state decoupled and hence there will be no contributions of the processes to/from that state. The third order contributions to the effective Hamiltonian are given by:

$$\begin{aligned} H_v(\tilde{D}) = (1-P_{\delta D})H_v \sum_{\alpha} G_\alpha H_v G_\alpha H_v (1-P^{\alpha}_{\delta D}) \\ - (1-P_{\delta D})H_v \sum_{\alpha} G_\alpha (\sum_{\alpha'} G_{\alpha'} H_v (1-P^{\alpha'}_{\delta D}) H_v (1-P^{\alpha}_{\delta D}) \end{aligned} \tag{3.31}$$

where $G_\alpha = \frac{P_{\delta D}}{E_\alpha - H_0}$ is the projected resolvent and α, α' are the indices for the degenerate states. Since we have excluded the doubly occupied state, the first term in the above equation will not contribute. So the second term is the only third order

contribution to the effective Hamiltonian. To get the scaling equation, we need to calculate this term for our model. We will see that the two terms of the hybridization ($c^\dagger_{k\sigma} d_\sigma$ and its Hermitian conjugate) get renormalized in different ways so we write them as follows and find the scaling equations separately for them.

$$H_v = \sum_{k\sigma} V_{k1} c^\dagger_{k\sigma} d_\sigma + V_{k2} d^\dagger_\sigma c_{k\sigma} \tag{3.32}$$

$$\begin{aligned} H^3_{eff} = \sum_{kk'q\sigma\sigma'} \sum_{\alpha\alpha'} \big(& - V_{k2} V_{k1} V_{k2} Q_{\delta D} d^\dagger_\sigma c_{k'\sigma} G_\alpha G_{\alpha'} c^\dagger_{k'\sigma'} d_{\sigma'} Q^{\alpha'}_{\delta D} d^\dagger_{\sigma'} c_{k\sigma} Q^\alpha_{\delta D} \qquad (3.33) \\ & - V_{k1} V_{k2} V_{k1} Q_{\delta D} c^\dagger_{k\sigma} d_\sigma G_\alpha G_{\alpha'} d^\dagger_\sigma c_{k\sigma} Q^\alpha_{\delta D} c^\dagger_{k\sigma} Q^\alpha_{\delta D} \big) \\ = & - \sum_{kq\sigma} V_{k2} V_{k1} V_{k2} \frac{d^\dagger c_{q\sigma} c^\dagger_{q\sigma} d_\sigma d^\dagger_\sigma c_{k\sigma}}{(-\epsilon_q - U_{fc} + \epsilon_d)(\epsilon_q - \epsilon_k)} - \sum_{qk\sigma} V_{k1} V_{k2} V_{k1} \frac{c^\dagger_{q\sigma'} d_{\sigma'} d^\dagger_{\sigma'} c_{q\sigma'} c^\dagger_{k\sigma} d_\sigma}{(-\epsilon_q - \epsilon_k)(-\epsilon_q - \epsilon_d)} \end{aligned} \tag{3.34}$$

Once again using the fact there are no particles/holes in high energy states and summing over the intermediate states, we get the renormalized hybridization expressions as follows:

$$V_2 - V_0 = \frac{-\rho_0 V_1 V_2^2 \delta D}{(D + U_{fc} - \epsilon_d)(D - \epsilon_k)} \tag{3.35}$$

$$V_1 - V_0 = \frac{-2\rho_0 V_2 V_1^2 \delta D}{(D + \epsilon_d)(D + \epsilon_k)} \tag{3.36}$$

The scaling equations for the hybridization can then be written from the above equations:

$$\frac{dV_2}{dD} = \frac{\rho_0 V_1 V_2^2}{(D + U_{fc} - \epsilon_d)(D - \epsilon_k)} \tag{3.37}$$

$$\frac{dV_1}{dD} = \frac{2\rho_0 V_2 V_1^2}{(D + \epsilon_d)(D + \epsilon_k)} \tag{3.38}$$

We will first present two analytically tractable limits for these equations, which will provide qualitative insight and the third scaling invariant.

I. In the mixed valent regime, and close to the Fermi level, we can choose $\epsilon_k = 0, \epsilon_d = 0$. In this regime also, we have two limits. First when $D >> U_{fc}$ in which case the scaling equation reduces to that of the SIAM as given in [14]. In the second case, when U_{fc} is comparable to the bandwidth, the scaling equations have different solutions and are given below. Also if we divide the two scaling equations for hybridizations and integrate, we find that V_1 and V_2 are related as $V_1 = \frac{V_2^2}{V_0}$. This relation implies that V_2 and V_1 renormalize in exactly the same way in this limit ($\epsilon_d = 0$ or $|\epsilon_d| \ll D$). It also needs to be noted that we have ignored the momentum dependence of the hybridization amplitudes which is physically reasonable in this regime because of the closeness to Fermi level. So the scaling equation for V_2 becomes:

$$\frac{dV_2}{dD} = \frac{V_2^2 V_1 \rho_0}{D(D + U_{fc})} \tag{3.39}$$

Solving for hybridization we obtain:

$$\frac{1}{V_2^3} - \frac{1}{V_0^3} = \frac{-\rho}{4V_0 U_{fc}} ln \left(\frac{D}{D_0} \frac{D_0 + U_{fc}}{D + U_{fc}} \right) \tag{3.40}$$

Once again using the fact that bandwidth is the largest energy scale of the model,we arrive at the simplified expression for hybridization.

$$\frac{1}{V_2^3} = \frac{-\rho}{4V_0} \left(\frac{1}{D_0} - \frac{1}{D} \right) + \frac{U_{fc}\rho}{4V_0} \left(\frac{1}{D_0} - \frac{1}{D} \right)^2 \tag{3.41}$$

We notice that U_{fc} enters this expression for hybridization at second order. For the case of vanishing U_{fc}, we arrive at following scaling invariant for Anderson impurity

model.

$$\frac{1}{V_2^3} - \frac{\rho_0}{4V_0 D} = \frac{1}{V_0^3} - \frac{\rho_0}{4V_0 D_0} \tag{3.42}$$

Solving for V_2 we arrive at the following equation which was obtained by Jefferson[14].

$$V_2 = V_0 \left(1 + \frac{\rho V_0^2}{4D_0}\left(\frac{D_0}{D} - 1\right)\right)^{-1/3} \tag{3.43}$$

As was shown by Jefferson for $U_{fc} = 0$, the hybridization becomes weaker under the scaling flow. The first term on the RHS of equation 3.41 shows that as $D \to 0$, V_2 also decreases. The second term is the contribution of U_{fc}, which is seen to enhance the reduction of V_2 even further. Combined with the fact that $|\epsilon_d| \ll D$ implies a flow to the empty orbital regime (see figure 3.5), we deduce that in presence of U_{fc}, valence fluctuations get enhanced.

II. In the LM regime, i.e $|\epsilon_d| \gg D$, equations 3.37,3.38 lead to a very different relation between V_2 and V_1, namely $V_1 V_2^2 = V_0^3$. Thus in this regime, V_1 and V_2 renormalize in opposite ways. So if V_1 diverges, V_2 vanishes and vice-versa. For $U_{fc} = 0$, we can solve equation 3.37 to get

$$V_2 = V_0 - \frac{\rho_0 V_0^3}{\epsilon_d} \ln \frac{D}{D_0}\,. \tag{3.44}$$

Since $\epsilon_d < 0$, V_2 decreases logarithmically as D decreases. As discussed above, V_1 increases concomitantly. Eventually, $V_2 \to 0$ as $D \to T_K$, and hence V_1 diverges. As is well known, this divergence is inherent in perturbative renormalization, and yields a closed form for the Kondo scale as

$$T_K \simeq D_0 \exp\left(\frac{-|\epsilon_d|}{\rho_0 V_0^2}\right)\,. \tag{3.45}$$

So, for $U_{fc} = 0$, the usual expression for Kondo scale is reproduced[15][30]. For

finite U_{fc}, we obtain the flows through a numerical solution of equations 3.37 and 3.38 in the next subsection.

3.5.3 Numerical solution

We use the usual Euler discretization to solve equations 3.37 and 3.38. Again, we restrict to flows of hybridization close to the Fermi level, so $\epsilon_k = 0$. It is important to note that ϵ_d, which also enters these equations, is also a function of D, but its flow is determined by a second order equation. So, we compute the flow of ϵ_d first keeping $V_1 = V_2 = V_0$ constant, and use this flow to solve for the flow of V_1 and V_2. Another issue is the discretization of the bandwidth. Since the Kondo scale is an exponentially small scale, the $D \to 0$ the regime must be sampled densely, while the non-universal scales can be sampled coarsely. Thus, a highly non-uniform the grid has been used to discretize the conduction band, which gets progressively dense as $D \to 0$.

We fix the initial $V_1 = V_2 = 0.35$, and investigate the effect of varying the initial ϵ_d on the flow of hybridization in the left panel of figure 3.6. For $|\epsilon_d| > D$, the V_1 diverges at a finite scale. As discussed in section 3.5.2, this scale is indeed the Kondo scale, and we will establish this shortly. For $|\epsilon_d| < D$, the hybridization vanishes algebraically, and as we know from section 3.5.1, the impurity orbital energy also vanishes as $D \to 0$, thus implying a flow to the empty orbital regime. It is interesting to note that in the flow to the empty orbital, the hybridization vanishes as $D^{1/2}$, while the divergence in the LM regime is $\sim (D - T_K)^{-2}$ as shown in the right panel of figure 3.6.

We can now investigate the effect of U_{fc} on the Kondo scale in the regime of $|\epsilon_d| > D$. We fix the initial $\epsilon_d = -2.4$, and $D = 0.375$, and find the Kondo scale as a function of several initial V values ranging from 0.35 to 0.55. The results presented in the left panel of figure 3.7 show the Kondo scale (T_K) as a function of $1/V^2$ for

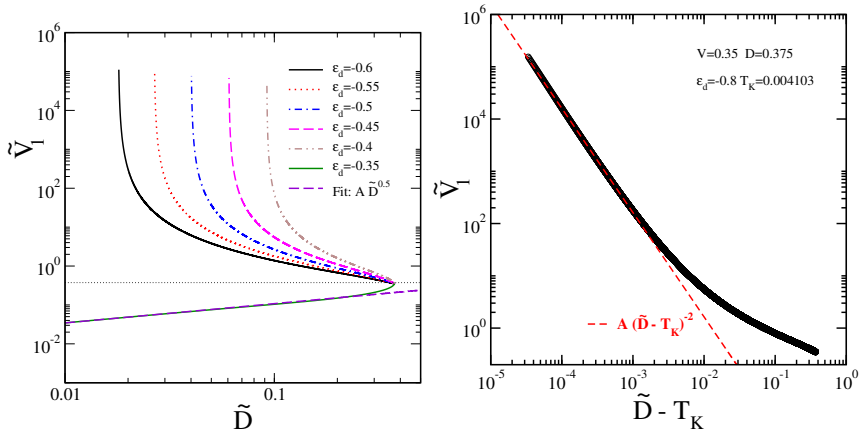

Figure 3.6: Left panel: Scaling flow of V_1 for various values of ϵ_d with an initial value of $V_0 = 0.35$ and the bare bandwidth, $D = 0.375$. Right panel: The divergence of V_1 shown in the left panel is analysed and it is found to be of the form $(D - T_K)^{-2}$.

three U_{fc} values of 0 (black circles), 0.5 (red squares) and 1.0 (triangles). The linear dependence of T_K on $1/V^2$ when plotted on a linear-log scale indicates an exponential dependence, and indeed, the slope correlates with ϵ_d (not shown). Again, the slope being independent of U_{fc} indicates that it does not enter the exponential, but in the prefactor. However, it is clear that the Kondo scale increases with increasing U_{fc}. This is shown in the right panel of figure 3.7, where $T_K - T_{K0}$ (with T_{K0} being the $U_{fc} = 0$ scale) is seen to depend on U_{fc} as a power law, i.e $T_K = T_{K0} + AU_{fc}^{\gamma}$. The exponent γ decreases with increasing V. The U_{fc} driven upward renormalization of the Kondo scale maybe interpreted as a crossover to a weaker coupling regime, and hence increased charge/valence fluctuations.

3.6 Summary

In this chapter, we have investigated the effect of a repulsive interaction between the correlated impurity electrons and the non-interacting conduction electrons in the extended single impurity Anderson model(e-SIAM) through unitary transformations and perturbative renormalization of the model. A Schrieffer-Wolff transformation

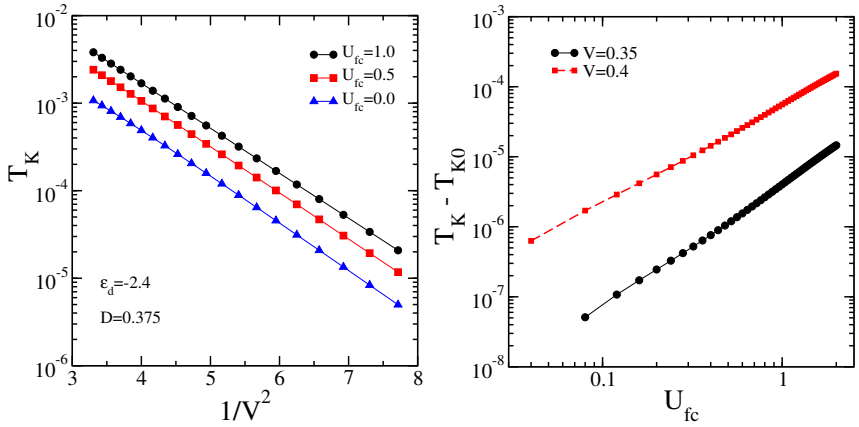

Figure 3.7: Left panel: Kondo scale as a function of $1/V^2$ for three U_{fc} values. Right panel: Kondo scale as a function of U_{fc} for two V values.

of the e-SIAM shows that the strong coupling regime is governed by a spin-charge Kondo model, unlike the Anderson impurity model where spin fluctuations dominate the strong coupling physics. Through perturbative renormalization to second and third order (following Haldane and Jefferson respectively), we found the scaling equations of the model parameters, with a focus on the effect of U_{fc} on the renormalization flows. The scaling invariants of the model were also found. A divergence in the flow of hybridization, signalling the breakdown of perturbative renormalization, can be used to identify a low energy scale, and is shown to be the Kondo scale, through analytical arguments and a numerical solution of the scaling flows. The U_{fc} interaction leads to an increase in the Kondo scale through a renormalization of the prefactor, and hence may be interpreted as leading to enhanced valence fluctuations. Our results are in agreement with NRG studies from Katsnelson's group who have found that enhanced valence fluctuations due to Falicov-Kimball interaction lead to the significant renormalization of the Anderson model parameters and hence of Kondo scale, which was found to increase with increasing U_{fc}. However, earlier NRG studies from Hewson's group have shown that though Kondo scale gets enhanced due to U_{fc}, the physics in the presence of U_{fc} interaction is still described by Anderson impurity model, albeit with renormalized parameters which is not in complete

agreement with our studies. From the numerical solution of the scaling equations of e-SIAM, we find that the system flows to the mixed valent regime. However, based on our perturbative renormalization method we were not able to show conclusively that Kondo fixed point becomes unstable to U_{fc} interaction. In future, we would like to do flow equation renormalization study of e-SIAM to explore the regimes when U_{fc} interaction becomes stronger or comparable to Hubbard repulsion.

Bibliography

[1] Grewe N and Steglich F 1991 *Handbook on the Physics and Chemistry of Rare Earths* vol **14**, ed K A Jr Gschneide and L L Eyring (Amsterdam: Elsevier) p 343.

[2] Wachter P 1994 *Handbook on the Physics and Chemistry of Rare Earths* vol **19**, ed K A Gschneider and L L Eyring (Amsterdam: Elsevier) p 177.

[3] Piers Coleman,*Local Moment Physics in Heavy Electron Systems*(Lectures on the Physics of Highly Correlated Electron Systems VI, Editor F. Mancini, American Institute of Physics, New York (2002), p 79 - 160

[4] K. Miyake and S. Watanabe, J. Phys. Soc. Jpn. **83**, 061006 (2014)

[5] S. Watanabe and K. Miyake, J. Phys : Condens. Matter **24**, 294208 (2012).

[6] J. K. Freericks and V. Zlatić, Rev. Mod. Phys. **75**,1333 (2003).

[7] T. A. Costi and A. C. Hewson, Physica C 185-189,2649-2656 (1991).

[8] A. C. Hewson, A. Oguri and D. C. Meyer, Eur. Phys. J. B **40**, 177189 (2004).

[9] V. Yu. Irkhin and M. I. Katsnelson, JETP Letters, Vol. 80, No.5,pp. 312316(2004).

[10] A. K. Zhuravlev, V. Yu. Irkhin and M. I. Katsnelson, Eur. Phys. J. B **55**,377-382 (2007)

[11] Ryu Takayama and Osamu Sakai, J. Phys. Soc. Jpn, Vol. 66, No. 5, pp. 1512-1525 (1997).

[12] P. W. Anderson, J. Phys. C **3**, 2436 (1970).

[13] F. D. M. Haldane, Phys. Rev. Lett, **40**, 6,416-419 (1978).

[14] J. H. Jefferson, J. Phys. C : Solid State Phys., Vol. 10. 1977. Printed in Great Britain. 1977.

[15] A. C. Hewson *The Kondo Problem to Heavy Fermions*, Cambridge University Press (1997).

[16] J. R. Schrieffer and P. A. Wolff, Phys. Rev. **149**, 2,491-492 (1966).

[17] H. Matsuura and K. Miyake, J. Phys. Soc. Jpn. **81**,113705 (2012).

[18] A. Kiss, J. Otsuki and Y. Kuramoto, J. Phys. Soc. Jpn. **82**,124713 (2013).

[19] P. Mehta and N. Andrei: Phys. Rev. Lett **96** 216802 (2006).

[20] L. Borda, K. Vladar and A. Zawadowski: Phys. Rev. B **75** 125107 (2007).

[21] L. Borda, A. Schiller and A. Zawadowski: Phys. Rev.B **78** 201301 (2008).

[22] J. H. Pixley, Stefan Kirchner, K. Ingersent, Q. Si, Phys. Rev. Lett. **109**, 086403 (2012).

[23] Olga Howczak and Jozef Spałek, J. Phys.: Condens. Matter **24**,205602 (2012).

[24] A. Taraphder and P. Coleman , Phys. Rev. Lett. **66** 2814 (1991).

[25] M. M. Salomaa ,Phys. Rev. B **37**, 9312 (1988).

[26] Rok Žitko and J. Bonča ,Phys. Rev. B **74**, 224411 (2006).

[27] A. H. Nevidomskyy and P. Coleman, Phys. Rev. Lett **103**,147205 (2009).

[28] A. Georges, L. Medici and J. Mravlje, Annu. Rev. Condens. Matter Phys.,**4**, 137-178 (2013).

[29] W. Hofstetter, R. Bulla and D. Vollhardt, Phys. Rev. Lett.**84** 4417 (2000)

[30] M. T. Glossop and D. E. Logan, Journal of Physics: Condensed Matter, **14** 6737 (2002).

Chapter 4

Continuous time Quantum Monte Carlo Study of Extended Periodic Anderson Model

Contents

4.1 Introduction

Heavy fermion systems(HFS) is another class of strongly correlated electron systems(SCES) in which the interactions cause the enhancement of electron mass by a very huge factor of three orders of magnitude. But they also constitute an extreme case where Fermi liquid theory(FLT) theory holds. Heavy fermion systems have competing interactions like Kondo and RKKY interaction. Due to these competing interactions, heavy fermion systems are very close to quantum phase transitions. In fact most of the quantum phase transitions have been studied in these systems only[1–3]. Doniach phase diagram[4] is considered standard phase diagram for heavy fermion systems. But it is based on Kondo lattice model and takes only spin fluctuations into consideration. The conventional theory of quantum criticality in heavy fermions is also based on spin fluctuations only[3]. But there are many systems which exhibit phase transitions which can not be explained on the basis of spin fluctuations alone. Valence/charge fluctuations play a very important role in such systems.

The prototypical example where valence fluctuations lead to phase transition is elemental Cerium in which there is an isostructural phase transition between α and γ phases. In high temperature α phase Cerium is metallic and spin susceptibility is temperature independent(Pauli type). In γ phase which is at low temperature Cerium develops local moments and spin susceptibility becomes temperature dependent(Curie type). This transition has been known for a long time but there is no unanimous microscopic understanding of the transition[5, 6]. Many experimental techniques have been used to investigate this transition and different theoretical models have been put forward to explain this transition. Two very important models are Hubbard-Mott scenario[7] and Kondo Volume Collapse(KVC)[8][9]. In Hubbard-

Mott picture, f electron of Cerium is delocalized in α phase and gets localized as Cerium changes to γ phase. In KVC the hybridization(and hence Kondo effect) between f electron and spd electrons plays an important role. In this picture f electron gets hybridized by spd electrons and leads to Kondo resonance in α phase while as in γ phase there is no quenching of local moments. Recent optical spectroscopy[11] and X-ray emission spectroscopy[12] experiments are in support of KVC picture. But the microscopic mechanism of the valence transitions is still debated. Crystal symmetry[13] and phonons[14][15] are also thought to play a role in this transition. It has also been suggested that valence transition can be Lifshitz transition[16].

Valence fluctuations are also believed to lead to unconventional superconductivity in $CeCu_2Si_2$ [17] and its isoelectronic compound $CeCu_2Ge_2$ [18]. $CeCu_2Si_2$ is the first discovered heavy fermion superconductor, but its superconductivity has remained a puzzle for conventional theory based on spin fluctuations. It shows anomalous behaviour in residual resistivity, Sommerfeld coefficient of resistivity and Kadowaki-Woods ratio [17][19]. In the doped case $CeCu_2(Si_{1-x}Ge_x)_2$ [20][21] the superconducting phase is split into two domes. In addition to a dome closer to anti-ferromagnetic(AF) quantum critical point (QCP), there is another dome which occurs at higher pressure and can not be related to spin fluctuations. There are other heavy fermion compounds with anomalous behaviour which can not be explained by the conventional theory of quantum criticality based on spin fluctuations alone. Many theoretical scenarios like local criticality theory[22][23], the theory of tricritical point[24] and others have been put forward to understand this unconventional quantum criticality. But these theories do not give a comprehensive understanding of the anomalies in these systems. So, an alternative theory based on critical valence fluctuations has been put forward which explains the critical exponents of the temperature dependence of resistivity, specific heat and susceptibility[25][26]. In a recent work[27] role of valence fluctuations in various transport properties in $CeCu_2Si_2$,

was experimentally probed. They have consolidated the role of valence fluctuations in the unconventional superconductivity of $CeCu_2Si_2$. In [28], review of the valence fluctuation theory of unconventional quantum criticality in heavy fermion systems has been presented.

To understand the role of valence fluctuations in heavy fermion systems, Miyake et al[29] have extended the periodic Anderson model by U_{fc} term which is the Hubbard repulsion between localized and itinerant electrons. This extended PAM(e-PAM) has been studied by many analytical and numerical methods. Analytical methods include Slave Boson mean field theory(SBMFT) [29][30], Gutzwiller variational method [31][32], Projection Renormalization group(PRM) [33]. Numerical methods include Density Matrix Renormalization Group(DMRG)[34] and Dynamical mean field theory(DMFT) with exact diagonalization(ED) as an impurity solver[35]. Though all these methods have investigated different aspects of valence fluctuations and have also confirmed that valence fluctuations lead to first order transition. But there is scope for more investigations because none of these methods can explore the full parameter regime of the model. SBMFT taking infinite U limit exclude the double occupancies and hence does not look at the competition between onsite Hubbard interaction U_{ff} and inter-orbital interaction U_{fc} which exists in real materials. Though DMFT takes into consideration the quantum fluctuations but using ED as impurity solver restricts it to small system sizes. Similarly, DMRG has been done only for one-dimensional case which can overestimate the role of valence fluctuations. Gutzwiller variational method is biased towards strong coupling regime while as valence transition takes place in the mixed valent regime. PRM like SBMFT does not consider finite U and being perturbative is being truncated after some order. All the calculations using above methods are at zero temperature which does not allow to see the effect of valence fluctuations in real materials which are at finite temperature. Considering all these limitations of the methods valence

fluctuations need to be investigated by a more powerful method which can explore a broader range of parameter space of the given model. We have chosen continuous time quantum Monte Carlo(CT-QMC) method which has been used within the framework of DMFT. CT-QMC is a very robust method and is a numerically exact method. It has been used to study other quantum phase transitions in spin systems. Though there has been a CT-QMC study of e-PAM[36] but in that study, only Kondo regime was explored, and the focus was on charge ordered phases.

In the previous chapter, we studied the effect of valence fluctuations in a quantum impurity model. In this chapter, we will extend that study and consider a lattice model for heavy fermion systems in which valence fluctuations lead to instabilities as well. We have considered extended PAM(e-PAM) which is the lattice version of extended SIAM which was studied in the previous chapter. Since within dynamical mean field theory (DMFT), e-PAM gets mapped to e-SIAM so the results of the last chapter become important for e-PAM as well. The rest of this chapter is organized in following way. We will give a brief description of algorithm and implementation of embedding CT-HYB quantum impurity solver with our DMFT code. Then we will present the results of our computations and discuss them in view of the questions we have asked in this chapter. Finally, we give the summary of our results.

4.2 Model and methods

Minimal model for heavy fermion systems is periodic Anderson model(PAM). In HFS there are two kinds of fermions called c and f electrons where former are itinerant electrons and latter are localized electrons. Hybridization between these two kinds of electrons leads to Kondo physics.

$$H = \sum_{k\sigma} \epsilon_k c^\dagger_{k\sigma} c_{k\sigma} + \sum_{i\sigma} \epsilon_f f^\dagger_{i\sigma} f_{i\sigma} + V(\sum_{i\sigma} c^\dagger_{i\sigma} f_{i\sigma} + h.c.) + \sum_i U n^f_{i\uparrow} n^f_{i\downarrow} \qquad (4.1)$$

The first term gives the kinetic energy of conduction electrons; second term gives the energy of localized f electrons, the third term is the hybridization terms which is important for Kondo physics and the final term gives the local Hubbard repulsion for the localized electrons. PAM has both Valence as well as Spin fluctuations. But valence fluctuations only lead to "Crossovers" from Kondo regime to Mixed-Valent Regime. So to capture the effects of valence fluctuations in heavy fermion systems, we need to extend this model by a Hubbard repulsion term between c and f electrons. This term is called U_{fc} term.

$$H_{U_{fc}} = U_{fc} \sum_{i\sigma\sigma'} n^c_{i\sigma} n^f_{i\sigma'} \tag{4.2}$$

This interaction term was first introduced in Falicov-Kimball model for valence transitions [37] and is also called Falicov-Kimball interaction. This interaction term was later on used by Miyake[29] for Periodic Anderson Model for valence fluctuations.

4.2.1 DMFT and CT-QMC

In this section, we give the details of the DMFT self-consistency loop which we have used for our calculations. Since we are dealing with a multi-orbital model so what we are using in this chapter is the matrix extension of DMFT equations given in chapter **1** which were for single-orbital Hubbard model. DMFT computations were done for finite temperature, and hence all the quantities are computed over Matsubara frequencies. Greens function for itinerant c electron is

$$G_c = \sum_k \frac{1}{iw + \mu - \epsilon_c - \Sigma_{fc} - \frac{V^2}{iw+\mu-\epsilon_f-\Sigma_{ff}}} \tag{4.3}$$

Greens function for localized f electron is

$$G_f = \sum_k \frac{1}{iw + \mu - \epsilon_f - \Sigma_{ff} - \frac{V^2}{iw+\mu-\epsilon_k-\Sigma_{fc}}} \tag{4.4}$$

where iw are Matsubara frequencies, μ is chemical potential, ϵ_c is the conduction electron energy, ϵ_f is the f orbital energy, Σ_{ff} is the self-energy of f electrons due to local Hubbard interaction, Σ_{fc} is the self-energy due to U_{fc} interaction and V is the hybridization between f and c electrons. We have used hybridization expansion Quantum Monte Carlo , CT-HYB impurity solver from ALPS[38]. To embed the solver with our DMFT code we have used the following algorithm which is slightly different from the standard DMFT self-consistency loop as given in chapter **1** because CT-QMC solver needs hybridization function on Matsubara time and returns self-energies and other quantities also on Matsubara time, and hence we need to take Fourier transform to bring them to Matsubara frequency domain used in DMFT computations.

The algorithm which we followed is given below:

1. Start with non-interacting Lattice Green's functions.
2. Using the Dyson equation get the Host Green's function.
3. Obtain hybridization function from host Green's function.
4. Fourier transform the hybridization function to Matsubara time domain and pass it on to the hybridization expansion ct-QMC solver which returns impurity self-energy and Green's functions on Matsubara time axis.
5. Fourier transform the self-energy obtained from solver to Matsubara frequency domain.
6. Obtain the full lattice Green's function with a new chemical potential obtained from Broyden solver.

7. Take Hilbert transform to obtain the local full Greens function.

8. Go to the next DMFT iteration and run the iterations until convergence is obtained.

In this DMFT algorithm convergence criterion was implemented using Greens function which is smoother function as compared to self-energy. To decrease the noise in data, we switched to Legendre function basis. Since we explored the mixed valent regime of our model, so we had to calculate the chemical potential as well to fix the total occupancy of electrons, n_{tot}. In our computations we have taken $n_{tot} = 1.8$. To fix n_{tot} we used Broyden solver[39] which was also part of the DMFT loop. Broyden solver was used in each DMFT iteration to calculate the chemical potential before hybridization was sent to the solver and after the solver had returned the interacting Greens functions, the chemical potential was again calculated. This increased the runtime of our DMFT computations.

4.3 Results and Discussion

In this section, we discuss the results of our computations. These computations were done using the high performance computing facilities from Louisiana State University[40]. Close to the first order phase transition we faced convergence issues which are known to happen from similar studies of Mott transition in case of Hubbard model. We, however, did capture the signatures of the first order valence transition in our computations.

4.3.1 Effect of U_{fc} on f electron Occupancy

Since valence fluctuations change the occupancy of the f electrons, so we, first of all, computed the effect of U_{fc} on f-level occupancy n_f. As shown in Figure 4.1, n_f decreases with increasing U_{fc}. This happens because, in presence of U_{fc}, f level gets

shifted towards the Fermi level and hence the valence fluctuations get enhanced. We have already seen for the e-SIAM in the previous chapter that in the presence of U_{fc} the impurity energy level ϵ_d gets shifted toward Fermi level. As we kept increasing U_{fc} we found the signatures of the first order valence transition as can be seen from Figure 4.1, for $U_{fc} = 3.0$ and higher, there is an abrupt jump in f electron occupancy. Our results are in agreement with other calculations[25][26][34][28] who have found based on slave boson mean field theory and DMRG computations that U_{fc} enhances valence fluctuations and eventually leads to first order phase transition. Earlier DMFT calculations[35] have also confirmed that U_{fc} leads to abrupt jumps in f level occupancy and eventually leads to first order transition. However, the model parameters that have been used are unrealistically high. They had to take $U_{fc} = 9$ which is very high value in view of that fact that U_{fc} is a weaker interaction as compared to local Hubbard interaction which typically is taken to be $U = 6$ in DMFT calculations. While in our case we see signatures of first order valence transition at $U_{fc} = 3$ which is very reasonable value. Similarly, Hubbard interaction parameter $U = 20$ which has been taken to get consistent results is very unrealistic. We did not face any sign problems which they had faced in their computations. It is known for PAM that as f level is moved closer to Fermi level, due to the valence fluctuations, there is cross-over from Kondo regime to Mixed valent regime. However, there is no valence transition in that model. In the presence of enhanced valence fluctuations due to U_{fc}, cross-over between Kondo and mixed valent regimes happens for lower values of ϵ_f. From Figure 4.1 we can see that for fixed ϵ_f , as we increase U_{fc}, the system moves away from Kondo regime even further.

4.3.2 Effect of U_{fc} on Valence Susceptibility

The dynamical quantity for the valence transition is the valence susceptibility which diverges close to first order phase transition. Valence susceptibility χ_v is defined as:

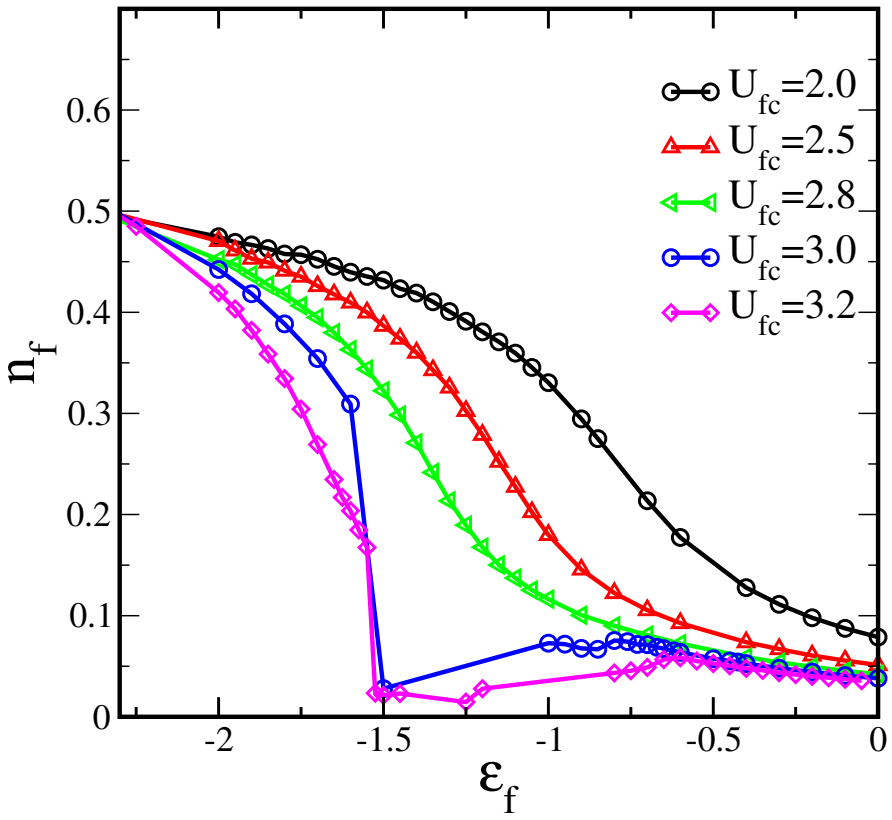

Figure 4.1: f orbital occupancy n_f is plotted versus f orbital energy ϵ_f for increasing values of U_{fc}. Other model parameters for this plot are : $U = 6.0$, $V = 0.77$, $\beta = \frac{1}{T} = 100$.

$\chi_v = -\frac{dn_f}{d\epsilon_f}$. As can been seen from Figure 4.2, as U_{fc} is increased, valence susceptibility also increases and finally jumps abruptly which is the signature of the valence transition. Though a similar behaviour of valence susceptibility has been reported before[35] but the values of U_{fc} were unrealistically high. Critical valence fluctuations leading to diverging valence susceptibility has been found in other studies[17]. It has been shown[41] that resistivity is related to valence susceptibility:

$$\rho_0 = B n_{imp} \left|u(0)\right|^2 \ln \left| \left(\frac{\partial n_f}{\partial \epsilon_f} \right)_\mu / N_f \right| + \rho_0^{unit} \tag{4.5}$$

where the co-efficient B depends on the band structure of host metal,n_{imp} is the concentration of the impurities with $u(q)$ being the scattering potential. N_f is the

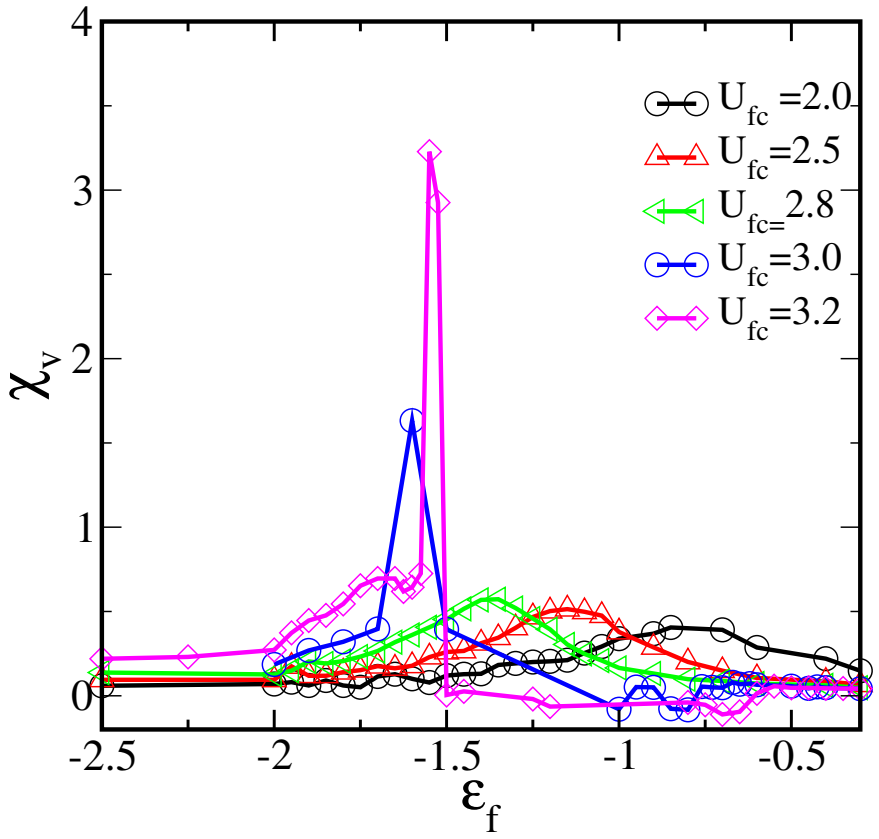

Figure 4.2: Valence susceptibility χ_v is plotted versus f orbital energy ϵ_f for increasing values of U_{fc}. Other model parameters for this plot are : $U = 6.0$, $V = 0.77$, $\beta = \frac{1}{T} = 100$.

density of states at Fermi level and ρ_0^{unit} is the residual resistivity. As can been from the above relation that valence susceptibility contributes to the resistivity and hence the critical valence fluctuations near the valence transition enhance the resistivity by coupling to the impurities or disorder. The enhancement in resistivity is hence directly related to the sharpness of the valence transition.

4.3.3 Enhancement of Quasiparticle Weight

Quasiparticle weight is another important quantity which captures the renormalization effects of interactions and hence is related to self-energy. In Quantum Monte Carlo, quasiparticle weight Z is extracted from the following expression:

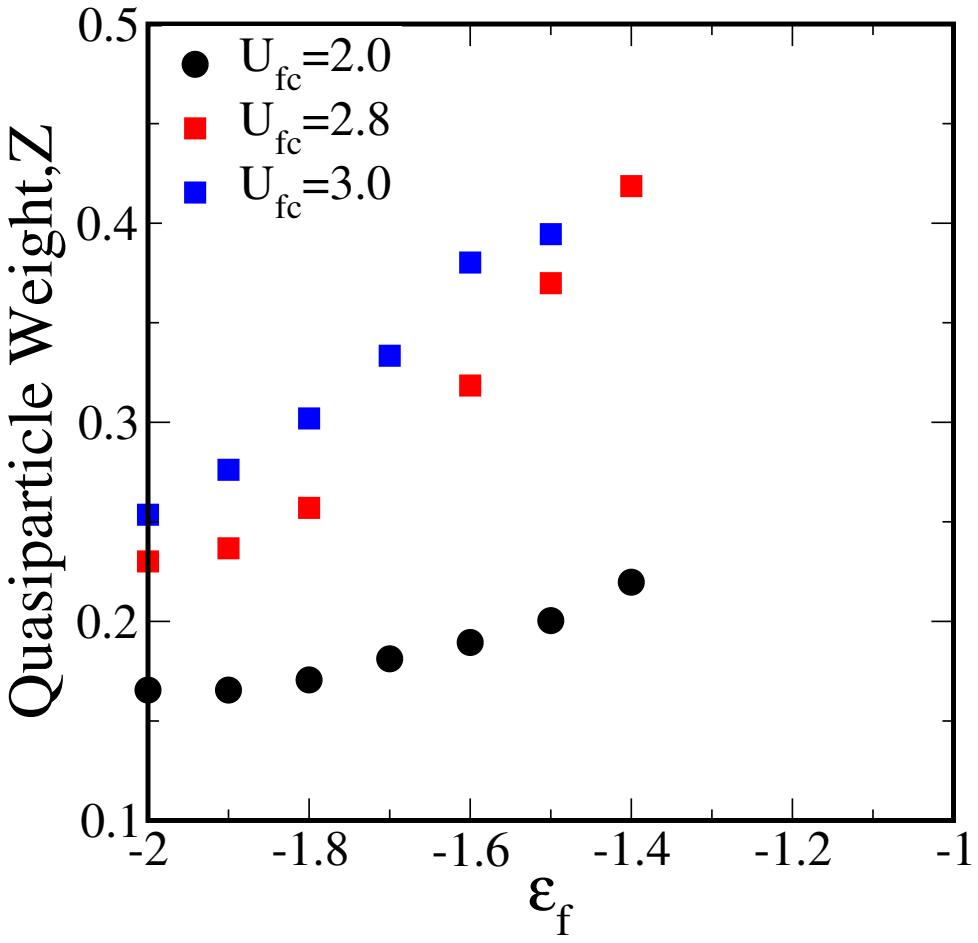

Figure 4.3: Quasiparticle weight of f electrons is plotted versus the f orbital energy ϵ_f for increasing values of U_{fc}. Other parameters are same as Figure 4.1

$Z = \frac{1}{1-\frac{Im\Sigma(i\pi T)}{\pi T}}$ When the local interactions are strong, quasiparticle weight decreases due to the renormalization effects of the interaction. But, as confirmed by other studies[17][19][32], quasiparticle weight increases when valence fluctuations become stronger and hence taking the systems from the correlated regime to a less correlated one. We have also found that quasiparticle weight gets enhanced as we increase U_{fc} as is shown in Figure 4.2. This behaviour can be understood from the fact that in the presence of U_{fc}, local Hubbard interaction U scales downwards and hence gets renormalized to a weaker interaction as shown in the previous chapter. This enhancement in the effective mass(quasiparticle weight) has been used to

explain the anomalies in the Sommerfeld co-efficient[17].

4.4 Conclusion

In this chapter, we have studied the extended Periodic Anderson model(e-PAM) to explore the role of valence fluctuations in heavy fermions systems, in view of recent measurements in which anomalous quantum critical behaviour (exponents) has been found. We have employed dynamical mean field theory within which, e-PAM gets mapped to a multi-orbital Anderson impurity model. For the impurity solver, we have used continuous time Quantum Monte Carlo, which is a state of art method for exploring the finite temperature dynamics of quantum impurity models. Exploring the effect of enhanced valence fluctuations due to U_{fc} we have found that f orbital occupancy n_f decreases and the system moves to the mixed valent regime, and as we increase U_{fc}, there is an abrupt jump in n_f which signals the first order valence transition(FOVT). Near the FOVT, valence susceptibility is supposed to show divergence and that is what we found that as we increase U_{fc} valence susceptibility undergoes abrupt jump above the critical U_{fc}. Our computations have confirmed that even for mild values of U_{fc}, critical valence fluctuations can lead to valence transitions. These critical valence fluctuations lead to the enhancement of the resistivity. Similarly, there is also a huge renormalization of quasiparticle weight due to the critical valence fluctuations which is consistent with our perturbative renormalization studies of extended Anderson impurity model where we have found that valence fluctuations lead to the downward renormalization of local Hubbard repulsion, as the systems moves away from the strong coupling fixed point. The enhancement in quasiparticle weight which we have found explains the renormalization of the Sommerfeld co-efficient due to valence fluctuations. Our studies have confirmed that valence fluctuations can lead to renormalizations of the resistivity and Sommerfeld coefficients and this renormalization has to be different than the

one due to spin fluctuations because as found in this chapter and previous chapter that the U_{fc} drives the system to the mixed valent regime where valence fluctuations are stronger.

Bibliography

[1] P. Gegenwart, Q. Si and F. Steglich, Nature Physics **4**,186-197 (2008).

[2] Q. Si and F. Steglich,Science Vol 329, Issue 5996,pp 1161-1166 (2010).

[3] O. Stockert and F. Steglich, Annu. Rev. Condens. Matter Phys. 2011, 2 : 79-99.

[4] S. Doniach, Physica B **91**, pp 231 (1977).

[5] Grewe N and Steglich F 1991 *Handbook on the Physics and Chemistry of Rare Earths* vol **14**, ed K A Jr Gschneide and L L Eyring (Amsterdam: Elsevier) p 343.

[6] Wachter P 1994 *Handbook on the Physics and Chemistry of Rare Earths* vol **19**, ed K A Gschneider and L L Eyring (Amsterdam: Elsevier) p 177.

[7] B. Johansson, Philos. Mag. **30**, 469 (1974).

[8] J. W. Allen and R. M. Martin, Phys. Rev. Lett.,**49**, 1106 (1982).

[9] J. W. Allen.,Phys. Rev. B **46**, 5047 (1992).

[10] M. Lavagna *et al*, Phys. Lett. A **90**, 210 (1982).

[11] J.W. van der Eb, A.B.Kuzmenko and D. van der Marel, Phys. Rev. Lett.,**86**, 3407 (2001).

[12] M. J. Lipp *et al.*, Phys. Rev. Lett. **109**, 195705 (2012).

[13] A.V.Nikolaev and K.H.Michel, Eur. Phys. J. B **9**, 619 (1999).

[14] Peng Zhang et al, Phys. Rev. B **87**, 121102(R) (2013).

[15] Michael Krisch et al, PNAS **108**, No.23, 9342 (2011).

[16] S.Burdin and C.Lacroix, Phys. Rev. Lett. **110**, 226403 (2013).

[17] A.T. Holmes, D. Jaccard and K. Miyake, Phys. Rev. B**69**,024508 (2004).

[18] D. Jaccard, H. Wilhelm, K. Alami-Yadri and E. Vargoz, Physica B **259-261**,1 (1999).

[19] A. T. Holmes, D. Jaccard and K. Miyake, Journal of the Physical Society of Japan, Vol. 76, No. 5, 051002 (2007).

[20] H. Q. Yuan, F. M. Grosche, M. Deppe,C. Giebel,G. Sparn and F. Steglich Science **302**,2104 (2003).

[21] H. Q. Yuan, F. M. Grosche, M. Deppe,G. Sparn,C. Giebel and F. Steglich, Phys. Rev. Lett. **96**, 047008 (2006).

[22] Q. Si, S. Rabello, K. Ingersent and J. L. Smith, Nature **413**,804 (2001).

[23] P. Coleman, C. Pepin, Q. Si and R. Ramazashvili, J. Phys: Condens. Matter **13**, R723 (2001).

[24] T. Misawa, Y. Yamaji and M. Imada, J. Phys. Soc. Jpn.**78**, 084707 (2009).

[25] S. Watanabe and K. Miyake, Phys. Rev. Lett. **105**, 186403 (2010).

[26] S. Watanabe and K. Miyake, J. Phys : Condens. Matter **24**, 294208 (2012).

[27] G. Seyfarth, A. S. Ruetschi, K. Sengupta, A. Georges, D. Jaccard ,S. Watanabe and K. Miyake, Phys. Rev B **85**, 205105 (2012).

[28] K. Miyake and S. Watanabe, *Philosophical Magazine* (2017).

[29] Y. Onishi and K. Miyake, Physica B **281-282** (2000).

[30] Onishi and Miyake JPSJ, **69**, No. 12 (2000).

[31] I. Hagymasi, K. Itai and J. Solyom, Acta Phys. Pol. A **121**, 1070 (2012)

[32] Katsunori Kubo, J.Phys.Soc.Jpn **80** (2011) 114711.

[33] V. Phan, A. Mai and K. Becker, Phys. Rev.B **82** 045101 (2010).

[34] S. Watanabe, M.Imada and K. Miyake, J. Phys. Soc. Jpn.**75**,043710 (2006).

[35] Y. Saiga, T. Sugibayashi and D. S. Hirashima, J. Phys. Soc. Jpn., **77**,114710 (2008).

[36] T. Yoshida and N. Kawakami, Phys. Rev. B **85** 235148 (2012).

[37] J. K. Freericks and V. Zlatić, Rev. Mod. Phys. **75** 1333(2003).

[38] E. Gull, A. Millis, A. Lichtenstein, A. Rubtsov, M. Troyer, and P. Werner, Rev. Mod. Phys. **83**, 349 (2011).

[39] We used the Broyden solver from Scipy.

[40] This has been done in collaboration with Professor Mark Jarrell from Department of Physics and Astronomy, Louisiana State University, USA.

[41] K. Miyake and H. Maebashi, J. Phys. Soc. Jpn. **71**, 1007 (2002).

[42] T. A. Costi and A. C. Hewson, Physica C 185-189 (1991).

[43] A. K. Zhuravlev *et al.*, Eur. Phys. J. B **55**, 377382 (2007).

Chapter 5

Z_2 Topological Order and Algebra of Majorana doubling in Kitaev chain Model

Contents

5.1 Introduction

Landau's symmetry breaking theory has been the paradigm for the classification of phases in condensed matter physics. Magnetic and superconducting orders are the prime examples which have been understood within this paradigm. However, the discovery of the quantum Hall effect gave rise to a counter example for symmetry breaking order. In this case, there is no symmetry breaking involved, and the classification is based on topology rather than on symmetry. The discovery of topological insulators[1, 2]has added more examples to the list for topological order, although in the latter case the order is not same as that of the quantum Hall fluid. Topological order in topological insulators and superconductors is called Z_2 topological order because it is associated with a Z_2 topological invariant. Discovery of topological insulators and superconductors has boosted the research in topological order. And more importantly, many model Hamiltonians have been shown to exhibit topological order. What is very interesting about these Hamiltonians is that they are quadratic, and hence can be analytically solved. Based on K-theory and Clifford algebras, by now there is a full classification for the topological order that arises in these Hamiltonians in various dimensions[3]. This classification came as the real breakthrough in understanding topological properties of matter. Nevertheless, the difficult task of taking interactions into considerations is going to take a lot more work.

In this Chapter, we will consider a Kitaev chain Hamiltonian[4] which, though simple and quadratic, has a topological phase in which there are Majorana modes at the edges of the chain. Kitaev employed a Majorana fermion representation to diagonalize the Hamiltonian and showed that there are Majorana edge modes. The Kitaev model is not an entirely new model. It can be obtained from the transverse field Ising model(TFIM) using a Jordan-Wigner transformation. So what Kitaev

did is that he took fermions as degrees of freedom instead of spins. This novel point of view opened up the way to understand the topological order in a well-known system. TFIM exhibits only Landau order, and the ordered phase arises due to the symmetry breaking of the model. The immediate question which comes to mind is how is Landau order in TFIM related to the topological order, or how does topological order arise in the Kitaev Chain when one maps to a fermionic representation. One important aspect of Kitaev's work is that he considered fermions as degrees of freedom, rather than spins in the TFIM model. But the question is how does the transformation from spin to fermionic representation give rise to topological order? This question has been asked in a recent work[5]. There it is concluded that spectral properties of the two models are same, which we will find below is not correct. Using duality, this question has been addressed by [6]. They find that in topological order one gets a non-local order parameter. So one tries to understand topological order from the symmetry point of view and tries to find out whether there are different kinds of symmetry breaking involved in the topological order. In [7] Fendley has come up with an algebraic approach for topological order in a Majorana chain and more generally for a parafermion chain. He identifies an operator which is a Majorana mode operator and its presence leads to topological order. This approach is close to our approach, and below we will show how we have also found an operator which satisfies the same algebra as that of the Fendley operator. We will show in this chapter that on the fermionic side, the algebra is larger and hence there are more symmetries and hence more conserved quantities which are non-local as compared to the spin model. We will show that in the Kitaev chain model there is an additional element in the algebra which had not been taken into consideration by Kitaev. That operator leads to topological degeneracy and edge modes. Hence we answer the question why there is topological order in Kitaev chain and not in its spin equivalent. The strength of our approach is that it can

be generalized to parafermion chains as well. Our construction holds good for the interacting case also.

The rest of this chapter is organized as follows: First, we briefly discuss the Kitaev chain model, its symmetries, and topological order. Then in the next section, we show how the algebra of Majorana fermions is conceptually incomplete, and we present the full Clifford algebra. In Section 4 we compare our results with Fendley's results and show that the operator which we introduce to complete the algebra of Majorana fermions satisfies the same algebra as that of the Majorana edge mode operator of Fendley. Then we briefly show how our construction can be generalized to parafermions as well. In the next section, we discuss the connection between topological order and the Yang-Baxter equation. In the final section, we summarize our results and conclusions.

5.2 Kitaev p-wave chain model

To study the relation between Landau order and topological order, we introduce two Hamiltonians which are related to each other by Jordan-Wigner transformation. Two models are transverse field Ising model(TFIM) and Kitaev p-wave chain model. Following Kitaev we will diagonalize Kiatev chain model using Majorana fermion representation and that way we will show that in its topological phase, Kitaev chain model has Majorana edge mode and also topological degeneracy. We will look closely at the algebra of Majorana fermions and how they are different from the standard(Dirac)fermions.

The Hamiltonian for the transverse field Ising model is:

$$H = -J \sum_{i=1}^{N-1} \sigma_i^x \sigma_{i+1}^x - h_z \sum_{i=1}^{N} \sigma_i^z \tag{5.1}$$

Where J is the ferromagnetic exchange constant and h_z is the Zeeman field in the Z direction. This model has Z_2 symmetry, due to which the global symmetry operator commutes with the Hamiltonian.

$$\left[\prod_i \sigma_i^z, H\right] = 0 \tag{5.2}$$

The global symmetry operator flips all the spins. There is a doubly degenerate ground state. This model exhibits two phases which can be understood on the basis of Landau's symmetry breaking theory. There is a ferromagnetically ordered phase which arises when the symmetry of the model is broken.There is a disordered phase in which symmetry is intact. We will now apply the Jordan-Wigner transformation to this model to map it to a fermionic model which will turn out to be the Kitaev chain model. The Jordan-Wigner transform maps the spin operators into Fermionic ones:

$$c_i = \sigma_i^\dagger \left(\prod_{j=1}^{i-1} \sigma_i^z\right) \quad c_i^\dagger = \sigma_i^- \left(\prod_{j=1}^{i-1} \sigma_i^z\right) \tag{5.3}$$

$$H = -t \sum_{i=0}^{N-1} (c_i^\dagger c_{i+1} + h.c.) + \triangle \sum_{i=0}^{N-1} c_i^\dagger c_{i+1}^\dagger + h.c. - \mu \sum_{i=0}^{N} c_i^\dagger c_i$$

where t, Δ, μ are hopping strength,superconducting order parameter and chemical potential respectively. Kitaev employed a Majorana fermion representation to diagonalize this Hamiltonian.

$$c_i = \frac{\gamma_{1,i} - i\gamma_{2,i}}{\sqrt{2}} \quad c_i^\dagger = \frac{\gamma_{1,i} + i\gamma_{2,i}}{\sqrt{2}} \tag{5.4}$$

In the Majorana representation the Hamiltonian gets transformed to:

$$H = it\sum_{i=0}^{N-1}(\gamma_{1,i}\gamma_{2,i+1} - \gamma_{2,i}\gamma_{1,i+1}) + i\Delta\sum_{i=0}^{N-1}(\gamma_{1,i}\gamma_{2,i+1} + \gamma_{2,i}\gamma_{1,i+1})$$
$$- \mu\sum_{i=0}^{N}(\frac{1}{2} - i\gamma_{1,i}\gamma_{2,i}) \tag{5.5}$$

The Hamiltonian has trivial phase and topological phase. Trivial phase is obtained for the choice of parameters: $t = \Delta = 0$. In this case two Majorana fermions at each site couple together to form a complex fermion, and there is no topological phase as there are no Majorana edge modes. Choosing $\mu = 0$ and $t = \Delta$ the Hamiltonian becomes.

$$H = 2it\sum_{i=0}^{N-1}\gamma_{1,i}\gamma_{2,i+1} \tag{5.6}$$

We can define a complex fermion:

$$a_i = \frac{\gamma_{2,i+1} - i\gamma_{1,i}}{\sqrt{2}} \tag{5.7}$$

The Hamiltonian becomes:

$$H = \left(t\sum_{i=0}^{N-1}a_i^{\dagger}a_i - \frac{1}{2}\right) \tag{5.8}$$

We can see that ground state of this Hamiltonian has no a-fermions. But there is more to the story because there are two Majorana fermions which have not been included in the Hamiltonian. Taking them together we can form another fermion which is non-local, residing at the two ends of the chain.

$$a_0 = \frac{\gamma_{1,N} - i\gamma_{2,0}}{\sqrt{2}} \tag{5.9}$$

So there is boundary term H_b corresponding to two Majorana edge modes. The presence of boundary term due to the bulk topology is another feature of topological order in which there is a bulk-boundary correspondence.

$$H_b = \epsilon_0 a_0^\dagger a_0 \quad \epsilon_0 = 0 \tag{5.10}$$

With this boundary term included in the Hamiltonian, we can see that it has a doubly degenerate ground state depending on presence or absence of the edge mode. It is this edge mode which is the feature of the topological phase of Kitaev chain and is related to the topological invariant of the bulk spectrum. The two ground states can be distinguished by a parity operator. They have even and odd parity respectively. $\mid 0\rangle$ has no a_0 fermion and hence an even number of fermions while as $\mid 1\rangle$ has one a_0 fermion and hence odd parity. So the presence of an edge mode gives rise to double degeneracy. This degeneracy is an example of topological degeneracy because it is protected by a topological invariant. Since the topological invariant comes from a particle-hole symmetry which is a discrete symmetry, such topological order has been called *symmetry protected topological order*.

5.2.1 Majorana fermions versus complex fermions

Majorana fermions can be taken algebraically as building blocks of (standard) Dirac fermions. The algebra of Majorana fermions makes them very different from the Dirac fermions. Dirac Fermions obey the Grassmann algebra:

$$\{c_i, c_i^\dagger\} = \delta_{ij} \quad c_i^2 = (c_i^\dagger)^2 = 0 \quad N = c^\dagger c \quad N^2 = N \tag{5.11}$$

where $c^\dagger$,c and N are creation, annihilation and number operator for a fermion.

$$| 1\rangle = c^\dagger | 0\rangle \quad | 0\rangle = c | 1\rangle \tag{5.12}$$

$$c | 0\rangle = c^\dagger | 1\rangle = 0 \tag{5.13}$$

Fermions have a vacuum state. Creation and annihilation operators are used to construct the states of fermions. Fermions have $U(1)$ symmetry, and hence the number of fermions is conserved, and occupation number is a well-defined quantum number. The number of fermions in a state is given by the eigenvalue of the number operator. Here the number operator is idempotent, and hence there are only two eigenvalues: $0, 1$. Also, different fermion operators anti-commute with each other and hence obey Fermi-Dirac statistics.

Majoranas are very different because they are self-hermitian and hence creation and annihilation operators are the same, which means that a Majorana fermion is its own anti-particle. A fermionic vacuum can not be defined for Majorana fermions because there is no well-defined number operator, or in other words, the number of Majorana fermions is not a well-defined quantity, and hence not a quantum number which can be used to label Majorana fermions. Majorana fermions don't have $U(1)$ symmetry, and hence a number operator can not be defined for them. However, they have Z_2 symmetry; parity is conserved for Majorana fermions. Majorana fermions also anti-commute among each other. However, Majorana fermions generate non-abelian braid statistics. They generate a braid group representation [16][17][18].

When taken abstractly Majorana fermions appear to be very unrealistic particles, but physically they can appear as Bogoliubov quasiparticles which exist as zero modes in topological superconductors. They are zero energy solutions of the BdG equation and are different from Majorana spinors which are solutions of the Dirac equation.

For a general choice of parameters, one finds that the Hamiltonian is an antisym-

metric matrix and hence has doubled spectrum. For every energy state, there is another degenerate eigenstate. So one can say that the presence of particle-hole symmetry turns a Hermitian matrix into a real anti-symmetric matrix which has doubled spectrum. The number of Majorana modes is a topological invariant called the Z_2 invariant, and is given by a Pfaffian of the Hamiltonian.

5.3 Algebra of Majorana doubling

In this section, we will revisit the algebra of Majorana fermions and see that in the way it is usually presented some of the significant higher order products are not used. In the Kitaev paper, the algebra of Majorana fermions is written as

$$\{a_i, a_j\} = 2\delta_{ij} \tag{5.14}$$

This equation defines the Clifford algebra of Majorana fermions. The full algebra is generated by all the ordered products of these operators. For the case of three Majorana fermions the full Clifford algebra is described below:

$$\{1, \gamma_1 = a_1, \gamma_2 = a_2, \gamma_3 = a_3, \gamma_{12} = a_1a_2, \gamma_{23} = a_2a_3, \gamma_{31} = a_3a_1, \gamma_{123} = a_1a_2a_3\} \tag{5.15}$$

The Clifford algebra of three Majorana fermions is 8 dimensional, with these eight independent generators. There are three bivectors γ_{12},γ_{23},γ_{31} and one tri-vector(also called pseudoscalar) γ_{123}. Bivectors are related to rotations and trivector will turn out to be very important for our discussion on topological order because it is a chirality operator which distinguishes between even and odd parity. We refer to [9] for more discussion on the role of chirality operator and Z_2 grading of Clifford algebra.

We ask whether there is a way to understand how topological order arises in the

Kitaev chain model as we do an algebraic transformation from TFIM. During this transformation, the degrees of freedom or the quasiparticles also get transformed. To answer this question, we revisit the algebra of Kitaev chain.

In [8] Lee and Wilczek gave an illuminating analysis of doubled spectrum of the Kitaev chain model. They showed that the algebra which has been considered for the Kitaev chain model is conceptually incomplete. Using the case of three Majorana fermions which are at the edges of superconducting wires, it is shown that the Hamiltonian of these Majorana fermions has more algebraic structure than anticipated. The difference lies in another Majorana operator which was missed in the Kitaev paper. This Majorana operator has been called *Emergent Majorana* for the reason that it obeys all the properties of a Majorana fermion. We briefly review their analysis here and later on generalize it. Let b_1,b_2 and b_3 are three Majorana fermions which can occur at the ends of three wires. They obey Clifford algebra:

$$\{b_j, b_k\} = 2\delta_{jk} \tag{5.16}$$

We can write down a Hamiltonian for these interacting Majorana fermions coming from three different wires.

$$H_m = -i(\alpha b_1 b_2 + \beta b_2 b_3 + \gamma b_3 b_1) \tag{5.17}$$

Now it is known that Majorana bilinears generate a spin algebra so one would naively think that it is a spin Hamiltonian. But the spin Hamiltonian neither has edge modes nor any topological degeneracy. To understand this one needs to realize that the Clifford algebra generated by Majorana fermions is larger than what is present in equation 5.14. There are other generators of the algebra. Physically the full implications of the parity operator need to be taken into consideration to conceptually complete the algebra. There is a special operator Γ in the algebra

which we call as *Emergent Majorana* because it has all the properties of a Majorana fermion.

$$\Gamma \equiv -ib_1 b_2 b_3 \tag{5.18}$$

$$\Gamma^2 = 1 \quad [\Gamma, b_j] = 0 \quad [\Gamma, H_m] = 0 \quad \{\Gamma, P\} = 0 \tag{5.19}$$

The emergent Majorana operator commutes with the Hamiltonian, and hence there is an additional symmetry present, as it anti-commutes with the parity operator and hence it shifts among the parity states. Both the P and Γ operators commute with Hamiltonian but anti-commute with each other due to which there is doubling of the spectrum. The presence of this extra symmetry leads to the doubled spectrum. This doubling is different from Kramer's doubling[10] because no time reversal symmetry is needed. In the basis in which P is diagonal with ± 1 eigenvalues, the Γ operator takes the states into degenerate eigenstates with eigenvalues ∓ 1.

The doubled spectrum of the Kitaev chain Hamiltonian comes from this algebraic structure which leads to extra symmetries. This algebraic structure is non-perturbative, and hence is robust to perturbations as long as they preserve the discrete symmetry. This algebraic structure survives the interactions also, though there can be dressing of the Majorana operators. So these properties are present in the Kitaev chain with interactions well. Γ operator can be defined for the interacting chain as well.

5.4 Topological order and Γ operator

What we have already found is that the complete algebra of Majorana fermions has extra operators which has been called as emergent Majorana fermions and represented by Γ operators. Emergent Majorana fermions have all the properties of the Majorana mode operators, and in fact, they are more robust to the effects of the environment. That is why it has been proposed to use them for quantum computing[11].

Due to the robustness of emergent Majorana fermions, they have been the focus of research recently [12][13][14][15] where their robustness to the environment and interactions has been studied in detail. Interesting things about emergent Majorana fermions is that they survive interactions as well while as Majorana fermions exist as zero modes of the mean-field(quadratic) Hamiltonians [12][13]. So it is clear that emergent Majorana fermions have something to do with topological order and in this section, we are going to make that connection explicit and rigorous. Though topological order has different definitions, we will use the definition as given in [7]. The presence of edge modes is a very important signature of topological order. First, we give a definition of fermionic zero mode, and then we will show how that is related to Emergent Majorana fermions or the Gamma operator. A fermionic zero mode is an operator Γ such that

- Commutes with Hamiltonian:$[H, \Gamma] = 0$
- anti-commutes with parity:$\{P, \Gamma\} = 0$
- has finite "normalization" even in the $L \to \infty$ limit:$\Gamma^\dagger \Gamma = 1$.

Now we can easily see that the first two properties are the defining properties of the Γ operator and hence are satisfied. Γ, like a Majorana operator, squares to unity and so is always normalized. So our Γ operator satisfies all the properties of the zero edge mode. We will reformulate the conditions in terms of the emergent Majoranas.

A system is said to be topologically ordered if there exists a zero mode which is given by an operator Γ *which is an emergent Majorana fermion and satisfies the above properties.* Therefore topological order is not just the presence of Majorana edge modes, rather it is the presence of emergent Majorana fermion that leads to the topological order in Kitaev chain model.

There are a few things that need to be understood here. Though there is a duality mapping between the spin model and the Fermion model, the algebra and hence the

symmetries and observables are not same. On the fermionic side, there is larger algebra in which there are extra operators which give rise to topological order while as there are spin analogues of these operators.The Jordan-Wigner transformation takes local observables to non-local observables, but it cannot give rise to a new algebra or the gamma operator. The Duality mapping can not find topological order because all it does is map observables on one side to other observables on another side.

5.5 Topological order and Yang-Baxter equation

Majorana fermions have been the focus of interest in research in topological quantum computation because as shown in [16] [18] that Majorana fermions have non-abelian braid statistics and generate representation of braid group. Kitaev chain realization of Majorana fermions have given ways to engineer Majorana fermions and there has already been some progress on that front[19]. It has also been realized[20] that the Majorana representation of braid group is different than the ones known in the literature. This representation has been called a type-II representation. Now the question which has been asked is that is the topological order which arises from quantum entanglement also related to topological entanglement which arises from the solutions of Yang-Baxter equation. Majorana fermions give new solutions to Yang-Baxter equations and hence the new type of topological entanglement. When there is topological order, we get a representation of braid group and also solutions to YBE.

Braiding operators arise from a row of Majorana Fermions $\{\gamma_1, \cdots \gamma_n\}$ as follows: Let

$$\sigma_i = (1/\sqrt{2})(1 + \gamma_{i+1}\gamma_i).$$

Note that if we define

$$\lambda_k = \gamma_{i+1}\gamma_i$$

for $i = 1, \cdots n$ with $\gamma_{n+1} = \gamma_1$, then

$$\lambda_i^2 = -1$$

and

$$\lambda_i\lambda_j + \lambda_j\lambda_i = 0$$

where $i \neq j$. From this it is easy to see that

$$\sigma_i\sigma_{i+1}\sigma_i = \sigma_{i+1}\sigma_i\sigma_{i+1}$$

for all i and that $\sigma_i\sigma_j = \sigma_j\sigma_i$ when $|i-j| > 2$. Thus we have constructed a representation of the Artin braid group from a row of Majorana fermions. This construction is due to Ivanov [18] and he notes that

$$\sigma_i = e^{(\pi/4)\gamma_{i+1}\gamma_i}.$$

In [20] authors make the further observation that if we define

$$\breve{R}_i(\theta) = e^{\theta\gamma_{i+1}\gamma_i},$$

Then $\breve{R}_i(\theta)$ satisfies the full Yang-Baxter equation with rapidity parameter θ. That is, we have the equation

$$\breve{R}_i(\theta_1)\breve{R}_{i+1}(\theta_2)\breve{R}_i(\theta_3) = \breve{R}_{i+1}(\theta_3)\breve{R}_i(\theta_2)\breve{R}_{i+1}(\theta_1).$$

This makes if very clear that $\breve{R}_i(\theta)$ has physical significance, and suggests examining

the physical process for a temporal evolution of the unitary operator $\breve{R}_i(\theta)$.
In fact, following [20], we can construct a Kitaev chain based on the solution $\breve{R}_i(\theta)$ of the Yang-Baxter Equation. Let a unitary evolution be governed by $\breve{R}_i(\theta)$. When θ in the unitary operator $\breve{R}_i(\theta)$ is time-dependent, we define a state $|\psi(t)\rangle$ by $|\psi(t)\rangle = \breve{R}_i|\psi(0)\rangle$. With the Schrödinger equation $i\hbar\frac{\partial}{\partial t}|\psi(t)\rangle = \hat{H}(t)|\psi(t)\rangle$ one obtains:

$$i\hbar\tfrac{\partial}{\partial t}[\breve{R}_i|\psi(0)\rangle] = \hat{H}(t)\breve{R}_i|\psi(0)\rangle. \tag{5.20}$$

Then the Hamiltonian $\hat{H}_i(t)$ related to the unitary operator $\breve{R}_i(\theta)$ is obtained by the formula:

$$\hat{H}_i(t) = \mathrm{i}\hbar\tfrac{\partial \breve{R}_i}{\partial t}\breve{R}_i^{-1}. \tag{5.21}$$

Substituting $\breve{R}_i(\theta) = \exp(\theta\gamma_{i+1}\gamma_i)$ into equation (5.21), we have:

$$\hat{H}_i(t) = \mathrm{i}\hbar\dot{\theta}\gamma_{i+1}\gamma_i. \tag{5.22}$$

This Hamiltonian describes the interaction between i-th and $(i+1)$-th sites via the parameter $\dot{\theta}$. When $\theta = n \times \frac{\pi}{4}$, the unitary evolution corresponds to the braiding progress of two nearest Majorana fermion sites in the system as we have described it above. Here n is an integer and signifies the time of the braiding operation. We remark that it is interesting to examine this periodicity of the appearance of the topological phase in the time evolution of this Hamiltonian. For applications, one may consider processes that let the Hamiltonian take the the system right to one of these topological points and then this Hamiltonian cuts off. One may also think of a mode of observation that is tuned in frequency with the appearances of the topological phase.

In [20] authors also point out that if we only consider the nearest-neighbour interactions between Majorana Fermions, and extend equation (5.22) to an inhomo-

geneous chain with $2N$ sites, the derived model is expressed as:

$$\hat{H} = \mathrm{i}\hbar \sum_{k=1}^{N} (\dot{\theta}_1 \gamma_{2k}\gamma_{2k-1} + \dot{\theta}_2 \gamma_{2k+1}\gamma_{2k}), \tag{5.23}$$

with $\dot{\theta}_1$ and $\dot{\theta}_2$ describing odd-even and even-odd pairs, respectively.

They then analyze the above chain model in two cases:

1. $\dot{\theta}_1 > 0$, $\dot{\theta}_2 = 0$.

   In this case, the Hamiltonian is:

   $$\hat{H}_1 = \mathrm{i}\hbar \sum_{k}^{N} \dot{\theta}_1 \gamma_{2k}\gamma_{2k-1}. \tag{5.24}$$

   The Majorana operators γ_{2k-1} and γ_{2k} come from the same ordinary fermion site k, $\mathrm{i}\gamma_{2k}\gamma_{2k-1} = 2a_k^\dagger a_k - 1$ ($a_k^\dagger$ and a_k are spinless ordinary fermion operators). $\hat{H}_1$ simply means the total occupancy of ordinary fermions in the chain and has U(1) symmetry, $a_j \to e^{i\phi} a_j$. Specifically, when $\theta_1(t) = \frac{\pi}{4}$, the unitary evolution $e^{\theta_1 \gamma_{2k}\gamma_{2k-1}}$ corresponds to the braiding operation of two Majorana sites from the same k-th ordinary fermion site. The ground state represents the ordinary fermion occupation number 0. In comparison to 1D Kitaev model, this Hamiltonian corresponds to the trivial case of Kitaev's. This Hamiltonian is described by the intersecting lines above the dashed line, where the intersecting lines correspond to interactions. The unitary evolution of the system $e^{-i\int \hat{H}_1 dt}$ stands for the exchange process of odd-even Majorana sites.

2. $\dot{\theta}_1 = 0$, $\dot{\theta}_2 > 0$.

In this case, the Hamiltonian is:

$$\hat{H}_2 = \mathrm{i}\hbar \sum_{k}^{N} \dot{\theta}_2 \gamma_{2k+1}\gamma_{2k}. \tag{5.25}$$

This Hamiltonian corresponds to the topological phase of 1D Kitaev model and has $\mathbb{Z}_2$ symmetry, $a_j \to -a_j$. Here the operators γ_1 and γ_{2N} are absent in $\hat{H}_2$. The Hamiltonian has two degenerate ground state, $|0\rangle$ and $|1\rangle = d^\dagger|0\rangle$, $d^\dagger = e^{-i\varphi/2}(\gamma_1 - i\gamma_{2N})/2$. This mode is the so-called Majorana mode in 1D Kitaev chain model. When $\theta_2(t) = \frac{\pi}{4}$, the unitary evolution $e^{\theta_2\gamma_{2k+1}\gamma_{2k}}$ corresponds to the braiding operation of two Majorana sites γ_{2k} and γ_{2k+1} from k-th and $(k+1)$-th ordinary fermion sites, respectively.

Thus the Hamiltonian derived from $\breve{R}_i(\theta(t))$ corresponding to the braiding of nearest Majorana fermion sites is exactly the same as the $1D$ wire proposed by Kitaev, and $\dot{\theta}_1 = \dot{\theta}_2$ corresponds to the phase transition point in the "superconducting" chain. By choosing different time-dependent parameter θ_1 and θ_2, one finds that the Hamiltonian $\hat{H}$ corresponds to different phases. These observations of Mo-Lin Ge give physical substance and significance to the Majorana Fermion braiding operators discovered by Ivanov [18], putting them into a robust context of Hamiltonian evolution via the simple Yang-Baxterization $\breve{R}_i(\theta) = e^{\theta\gamma_{i+1}\gamma_i}$. Yu and Mo-lin Ge[20] make another observation, that we wish to point out. In [21], Kauffman and Lomonaco observe that the Bell Basis Change Matrix in the quantum information context is a solution to the Yang-Baxter equation. Remarkably this solution can be seen as a 4×4 matrix representation for the operator $\breve{R}_i(\theta)$.

This lets one can ask whether there is relation between topological order and quantum entanglement and braiding [21] which is the case for the Kitaev chain where non-local Majorana modes are entangled and also braiding.

The Bell-Basis Matrix B_{II} is given as follows:

$$B_{II} = \frac{1}{\sqrt{2}} \begin{bmatrix} 1 & 0 & 0 & 1 \\ 0 & 1 & 1 & 0 \\ 0 & -1 & 1 & 0 \\ -1 & 0 & 0 & 1 \end{bmatrix} = \frac{1}{\sqrt{2}}\big(I + M\big) \quad \big(M^2 = -1\big) \tag{5.26}$$

and

$$M_i M_{i\pm 1} = -M_{i\pm 1} M_i, \quad M^2 = -I, \tag{5.27}$$

$$M_i M_j = M_j M_{i,} \quad \big|i - j\big| \geq 2. \tag{5.28}$$

Remarks. The operators M_i take the place here of the products of Majorana Fermions $\gamma_{i+1}\gamma_i$ in the Ivanov picture of braid group representation in the form

$$\sigma_i = (1/\sqrt{2})(1 + \gamma_{i+1}\gamma_i).$$

This observation of authors in [20] gives a concrete interpretation of these braiding operators and relates them to a Hamiltonian for the physical system. This goes beyond the work of Ivanov, who examines the representation on Majoranas obtained by conjugating by these operators. The Ivanov representation is of order two, while this representation is of order eight. The reader may wish to compare this remark with the contents of [22] where we associate Majorana fermions with elementary periodic processes. These processes can be regarded as prior to the periodic process associated with the Hamiltonian of Yu and Mo-Lin Ge[20].

5.5.1 Topological order and topological entanglement

To understand the relation between quantum entanglement in Kitaev chain and the corresponding topological entanglement which manifests as braid group representation,we point out that *it is only in the topological phase of the Kitaev chain braid group representation arises while as in topologically trivial phase there are no Majorana edge modes and hence no braid representation.* To see this relation mathematically, we rewrite the Kitaev chain Hamiltonian corresponding to topological phase.

$$H = 2it \sum_{i=0}^{N-1} \gamma_{1,i+1}\gamma_{2,i} \tag{5.29}$$

and now find out that for Majorana representation as shown by Ivanov we need the operator of the form $1 + \gamma_{i+1}\gamma_i$ which arises only in topological phase. So this brings out the relation between topological order and the topological entanglement(braiding).

Using this relation we give a new characterization of topological order. *A system is said to be topological ordered if it also gives a solution to Yang-Baxter equation.* This is true both for Kitaev chain and its parafermion generalization. In both cases, there are edge modes which give a solution to Yang-Baxter equation.

5.6 Conclusion

In this chapter, we answer the question of how topological order and Landau order are related in the context of Kitaev p-wave chain. We show that on the fermionic side there are extra symmetries and particularly we identify γ operator which is needed to have topological order. The same gamma operator was shown to lead to doubled spectrum for the Kitaev chain Hamiltonian. It is interesting to note that the γ operator which we have used to define topological order has same algebraic properties

as Ψ operator which Fendley has defined. Our construction can be easily generalized to parafermion case as well. We have also shown how non-locality of Majorana fermions(quantum entangelemt) is related to topological entangelent which arises for the solutions of Yang-Baxter equation. Since understanding topological order is very important not only for the topological quantum computation rather is is also very important within condensed matter physics where more and more systems are being discovered which exhibit topological order. In that direction, our work is very important because it clearly shows how topological order occurs when there are more symmetries and larger algebra.

Bibliography

[1] M. Z. Hasan and C. L. Kane, Rev. Mod. Phys. **82**, 3045 (2010).

[2] Xiao-Liang Qi and Shou-Cheng Zhang, Rev. Mod. Phys. **83**, 1057 (2011).

[3] C. K. Chiu, J. C. Y. Teo, A. P. Schnyder and S. Ryu, Rev. Mod. Phys. **88**, 035005 (2016).

[4] A. Kitaev, Phys. Usp. **44**,131 (2001).

[5] M. Greiter,V. Schnells and R. Thomale, Annals of Physics **351**,1026 (2014).

[6] E. Cobanera, G. Ortiz and Z. Nussinov, Phys. Rev. B. **87**, 0411705 (2013).

[7] P. Fendley, J. Phys. A: Math. Theor. **49** (2016).

[8] J. Lee and F. Wilczek, Phys. Rev.Lett.**111**, 226402 (2013).

[9] Rukhsan Ul Haq, Resonance, Vol. 21, **12** (2016).

[10] B. A. Bernevig, *Topological Insulators and Toplogical Superconductors* (Princeton University Press, Princeton) (2013).

[11] A. R. Akhmerov, Phys. Rev. B **82**, 020509 (2010).

[12] G. Goldstein and C. Chamon, Phys. Rev. B **86**, 115122 (2010).

[13] Guang Yang and D.E. Feldman, Phys. Rev B**89**, 035136 (2014).

[14] G. Kells, Phys. Rev. B**92**, 081401 (2015).

[15] H. Katsura, D. Schuricht and M. Takahashi, Phys. Rev. B **92**, 115137 (2015).

[16] G. Moore and N. Read, Nucl. Phys. B **360**, 362 (1991).

[17] N. Read and D. Green, Phys. Rev. B **61**, 10267 (2000).

[18] D. A. Ivanov, Phys. Rev. Lett. **86**, 268 (2001).

[19] V. Mourik *et al*, Science **336**, 1003 (2012).

[20] Li-Wei Yu and Mo-Lin Ge, Sci. Rep. **5**, 8102 (2015).

[21] L. H. Kauffman and S. J. Lomonaco, New. J. Phys. **4**,73(2002).

[22] L. H. Kauffman. Knot logic and topological quantum computing with Majorana fermions. In "Logic and algebraic structures in quantum computing and information", Lecture Notes in Logic, J. Chubb, J. Chubb, Ali Eskandarian, and V. Harizanov, editors, 124 pages Cambridge University Press (2016).

Chapter 6

The interplay of Majorana fermions and Kondo effect in quantum dots: Flow equation Renormalization

Contents

6.1 Introduction

Majorana fermions(Majorana zero modes) have recently attracted a lot of attention in condensed matter physics community due to their special topological properties which make them a promising candidate for quantum computing. Majorana fermions make topological qubits which can store the information non-locally and hence are immune to local perturbations. Their topological protection comes from Z_2 parity symmetry. Majorana fermions are Ising anyons and obey non-abelian statistics. Though it was known that Majorana fermions exist in topological superconductors[1][2] but after Kitaev[3] introduced a simple Hamiltonian and it was realized that it could be experimentally realized[4], it gave a boost to the research on Majorana fermions. So the search for Majorana fermions in solid state systems started. Since as of now there is no conclusive evidence for the topological superconductivity in nature, it was realized that we could engineer systems which harbour Majorana fermions. The recent successes in the detection and control of the Majorana fermions[5][6][7] have created a lot of hope about Majorana fermion based quantum computing[8]. However, the experimental detection of Majorana fermions is based on spectroscopic signatures, and there are physical effects which contribute to the zero-bias spectral peaks including Kondo impurities and disorder. So the search for unambiguous signatures of Majorana fermions is still on. In [11] it was proposed that Kondo effect can be used for the detection of Majorana fermions. Kondo effect is known to have a high level of experimental tunability in quantum dots. So quantum dot systems offer a very feasible and controllable way for the detection of Majorana fermions.There are other reasons also to consider a setup where

Majorana fermions are coupled to quantum dots. It was shown in[9][10] that Majorana fermions tunnel-coupled to conduction leads do not preserve the information in qubit and also parity time of Majorana fermions can not be determined in those experiments. They proposed an experimental setup in which Majorana fermions are coupled to quantum dot which can be coupled to normal lead(s) as well. To explore the signatures of Majorana fermions in Kondo effect and hence the interplay between Majorana fermions and Kondo effect, there have been recent theoretical studies [11][12][13][14]. In [11] poor man's scaling was applied to study the stability of Kondo effect. Though they find that Majorana fermions have a drastic effect on Kondo effect, they have got the same scaling equations as for the standard Kondo model. In [12] based on numerical renormalization group(NRG) calculations, it has been found that there is Majorana fermion induced Zeeman field which shifts the spectral function of one species of fermions and also there is the contribution of Majorana fermions to differential conductance. In [14] similar results have been obtained using recursive Greens function method. However, none of these studies has found a new fixed point arising due to the Majorana fermions. In [13] based on perturbative renormalization, slave boson mean field theory and density matrix renormalization group calculations, the authors have come to the conclusion that in the strong Majorana-Dot coupling regime, physics of the system is governed by a new fixed point rather than Kondo fixed point. The signatures of the new fixed point can be found in spin susceptibility, and they find that, quite unlike Kondo fixed point, spin susceptibility is dependent on gate-voltage(particle-hole asymmetry).

There are still many questions which have not been addressed in these studies. The existence of a new fixed point needs to be put on more firm analytical and computational basis and needs to be confirmed by more direct ways than has been done. Since Kondo effect is associated with the strong coupling fixed point and hence to capture the effects of Majorana fermions, we need to employ a method

which can capture the physics in the strong coupling regime where perturbative renormalization methods can not be relied upon. Similarly, it has been realized that dynamic spin susceptibility is an important quantity which can be used to capture the signatures of Majorana fermions. However, a detailed study of this quantity has not been done. Yet another aspect of the interplay between Majorana fermions and Kondo effect which needs further exploration is the particle-hole asymmetry. In the presence of Majorana fermions, particle-hole asymmetry becomes a relevant perturbation for Kondo physics. Physics is different for the cases when particle-hole symmetry is present or absent. Motivated by these questions which need detailed study, we employed flow equation renormalization method to study the interplay between Majorana fermions and Kondo effect. Flow equation method retains the full momentum dependence of the coupling constants of the Hamiltonian and is not restricted to the excitations closer to the Fermi level, as is the case with perturbative renormalization methods like poor man's scaling. Due to this restriction, many renormalization processes are not captured. In our present study, flow equation method has brought out one important difference between the particle-hole symmetric and asymmetric cases. In other studies, it has been found that the emergent Zeeman field which arises due to the Majorana fermions vanishes at particle-hole symmetry and hence does not contribute to the renormalization of the Kondo couplings. However, in flow equation method studies we have found that even though the emergent field is zero initially, it emerges again under the renormalization flow and hence leads to anisotropic Kondo model. So while other studies have found that Majorana fermions have drastic effects only away from particle-hole symmetry, our results show that even at the particle-hole symmetric case, Majorana fermions lead to significant renormalization of Kondo couplings and hence dynamic spin susceptibility also changes. And to see the effect of Majorana fermions on Kondo effect in quantum dots, there is no need to tune the gate voltage, as has been shown in

other works. This is one of the main results of our studies, and it brings out the new aspects of the renormalization effects of Majorana fermions on Kondo physics which were not explored in literature and due to which there was an impression that to see the strong renormalization effects of Majorana fermions, we need to tune the gate voltage away from particle-hole symmetric point. Flow equation method gives us access to the renormalization flow of observables and correlation and response functions. Since spin susceptibility is a key observable which can be used in the experiment for the unambiguous detection of Majorana fermions, we have done a detailed study of spin susceptibility both at the particle-hole symmetric point and away from it. Once again though there were some results about how away from the particle-hole symmetric point, the emergent Zeeman field will effect the spin susceptibility, a detailed study of the signatures of Majorana fermions in spin susceptibility was lacking and has been done in this chapter.

The rest of this chapter is organized in following way. First, we consider the Hamiltonian for the system in which a quantum dot is coupled to a normal lead on one side and is side-coupled to the topological superconductor. In the long chain limit, there is only one Majorana fermion in the topological superconductor. We calculate the effective Hamiltonian, Majorana-Kondo model, which has both Kondo interaction and terms arising from the coupling to Majorana fermion. To find the stability of Kondo fixed point in the presence of Majorana fermions, we calculate the flow equations for the couplings constants of the Majorana-Kondo model. We solve the flow equations numerically. Then we calculate the flow equations of Kondo spin observable and solving the flow equations numerically, we calculate dynamic spin susceptibility, and we find clear signatures of Majorana fermions in this key observable quantity. Once again we explore both the cases, with particle-hole symmetry being present and absent. Finally, we summarize our conclusions and discuss the interplay between Majorana fermions and Kondo effect and hence point to the

unambiguous ways for the detection of Majorana fermions.

6.2 Hamiltonian for Normal Lead-Quantum Dot-Topological Superconductor System

We consider a set-up in which a quantum dot is connected to a topological superconductor on one side and to a normal lead on another side. Topological superconductor is an experimental realization of Kitaev chain model and hence has two Majorana fermions on the edges of the chain. We work in the long chain limit and couple only one of the Majorana fermions to the quantum dot. The Hamiltonian for this system is:

$$H = \sum_{k\sigma} \epsilon_k c^\dagger_{k\sigma} c_{k\sigma} + \sum_{\sigma} \epsilon_d d^\dagger_\sigma d_\sigma + U n_{d\uparrow} n_{d\downarrow} + t \sum_{k\sigma} (c^\dagger_{k\sigma} d_\sigma + h.c.) + \sum_{\sigma} i\lambda_\sigma \gamma (d_\sigma + d^\dagger_\sigma) \tag{6.1}$$

The first four terms constitute the Anderson impurity model for quantum dot connected to a normal lead. The last term represents the coupling of Majorana fermion with quantum dot electron, λ being the coupling strength. We have taken general coupling, but later on, we will see that Majorana fermion gets coupled to only one species of electrons. To get an insight into the effect of Majorana fermions on the dynamics of our system, we first consider the case when Majorana fermions are coupled to quantum dot only[9]. The Hamiltonian for this system is:

$$H = H_D + \frac{i}{2}\gamma_1\gamma_2 + i\sum_{\sigma} \lambda_\sigma \gamma (d_\sigma + d^\dagger_\sigma) \tag{6.2}$$

Where H_D is the Hamiltonian for the quantum dot which is actually the impurity part of the Anderson impurity model. For the case $\lambda = 0$, all the terms commute among themselves and hence can be diagonalized. We denote the eigenstates of the Hamiltonian as $\mid n_d n_f \rangle$ where n_f is the number operator for the fermionic state

corresponding to Majorana fermion. In the absence of the Majorana fermion, local Hilbert space of the quantum dot is four dimensional corresponding to the empty, singly occupied(up and down) and doubly occupied states. But due to the parity conservation in the presence of Majorana fermions, Majorana-dot Hamiltonian will be block-diagonal where the two blocks refer to the even and odd parity sectors. Since number of their fermions is not conserved, it is only the parity which is a good quantum number for this system. The tunnelling part of the Hamiltonian connects even and odd parity sectors by changing the occupation by ∓ 1. We have assumed the long chain limit of topological superconductor in which case the two Majorana edge modes are degenerate, and this degeneracy breaks for the case of finite chain and the Majorana edge modes have actually finite energy. Like Anderson impurity model, our Hamiltonian has many parameter regimes but to study the interplay between Majorana fermions and Kondo effect; we need to project our Hamiltonian into its Kondo regime. We will use the projection operator method to calculate the effective Hamiltonian in the Kondo regime of our model. The details of the projection operator method have been given in chapter **3** where it was used to calculate the effective Hamiltonian for another extended version of Anderson impurity model. Effective Hamiltonian in singly occupied space is given by

$$H_{eff} = H_{11} + H_{10}\frac{1}{E - H_{00}}H_{01} + H_{12}\frac{1}{E - H_{22}}H_{21} \tag{6.3}$$

To get the effective Hamiltonian we need to calculate the projected Hamiltonian terms H_{12} and H_{10}. Since there are only two tunneling terms so only these will contribute to off-diagonal part of the effective Hamiltonian.

$$H_{12} = \sum_{\sigma}(tc^{\dagger}_{k\sigma} + i\lambda_{\sigma}\gamma)d_{\sigma}n_{d\bar{\sigma}} \quad H_{21} = H^{\dagger}_{12} \tag{6.4}$$

$$H_{01} = \sum_{\sigma} (t c^{\dagger}_{k\sigma} + i\lambda_{\sigma}\gamma) d_{\sigma}(1 - n_{d\bar{\sigma}}) \quad H_{10} = H^{\dagger}_{01} \tag{6.5}$$

To calculate the effective Hamiltonian, we need to evaluate following two terms.

$$\begin{aligned}
&H_{12} \frac{1}{E - H_{22}} H_{21} \\
&= \sum_{\sigma} t c^{\dagger}_{k\sigma} d_{\sigma} n_{d\bar{\sigma}} \frac{1}{E - H_{22}} \sum_{k'\sigma'} t d^{\dagger}_{\sigma'} c_{k'\sigma'} n_{d\bar{\sigma'}} \\
&+ \sum_{k\sigma} t c^{\dagger}_{k\sigma} d_{\sigma} n_{d\bar{\sigma}} \frac{1}{E - H_{22}} \sum_{k'\sigma'} i\lambda_{\sigma'}\gamma d^{\dagger}_{\sigma'} c_{k'\sigma'} n_{d\bar{\sigma'}} \\
&+ \sum_{k\sigma} i\lambda_{\sigma}\gamma d_{\sigma} n_{d\bar{\sigma}} \frac{1}{E - H_{22}} \sum_{k'\sigma'} i t_{\sigma'} d^{\dagger}_{\sigma'} c_{k'\sigma'} n_{d\bar{\sigma'}} \\
&+ \sum_{k\sigma} i\lambda_{\sigma}\gamma d_{\sigma} n_{d\bar{\sigma}} \frac{1}{E - H_{22}} \sum_{k'\sigma'} i\lambda_{\sigma'} d^{\dagger}_{\sigma'} n_{d\bar{\sigma'}}
\end{aligned} \tag{6.6}$$

$$\begin{aligned}
&H_{10} \frac{1}{E - H_{00}} H_{01} \\
&= \sum_{k\sigma} \sum_{k'\sigma'} t d^{\dagger}_{\sigma} c_{k\sigma}(1 - n_{d\bar{\sigma}}) \frac{1}{E - H_{00}} t c^{\dagger}_{k'\sigma'} d_{\sigma'}(1 - n_{d\bar{\sigma'}}) \\
&+ \sum_{k\sigma} \sum_{k'\sigma'} t d^{\dagger}_{\sigma} c_{k\sigma}(1 - n_{d\bar{\sigma}}) \frac{1}{E - H_{00}} i\lambda_{\sigma'}\gamma d_{\sigma'}(1 - n_{d\bar{\sigma'}}) \\
&+ \sum_{k\sigma} \sum_{k'\sigma'} i\lambda_{\sigma}\gamma d^{\dagger}_{\sigma} c_{k\sigma}(1 - n_{d\bar{\sigma}}) \frac{1}{E - H_{00}} t c^{\dagger}_{k'\sigma'} d_{\sigma'}(1 - n_{d\bar{\sigma'}}) \\
&+ \sum_{k\sigma} \sum_{k'\sigma'} i\lambda_{\sigma}\gamma d^{\dagger}_{\sigma} c_{k\sigma}(1 - n_{d\bar{\sigma}}) \frac{1}{E - H_{00}} i\lambda_{\sigma'}\gamma d_{\sigma'}(1 - n_{d\bar{\sigma'}})
\end{aligned} \tag{6.7}$$

Using the Abrikosov's fermion representation of spin operators, we can write the effective Hamiltonian as(also calculated in[12][13]):

$$H_{eff} = \sum_{kk'} J(k,k') S.s_{kk'} - hS^z + \sum_k J_1(k) i\gamma (c_{k\uparrow} + c^\dagger_{k\uparrow}) + \sum_k J_2(k) i\gamma (c_{k\uparrow} + c^\dagger_{k\uparrow}) S^z + \sum_k J_3(k) i\gamma (c^\dagger_{k\downarrow} S^+ + c_{k\downarrow} S^-) \tag{6.8}$$

where $J(k,k') = t^2\zeta_{1+}$, $h = \lambda^2\zeta_-$, $J_1 = t\lambda\zeta_-$, $J_2 = J_3 = t\lambda\zeta_{2+}$.

$$\zeta_{1+} = \frac{1}{\epsilon_d + U - \epsilon_k} + \frac{1}{\epsilon_k - \epsilon_d} + \frac{1}{\epsilon_d + U - \epsilon_{k'}} + \frac{1}{\epsilon_{k'} - \epsilon_d} \tag{6.9}$$

$$\zeta_{2+} = \frac{1}{\epsilon_d + U - \epsilon_k} + \frac{1}{\epsilon_k - \epsilon_d} \tag{6.10}$$

$$\zeta_- = \frac{1}{\epsilon_d + U - \epsilon_m} - \frac{1}{\epsilon_m - \epsilon_d} \tag{6.11}$$

6.2.1 Majorana-Kondo Model

The effective Hamiltonian that we have obtained has terms arising from the Quantum Dot-Majorana coupling. We call this model Majorana-Kondo model (MKM).

$$H_{eff} = \underbrace{\sum_{k\sigma} \epsilon_k c^\dagger_{k\sigma} c_{k\sigma} + J_k \sum_{kk'} S.s_{kk'}}_{\text{Kondo model}} - \underbrace{h_z S^z}_{\text{Zeeman term}} + \underbrace{\sum_k J_1 (i\gamma)(c_{k\uparrow} + c^\dagger_{k\uparrow})}_{\text{Andreev term}} + \sum_k J_2 (i\gamma)(c_{k\uparrow} + c^\dagger_{k\uparrow}) S^z + \sum_k J_3 (i\lambda)\gamma (c^\dagger_{k\downarrow} S^+ + c_{k\downarrow} S^-)$$

In Majorana-Kondo model there are four other terms in addition to the standard Kondo interaction term. 1. Zeeman term which has Majorana induced Zeeman field. 2. Andreev Scattering term. Since there is no direct tunneling between lead and Majorana so this term arises due to the virtual charge fluctuations. 3. Then there are two more terms in which impurity spin couples both to Majorana and lead electrons.

To get insight into last two terms it is helpful to consider Majorana-Kondo model in particle-hole symmetric limit. The particle-hole symmetric case gives an insight into the dynamics of Majorana fermion and also about the competition between Majorana and Kondo physics. In this case $\zeta_- = 0$ and hence there is no Zeeman field and Andreev scattering at the effective Hamiltonian level which has only two Majorana terms. We will ignore the Kondo term for now and study the Majorana terms alone.

$$H = iJ_3 \left((c_{0\uparrow} + c_{0\uparrow}^\dagger)\gamma S^z + (c_{0\downarrow}^\dagger S^+ + c_{0\downarrow} S^-)\gamma \right) \tag{6.12}$$

We can switch to Majorana fermion representation for lead electrons as well.

$$c_{0\uparrow} + c_{0\uparrow}^\dagger = \eta_z \tag{6.13}$$

$$c_{0\downarrow} + c_{0\downarrow}^\dagger = \eta_x \tag{6.14}$$

$$i(c_{0\downarrow}^\dagger - c_{0\downarrow}) = \eta_y \tag{6.15}$$

In Majorana representation Hamiltonian takes the following form:

$$H = iJ_3 \sum_a \gamma \eta_a S^a \quad a \in (x, y, z) \tag{6.16}$$

This Hamiltonian has not only particle-hole symmetry but also an emergent time reversal due to which $\langle S \rangle = 0$ and hence there are impurity spin fluctuations. So at particle-hole symmetric point, there is no impurity spin polarization due to the emergent time reversal symmetry. Impurity spin gets entangled with the parity of the lead electrons which can be seen from Majorana representation of Hamiltonian. Since there are two Majorana fermions present for each spin direction hence, there are four fermion states which are present, but due to the parity constraint, only linear combinations of these states are eigenstates of the Hamiltonian. Impurity

spin couples with these two states of the lead electrons. Four states are: $|\ 00\rangle, |\ 11\rangle, |\ 10\rangle, |\ 01\rangle$. Parity states: $|\ even\rangle = |\ 00\rangle + |\ 11\rangle, |\ odd\rangle = |\ 10\rangle + |\ 01\rangle$.

Particle-hole asymmetry is not relevant perturbation for Kondo physics (model) while it is a relevant perturbation for Majorana physics. In the case of Kondo model(zero Majorana coupling) detuning of the gate voltage away from particle-hole symmetric point does not change impurity magnetization while in presence of Majorana coupling impurity magnetization is different for particle-hole symmetric and asymmetric case. So impurity susceptibility has the signatures of Majorana physics.

6.3 Flow equations for Majorana-Kondo Model

In this section, we will apply the flow equation renormalization group method to Majorana-Kondo model. We will calculate the flow equations for the parameters of the model. In chapter **2** we have given the formalism of this method and calculated the flow equations for Kondo model. We have seen that Kondo couplings show divergence which is one important signature of Kondo effect. In the case of Majorana-Kondo model, our interest is to explore the interplay between the Kondo effect and Majorana fermions, so we will find out what happens to Kondo divergence(scale) in the presence of Majorana fermions. We will increase the QD-TSC coupling λ and find out whether Kondo effect survives in the strong λ regime. To calculate the flow equation for our model, we first need to calculate the generator.

Generator for the flow equations for Majorana-Kondo model is given below:

$$\begin{aligned}\eta =&\frac{1}{2}\sum_{pq}(\epsilon_p-\epsilon_q)(J^{\uparrow}(p,q):c^{\dagger}_{p\uparrow}c_{q\uparrow}:-J^{\downarrow}(p,q):c^{\dagger}_{p\downarrow}c_{q\downarrow}:)S^z\\&+\frac{1}{2}\sum_{pq}(\epsilon_p-\epsilon_q+h)J^{\perp}(p,q)(:c^{\dagger}_{p\uparrow}c_{q\downarrow}:S^{-}-:c^{\dagger}_{q\downarrow}c_{p\uparrow}:S^{+})\\&+\sum_{p}\epsilon_pJ_1(p)(i\gamma)(c^{\dagger}_{p\uparrow}-c_{p\uparrow})+\epsilon_pJ_2(p)(i\gamma)(c^{\dagger}_{p\uparrow}-c_{p\uparrow})S^z\\&+\sum_{p}(\epsilon_p+h)J_3(p)(i\gamma)(c^{\dagger}_{p\downarrow}S^{\dagger}-c_{p\downarrow}S_{-})\end{aligned}\tag{6.17}$$

$$\eta=\eta^{\parallel}_K+\eta^{\perp}_K+\eta^1_M+\eta^2_M+\eta^3_M\tag{6.18}$$

In equation 6.18 flow equation generator has been written as sum of generators corresponding to different terms in the interaction of the Hamiltonian. To calculate the flow equations we need to evaluate the commutators of the generators with the full Hamiltonian. These commutators have been evaluated in Appendix A. Putting all the commutators together and comparing with the original Hamiltonian we obtain the flow equations for the Majorana-Kondo Hamiltonian.

For spin-up Kondo coupling, the flow equation is

$$\begin{aligned}\frac{dJ^{\uparrow}(p,q)}{dl}=&-(\epsilon_p-\epsilon_q)^2J^{\uparrow}(p,q)+\\&\frac{1}{2}\sum_{s}\Big(2(\epsilon_s-h)-(\epsilon_p+\epsilon_q))J^{\perp}(p,s)J^{\perp}(q,s)(1-2n(s)\Big)\end{aligned}\tag{6.19}$$

Similarly for spin down Kondo Coupling, flow equation is

$$\begin{aligned}\frac{dJ^{\downarrow}(p,q)}{dl}=&-(\epsilon_p-\epsilon_q)^2J^{\downarrow}(p,q)+\\&\frac{1}{2}\sum_{s}\Big(2(\epsilon_s+h)-(\epsilon_p+\epsilon_q))J^{\perp}(s,p)J^{\perp}(s,q)(1-2n(s)\Big)\end{aligned}\tag{6.20}$$

Flow equation for transverse Kondo coupling is

$$\begin{aligned}\frac{dJ^{\perp}(p,q)}{dl} =& -(\epsilon_p - \epsilon_q + h)^2 J^{\perp}(p,q) + \\ & \frac{1}{4}\sum_s (1-2n_f(s))\Big[(2\epsilon_s - (\epsilon_p+\epsilon_q)+h)J^{\perp}(s,q)J^{\uparrow}(p,s)) \\ & + (2\epsilon_s - (\epsilon_p+\epsilon_q)-h)(J^{\perp}(p,s))J^{\downarrow}(q,s))\Big] \end{aligned} \tag{6.21}$$

Fot the Majorana induced Zeeman field, flow equation has contributions both from Kondo interaction as well as Majorana coupling terms.

$$\begin{aligned}\frac{dh}{dl} =& \frac{1}{2}\sum_{pq}(\epsilon_p - \epsilon_q + h)(n(p)+n(q)-2n(p)n(q))(J_{\perp}^2(p,q)) + \\ & (\epsilon_p + h)^2 J_3^2(1-2n(p)) \end{aligned} \tag{6.22}$$

Flow equation for Andreev scattering term is

$$\begin{aligned}\frac{dJ_1(p)}{dl} =& -\epsilon_p J_1(p) + \frac{1}{4}\sum_q(\epsilon_p - \epsilon_q)J^{\uparrow}(p,q)J_2(q) + \frac{1}{2}\sum_q(\epsilon_p - \epsilon_q + h)J_3(q)J^{\perp}(p,q) \\ & - \frac{1}{2}\sum_q(\epsilon_q + h)J_3(q)J^{\perp}(p,q)) - \frac{1}{4}\sum_q \epsilon_q J_2(q)J^{\uparrow}(p,q) \end{aligned} \tag{6.23}$$

Flow equation for Majorana couplings J_2 is:

$$\begin{aligned}\frac{dJ_2(p)}{dl} =& -\epsilon_p J_2(p) + \sum_q(\epsilon_p - \epsilon_q)J^{\uparrow}(p,q)J_1(q) - \sum_q \epsilon_q J_1(q)J^{\uparrow}(p,q) \\ & - \sum_q(\epsilon_p - \epsilon_q + h)J_3(q)J^{\perp}(p,q)(1-2n(q)) \\ & + \sum_q(\epsilon_q + h)J_3(q)J^{\perp}(p,q)(1-2n(q)) \end{aligned} \tag{6.24}$$

Flow equation for Majorana coupling J_3 is:

$$\begin{aligned}\frac{dJ_3(p)}{dl} =& -\epsilon_p J_3(p) - \frac{1}{2}\sum_q(\epsilon_p-\epsilon_q)(1-2n(q))(J^{\downarrow}(p,q)J_3(q)\\ &-\sum_q(\epsilon_q-\epsilon_p+h)J^{\perp}(q,p)J_1(q)\\ &+\frac{1}{2}\sum_q(\epsilon_q-\epsilon_p+h)J^{\perp}(q,p)J_2(q)(1-2n(q))+\\ &-\sum_q\epsilon_q J_1(q)J^{\perp}(p,q)-\frac{1}{2}\sum_q\epsilon_q J_2(q)J^{\perp}(q,p)(1-2n(q))\\ &-\frac{1}{2}\sum_q(\epsilon_q+h)J_3(q)J^{\downarrow}(p,q)(1-2n(q)) \qquad (6.25)\end{aligned}$$

6.3.1 Numerical Solution of Flow Equations

As we have seen in chapter **2** where we have solved flow equations for Kondo model, flow equations need to be solved numerically because they are non-linear coupled differential equations and analytical solution can be obtained only in some special limits like infrared limit where momentum dependence of coupling constants can be dropped off. In case of Majorana-Kondo model, since there is larger number of coupling constants so the system of differential equations becomes larger and even more coupled which increases the computational complexity of the problem. Also there are more energy scales in addition to the Kondo scale. Due to the interplay of various energy scales present in the system flow equations generally become stiff. For the numerical solution of the flow equation of Majorana-Kondo model we have taken conduction bath to have flat density of states. Conduction band has been discretized and typically we have kept 200 energy states and since number of flow equations to be solved scales as $O(N^2)$ where N is the number of states kept in conduction band, the dimension of systems of flow equations is of the order 10^4. The computational expense however scales as $\mathcal{O}N^3$. We have used DOPRI5 which is the fifth order Runga-Kutta method for solving ODEs. The method has proved

stable for the flow equations except that due to the stiffness of the flow equations we often had to tweak the discretization of the flow parameter l grid so that the lowest energy scale gets resolved.

Particle-hole asymmetry is not a relevant perturbation for Kondo model and hence in chapter **2** we solved the Kondo model without incorporating it. However as shown above for Majorana-Kondo model, particle-hole asymmetry becomes relevant and hence we need to solve the flow equations separately for the two cases. We will first solve the flow equations for particle-hole symmetric case and then for the general case.

6.3.2 Particle-hole symmetric Case

At particle-hole symmetric point, Andreev scattering term vanishes because $\zeta_- = 0$. Similarly emergent Zeeman field is also zero initially. However, as can been seen from the flow equation for the Zeeman field, it grows under unitary flow and hence needs to be taken into consideration even at particle-hole symmetric case. This is one of the main differences between our studies and earlier studies in which they have found that Zeeman field does not contribute to renormalization at particle-hole symmetric case because it vanishes at the effective Hamiltonian level. Using the flow equation method, we have been able to capture the effect of emergent Zeeman field on Kondo fixed point even at particle-hole symmetric case where perturbative renormalization have missed it because Zeeman field does not have a scaling equation and hence does not grow. Consequently the scaling equations for the Kondo couplings which were obtained using poor man's scaling[11] or other perturbative renormalization method[13], are same as that of isotropic Kondo model. So the effect of Majorana fermions on Kondo effect and the consequent emhancement of Kondo scale even at particle-hole symmetric point is one of the main results of our work. It shows that the effect of Majorana fermions of Kondo effect is stronger than has been anticipated

by earlier works. Later on we will see that the signatures of Majorana fermions are present in spin susceptibility even at partice-hole symmetric case.

Now we will present the numerical solutions of the flow equations. In Figure 6.1,

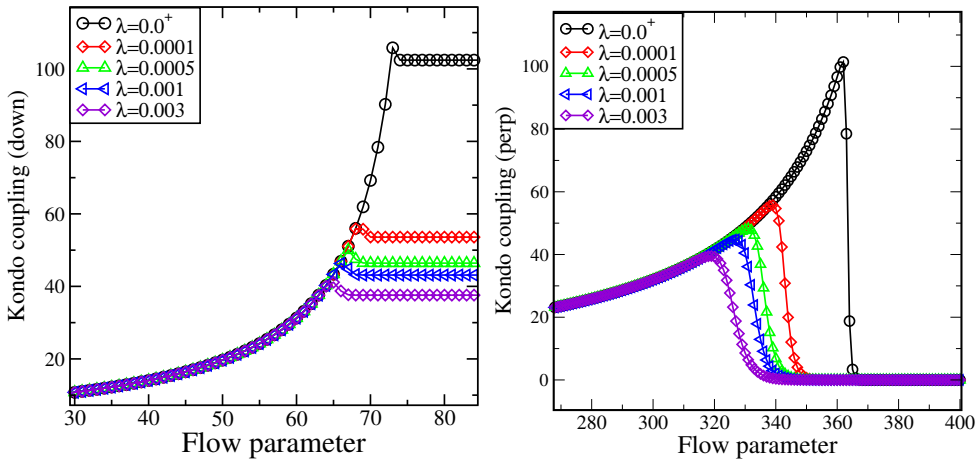

Figure 6.1: In left panel, longitudinal Kondo coupling is plotted versus flow parameter. In right panel, transverse Kondo coupling is plotted versus flow parameter. Other parameters are: U= 6.0, ϵ_d= -3.0, t= 3.0.

Kondo couplings, both longitudinal and transverse have been plotted versus flow parameter. First thing to be noted is that longitudinal and transverse Kondo couplings get renormalized in an anisotropic way due to Majorana fermions. This behaviour was not captured by earlier studies[11][13][14]. Since there is Majorana fermion induced Zeeman field which is contributing to the renormalization flow of Kondo couplings, we find that the Kondo divergence is being cut off as shown in Figure 6.1. As λ increases, divergence gets cut off earlier in the renormalization flow which is tantamount to the change in Kondo scale. Kondo scale has been calculated from longitudinal Kondo coupling using the expression $g = \frac{1}{\frac{1}{g_0} - \ln(\frac{\sqrt{l_c}}{\sqrt{l_0}})}$. g is dimensionless Kondo coupling and l_c is the value of the flow parameter where Kondo divergence occurs. We have also used the relation $D = \frac{1}{\sqrt{l}}$ which relates energy scale D with flow parameter l. We have plotted Kondo scale versus λ in Figure 6.2, and as can be seen, Kondo scale increases in the presence of Majorana fermion. Similar enhance-

ment of Kondo scale has been found in [14] where recursive Green's function method has been used. Through curve fitting we found that $T_k(\lambda) = T_k(\lambda = 0) + A\lambda^\theta$ where $\theta \sim 0.15$. So the dependence of Kondo scale on QD-TSC coupling λ is sub-linear. In Figure 6.2(left panel) flow of the emergent Zeeman field has been plotted. It is interesting to note that Zeeman field is zero until certain scale which is roughly same scale at which longitudinal Kondo coupling gets cut off, and Zeeman field makes an abrupt jump. Even more interesting is the fact that smaller is the value of λ, the higher is the value to which Zeeman field jumps to. Zeeman field finally saturates to a universal value at which all curves collapse.

The plots corresponding to $\lambda = 0^+$ in Figure 6.1 also show the Kondo divergence gets cut off. However, this is known in case of anisotropic Kondo model, $h(l) \equiv 0$, $J^\uparrow(p,q) = J^\downarrow(p,q)$ and $J^\perp(p,q) = J^\perp(q,p)$ are fulfilled during the flow for the case $h(l = 0) = 0$. The relations $J^\uparrow(p,q) = J^\uparrow(q,p)$ and $J^\downarrow(p,q) = J^\downarrow(q,p)$ are always fulfilled due to hermiticity[16]. So what we see in these plots shows that flow equations have essential instability to particle-hole asymmetry. The slightest asymmetry makes the Zeeman field to grow. Since in numerical solutions of flow equations the condition $J^\perp(p,q) = J^\perp(q,p)$ which holds for zero initial field, is maintained only within the machine error which propagates along the flow and leads to the flow of the field as well. That is what we see in the plots for $\lambda = 0$. This result has physical implications for the experimental situations where particle-hole asymmetry is generic, and consequently Majorana physics is going to dominate over Kondo physics even for weaker QD-TSC coupling. This is one of our important observations which gives the insight into the interplay between Majorana fermions and Kondo physics.

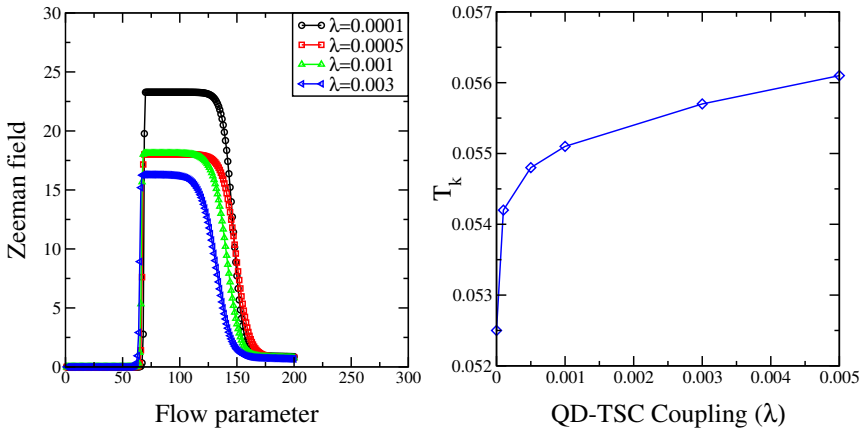

Figure 6.2: In the left panel, flow of Zeeman field has been plotted. In the right panel, Kondo scale has been plotted as a function of λ, coupling of quantum Dot to the topological superconductor. Other parameters are same as given in Figure 6.1

6.3.3 Particle-hole asymmetric case

Away from particle-hole symmetry, both Zeeman field and Andreev scattering terms are present in the Majorana-Kondo model and hence both contribute to the flow equations of Kondo couplings. In Figure 6.3 longitudinal (left panel) and transverse(right panel), Kondo couplings for asymmetric Majorana-Kondo model are plotted versus the flow parameter. We once again see that Kondo divergence gets cut off. However, what needs to be noted is that as compared to the similar plots for particle-hole symmetric case(Figure 6.1), Kondo divergence gets cut off at different values of flow parameter for the same values of λ which signifies the change in Kondo scale. This is because in asymmetric case Andreev scattering also contributes to the renormalization of Kondo couplings. Earlier renormalization studies[11][13] have explored the particle-hole asymmetric case of Majorana-Kondo model and found how Majorana fermions renormalize Kondo couplings. However what was not found in those studies is that Majorana fermions renormalize Kondo couplings in anisotropic manner. The conclusion that Kondo fixed point becomes unstable to Majorana fermion coupling was arrived by looking at renormalization flow of Majorana fermions rather

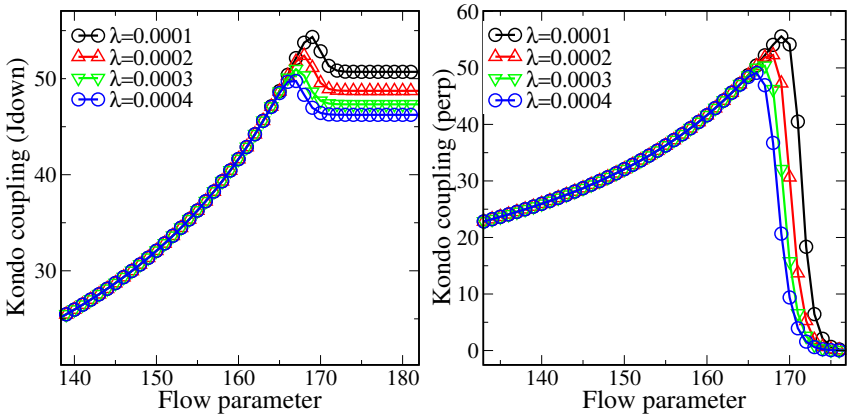

Figure 6.3: Flow of the Kondo couplings for the asymmetric case of Majorana-Kondo model: In the left panel, longitudinal Kondo coupling is plotted versus the flow parameter. In the right panel, transverse Kondo coupling versus flow parameter is plotted. Other parameters are: $U = 6.0$, ϵ_d = -3.1, t= 3.0

than directly from the scaling equations of Kondo couplings which were found to be same as for the isotropic Kondo model. In our studies, we have found the effect of Majorana fermion induced couplings directly from the flow equations of Kondo couplings, and as shown in Figure 6.3 we see clearly how Kondo divergence gets cut off, and hence Kondo scale also changes. Kondo scale for the asymmetric case is plotted in Figure 6.4(right panel). Kondo scale has been extracted by following the procedure of the particle-hole symmetric case. Kondo scale gets enhanced, but the dependence of Kondo scale on λ is linear in this case which needs to be compared with the symmetric case where we have found sub-linear dependence. Similarly, the behaviour of emergent Zeeman field, shown in Figure 6.4(right panel) is also different than the symmetric case. However, Zeeman field once again makes an abrupt jump and the higher values to which it jumps are for lower values of λ. Again the value of flow parameter at which Zeeman field jumps is roughly same as the one where the divergence of longitudinal Kondo coupling gets cut off.

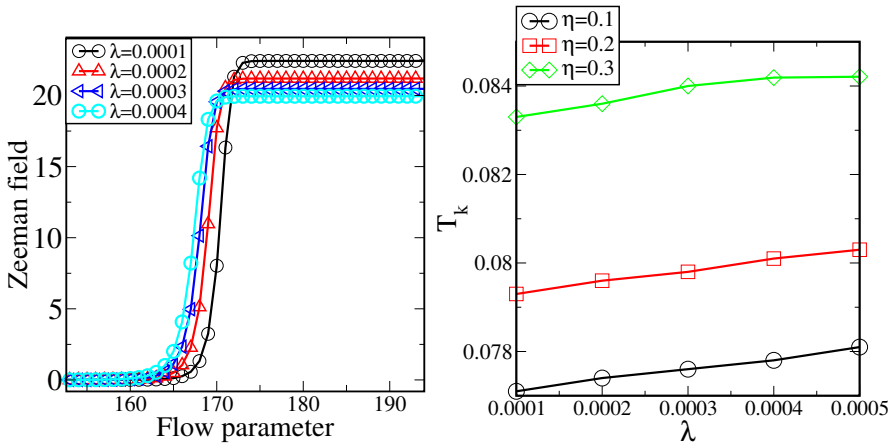

Figure 6.4: Plots for asymmetric Majorana-Kondo model: In the left panel, the flow of the emergent Zeeman field has been plotted. In right panel, Kondo scale has been plotted as function of λ, coupling of quantum dot to topological superconductor, for different asymmetry parameters.

6.4 Flow equations for Kondo impurity spin

One main difference between flow equations and conventional renormalization methods is that in flow equations observables also undergo unitary flow and hence renormalization. In the case of fermionic systems, fermion operators get transformed under unitary flow. The new fermion operators are then written as operator product expansion of fermion operators. In the case of Kondo model, the spin operator gets transformed under unitary flow. To check the consistency, there are many checks which one can make using the properties of the unitary flow. Unitary flow keeps the operator algebra(commutation/anti-commutation) invariant. There are other sum rules also which can be used to check the consistency of the operator product expansion. There are physical plausibility arguments as well which can be used to make sense of these operator product expansions. In the case of Kondo model, it is known that as renormalization flow proceeds to strong coupling fixed point, the magnetic moment of Kondo impurity gets quenched. This physical process has an algebraic mapping in flow equation method as shown below. Using the transformed observables, we can calculate correlation and response functions for a

given Hamiltonian. In chapter **2** dynamic spin susceptibility was obtained from the numerical solution of the flow equations for the isotropic Kondo model. In this section, we will calculate flow equations for the Kondo impurity spin and upon solving the flow equations, obtain the dynamic spin susceptibility for the Majorana-Kondo model. This quantity will give us access to the signatures of Majorana fermions which can be detected easily in an experiment. Hence dynamic spin susceptibility is a very important quantity to understand the interplay between Majorana fermions and Kondo effect and hence for the detection of Majorana fermions.

We make following ansatz for the spin operator S^z:

$$S^z(l) = h^z(l)S^z + \frac{M(l)}{2} + \sum_{pq} \gamma_{pq}(l)(: c^\dagger_{p\uparrow} c_{q\downarrow} : S^- + : c^\dagger_{q\downarrow} c_{p\uparrow} : S^+)$$
$$+ \sum_p \zeta_p(l)(i\gamma)(c_{p\uparrow} + c^\dagger_{p\uparrow})S^z) + \sum_p \eta_p(l)(\gamma(c^+_{p\downarrow} S^+ + c_{p\downarrow} S^-) \tag{6.26}$$

where $h^z(l = 0) = 1$ and initial values of all other parameters are zero. For the Kondo model, the ansatz for the spin operator[15] is motivated by the fact that Kondo effect quenches the magnetic moment. So for isotropic Kondo model, the decomposition of the spin operator has only two terms referring to the Kondo spin and the Kondo interaction. We have used this ansatz in chapter **2** of this thesis. For the anisotropic case, since there is Zeeman field and hence magnetization also, so the ansatz for spin observable needs to include these terms as well[16]. For the case of Majorana-Kondo model, there are Majorana fermion induced couplings due to which Kondo impurity spin couples to Majorana fermion also and hence these interactions need to be included in the ansatz. Andreev scattering term does not couple to Kondo impurity spi and hence has not been included in the ansatz.
To calculate the flow equation of the spin operator , we will use one-loop generator

as given in equation 6.17. .

$$\frac{dS^z}{dl} = [\eta(l), S^z(l)] \tag{6.27}$$

The commutators are evaluated in Appendix A. In the following we will present the flow equations for the various parameters in Equation 6.26.

Flow equation for magnetization is:

$$\begin{aligned}\frac{dM}{dl} =& \sum_{pq}(n(p) - n(q))(\epsilon_p - \epsilon_q + h)J_\perp(p,q)\gamma_{pq}(l) \\ &+ \sum_p(\epsilon_p + h)\eta_p(l)J_3(p)\end{aligned} \tag{6.28}$$

Flow equation for h^z co-efficient is:

$$\begin{aligned}\frac{dh^z}{dl} =& -\sum_{pq}(\epsilon_p - \epsilon_q + h)(J_\perp(p,q)\gamma_{pq})(n(p) + n(q) - 2n(p)n(q)) \\ &+ \sum_p(\epsilon_p + h)\eta_p(l)J_3(p)(1 - 2n(p))\end{aligned} \tag{6.29}$$

Flow equation for γ co-efficient is:

$$\begin{aligned}\frac{d\gamma_{pq}}{dl} =& \frac{1}{2}\sum_r \left(J^\uparrow(p,r)(\epsilon_r - \epsilon_p)\gamma_{rq}(l) + J^\downarrow(r,q)(\epsilon_r - \epsilon_q)\gamma_{pr}(l)\right)(1 - 2n(q)) \\ &+ \frac{1}{2}(\epsilon_p - \epsilon_q + h)J^\perp(p,q)h^z(l)\end{aligned} \tag{6.30}$$

Flow equation for ζ co-efficient is:

$$\frac{d\zeta_p}{dl} = \sum_q(\epsilon_q + h)J_3(q)\gamma_{pq}(1 - 2n(q)) \tag{6.31}$$

$$- \sum_q(\epsilon_p - \epsilon_q + h)J_\perp(p,q)\eta_q(1 - 2n(q)) \tag{6.32}$$

Flow equation for η co-efficient is:

$$\frac{d\eta_p(l)}{dl} = -(\epsilon_p + h)J_3(p)h^z(l) - \sum_q \epsilon_q J_1(q)\gamma_{qp}(l) \tag{6.33}$$

$$- \frac{1}{2}\sum_q \epsilon_q J_2(q)\gamma_{qp}(l)(1-2n(q))$$

$$+ \frac{1}{2}\sum_q (\epsilon_p - \epsilon_q + h)J_\perp(p,q)\zeta_q(l)(1-2n(q)) \tag{6.34}$$

$$- \frac{1}{2}\sum_q (\epsilon_p - \epsilon_q)J^\downarrow(p,q)\eta_q(1-2n(q)) \tag{6.35}$$

6.4.1 Numerical solution

In this section we will solve the flow equations for the spin operator and calculate the dynamic spin susceptibility. The formalism for the calculation of correlation and response functions is given in chapter **2**. For the Majorana-Kondo model, dynamical spin susceptibility is given by:

$$\begin{aligned}\chi(\omega) =& \frac{\pi(1-sgn(\tilde{h}))}{2}\sum_p \Big(\tilde{\gamma}^2_{\epsilon_p,\epsilon_p+\omega+\tilde{h}} n_f(\epsilon_p)(1-n_f(\epsilon_p+\omega+\tilde{h}))\\ &- \tilde{\gamma}^2_{\epsilon_p,\epsilon_p+\omega+\tilde{h}} n_f(\epsilon_p)(1-n_f(\epsilon_p-\omega+\tilde{h}))\Big)\\ &+ \frac{\pi(1+sgn(\tilde{h}))}{2}\sum_p \Big(\tilde{\gamma}^2_{\epsilon_p,\epsilon_p+\omega+\tilde{h}} n_f(\epsilon_p+\omega+\tilde{h})(1-n_f(\epsilon_p))\\ &- \tilde{\gamma}^2_{\epsilon_p,\epsilon_p+\omega+\tilde{h}}(1-n_f(\epsilon_p))(n_f(\epsilon_p-\omega+\tilde{h}))\Big)\end{aligned} \tag{6.36}$$

It is the imaginary part of the Fourier transformed response function[16]. To compute dynamic susceptibility we need the solve the flow equations for the spin observable numerically. Once again the flow equations need to be solved separately for the particle-hole symmetric and asymmetric cases.

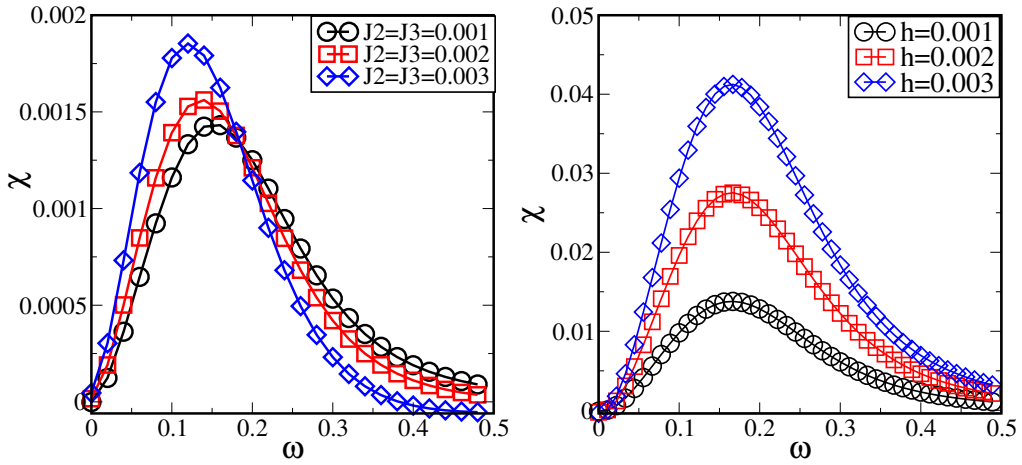

Figure 6.5: Dynamical spin susceptibility plots for Majorana-Kondo model at particle-hole symmetric point: In left panel, spin susceptibility has been plotted on frequency axis for different J_2 coupling constants. In right panel, spin susceptibility has been plotted for increasing values of Zeeman field.

6.4.2 Particle-hole symmetric case

To capture the effects of Majorana fermions in spin susceptibility we have plotted dynamic spin susceptibility on frequency axis in Figure 6.5 . In left panel, we see the effect of increasing J_2 Majorana coupling. As we increase J_2, spin susceptibility increases because as we have shown earlier in section 6.2.1 that coupling to the topological superconductor lets Kondo spin to interact with Majorana fermion which competes with Kondo effect which arises from the interaction between Kondo spin and lead electrons consequently Kondo effect weakenes. Similarly, as we increase Zeeman field, we find that dynamic spin susceptibility gets enhanced. What is very interesting to note is that very small values of Zeeman field lead to quite significant effects on spin susceptibility which shows the effect of Majorana fermions on Kondo effect is quite strong.

6.4.3 Particle-Hole Asymmetric Case

Away from the particle-hole symmetry, we expect that the effects of Majorana fermions on spin susceptibility will be even stronger because Andreev scattering

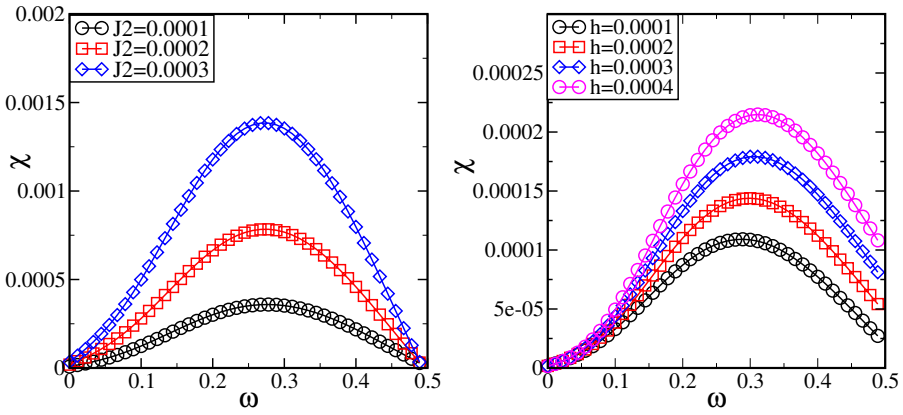

Figure 6.6: Dynamic spin susceptibility for asymmetric Majorana-Kondo model: In the left panel, spin susceptibility has been plotted on the frequency axis for increasing values of J_2 coupling. In right panel, spin susceptibility has been plotted for increasing values of Zeeman field.

term is also present at the effective Hamiltonian level and contributes to the flow equations of the spin operator as well. As can be seen from the Figure 6.6, spin susceptibility has huge effects even for smaller values of J_2(left panel) and Zeeman field(right panel). These values are the order of magnitude smaller than the ones shown in plots in Figure 6.5 for the particle-hole symmetric case.

6.5 Conclusion

In this chapter, we have done a detailed study of the interplay between Majorana fermions and Kondo effects considering an experimental set-up in which a quantum dot is coupled to a normal lead on one side and tunnel-coupled to a topological superconductor, which itself is an experimental realization of Kitaev p-wave chain model. Our motivation comes from the recent surge in the research on Majorana fermions as being the promising candidates for topological quantum computing. Hence searching for umambiguous ways of their detection has assumed utmost importance. Kondo effect in quantum dots offers a lot of tunability and hence very feasible way to detect Majorana fermions. However, to single out the signatures of Majorana fermions in

Kondo physics, needs careful and detailed study. There are questions which need to be addressed to have conclusive evidence for the signatures of Majorana fermions. Firstly Kondo effect is associated with the strong coupling fixed point of Anderson impurity model and is very stable to perturbations and hence to show that Majorana fermions make Kondo fixed point unstable and lead to new fixed point, one has to take recourse to methods which can be relied upon in the strong coupling regime of the model. In our work, we have employed flow equation method which has already been applied to Kondo model to study its strong coupling physics both in equilibrium and non-equilibrium. Based on this method we did the renormalization group study of the Majorana-Kondo model which is the effective Hamiltonian in the strong coupling regime of the Hamiltonian for NL-QD-TSC system. We calculated the flow equations for the coupling constants of the Majorana-Kondo model, and after solving them numerically, we clearly found how Majorana fermion induced terms, cut off Kondo divergence and also change the Kondo scale. One important signature of Majorana fermions in Kondo physics is that they make particle-hole asymmetry relevant for Kondo effect. Away from the particle-hole symmetric point, there is a Majorana fermion induced Zeeman field and also Andreev scattering term , both of which vanish at particle-hole symmetry. Hence the renormalization effects of Kondo couplings in both cases are different. One of our novel results of our works is that though Andreev scattering vanishes at particle-hole symmetric point and hence does not contribute to the renormalization flow of the Kondo couplings, the same is not true for the Zeeman field which initially is zero, but it gets generated during the flow and hence contributes to the renormalization of Kondo couplings. In fact, Zeeman field makes the renormalization flow of the Kondo couplings same as that of anisotropic Kondo model which is what earlier studies have missed due to the nature of perturbative renormalization methods. In the presence of Majorana fermions, particle-hole asymmetry becomes relevant perturbation for Kondo effect

which is not true for the standard Kondo fixed point for which particle-hole asymmetry is irrelevant. We explored both particle-hole symmetric and asymmetric cases and found that Kondo couplings renormalize differently in two cases. Also, Kondo scale shows a different kind of dependence on QD-TSC coupling parameter. From the numerical solution of flow equations of Kondo couplings of Majorana-Kondo model, we have made an important observation that these flow equations have an essential instability to particle-hole asymmetry due to which Majorana fermions dominate the physics even in the QD-TSC coupling regime. This observation has physical implications for the realistic experimental situations where particle-hole asymmetry being generic and particle-hole symmetric point being a very special point.

Dynamic spin susceptibility is an experimentally accessible quantity. We find clear signatures of Majorana fermions in this quantity and we propose these signatures can be feasibly found in experiments on quantum dots. Our studies have confirmed and consolidated the interplay between Majorana fermions and Kondo effect and hence showed that Kondo effect in quantum dots provides an experimentally feasible and unambiguous way for the detection of Majorana fermions.

Bibliography

[1] G. Volovik, JETP Lett. **70**, 609(1999).

[2] N. Read and D. Green, Phys. Rev. B **61**, 10267 (2000).

[3] A. Kitaev, Phys. Usp. **44**, 131 (2001).

[4] L. Fu and C.L. Kane, Phys. Rev. Lett. **100**, 096407 (2008).

[5] V. Mourik *et al* Science **336**, 1003 (2012).

[6] S.Nadj-Perge*et al* Phys. Rev. B **88**, 020407 (2013).

[7] M.T. Deng *et al* Science, Vol. 354, Issue 6319, pp.1557-1562 (2016).

[8] David Aasen*et al* Phys. Rev. X **6**, 031016 (2016)

[9] Martin Leijnse and Karsten Flensberg, Phys. Rev. B **84**, 140501 (2011).

[10] D.E. Liu and H. U. Baranger, Phys. Rev. B **84**, 201308 (2011)

[11] A. Golub, I. Kuzmenko and Y. Avishai, Phys. Rev. Lett. **107** 176802 (2011)

[12] M. Lee, J. S. Lim and R. Lopez, Phys. Rev. B **87**, 241402 (2013).

[13] M. Cheng, M. Becker, B. Bauer and R. M. Lutchyn, Phys. Rev. X **4**, 031051 (2014).

[14] R. Chirla, I.V. Dinu, V. Moldoveanu and C. P. Moca, Phys. Rev. B **90**, 195108 (2014).

[15] S. Kehrein *The flow equation approach to many particle systems* Springer, Berlin (2006).

[16] P. Fritsch and S. Kehrein, Phys. Rev. B. **81**, 035113 (2010).

[17] W. Hofstetter and S. Kehrein, Phys. Rev. B, **63**, 140402 (2001).

Chapter 7

Summary

The research work reported in the thesis belongs to the broad area of strongly correlated electron systems. Kondo physics is the underlying theme of the thesis and renormalization group method is the main method applied to explore the interplay of Kondo physics with other quantum fluctuations. The thesis can be divided into two sections : the first section is about the interplay between Kondo physics, and valence fluctuations which is explored in chapters 3 and 4 and the other section is about the interplay between Kondo physics and the topological order which is explored in chapter 6 and chapter 5 sets the background for that work. Introduction to the field of strongly correlated electron systems is given in chapter 1 where the various models are described which include quantum impurity models as well as Hubbard model. There is also a brief description of dynamical mean field theory which is used in chapter **4** to study the lattice model for heavy fermion systems. A detailed discussion of the various renormalization group methods used in the thesis is given in chapter **2**. In this chapter, we will summarise the main results of the research projects described in chapter **3** to chapter **6**. We will also discuss the future directions of these projects.

In chapter **3** the main goal of the project is to understand the role of valence

fluctuations on the Kondo fixed point and to find out whether valence fluctuations can lead to quantum criticality in the lattice case. To capture the effects of the valence fluctuations, a local, Hubbard repulsive interaction term between conduction electrons and impurity electrons is added to Anderson impurity model and this way we get what has been called extended Anderson impurity model (e-SIAM). We have employed Haldane's and Jefferson's perturbative renormalization methods to e-SIAM and have calculated scaling equations for various parameters of the model. The scaling equations have been solved both numerically and analytically, and effects of the valence fluctuations on the Kondo scale have been explored, since this would yield information about the stability of the Kondo fixed point. We have found that the Kondo scale gets enhanced due to valence fluctuations. To get the effective Hamiltonian in the strong coupling regime of e-SIAM, we have carried out Schrieffer-Wolff transformation and found that the strong coupling physics of the model is governed by spin-charge Kondo model which has anisotropic charge Kondo interaction in addition to the spin Kondo interaction. Our scaling equations did not confirm these results from SWT because our scaling analysis is restricted to infinite U case due to which the doubly occupied subspace gets decoupled. So, in future, we would like to explore the finite U case and confirm the co-existence of the spin and charge Kondo effects together. We are planning to apply flow equation renormalization method and see if the spin-charge Kondo model arises in the flow equations as well.

In chapter **4** we have explored the lattice version of extended single impurity Anderson model. The lattice version is called extended Periodic Anderson model. Once again the motivation here was to explore the role of the valence fluctuations in the quantum criticality in heavy fermions systems for which the Periodic Anderson model is the minimal model. We have employed the framework of dynamical mean field theory(DMFT) in which e-PAM gets mapped to e-SIAM. Hybridization ex-

pansion continuous time quantum Monte Carlo has been used as quantum impurity solver. We find that as we increase the U_{fc} interaction and hence as the valence fluctuations get enhanced, the occupancy of the f electrons decreases which signifies that f electron level is getting closer to the Fermi level, in agreement with the scaling behaviour of the impurity energy level of e-SIAM, as found in the chapter **3**. Based on slave boson mean field theory studies of e-PAM, it has been found that critical valence fluctuations lead to first order phase transition where the valence susceptibility diverges. We also calculated this quantity and found that at some critical value of U_{fc}, valence susceptibility diverges. We also calculated quasiparticle weight and once again, in agreement with our renormalization calculations of e-SIAM, we found that quasiparticle weight increases and hence the system moves away from the strong coupling regime. Though our results suggest that valence fluctuations can lead to quantum criticality in heavy fermion systems, in future, we would like to carry out a more detailed study of e-PAM and actually locate the quantum critical point in the phase diagram. We would also like to see how the valence fluctuations mediated charge Kondo effect, which we have found in case of e-SIAM, manifests in case of lattice model and what are the physical implications of the competition between spin and charge Kondo effects for the heavy fermion systems.

In chapter **5** we have explored two models which are related to each other via Jordan-Wigner transformation. One model is the transverse field Ising model which has been studied extensively as a model for the quantum phase transition. Another model is the Kitaev chain model which has become the celebrated model which exhibits Z_2 topological order and has Majorana edge modes. The natural question which one can ask is that why there is topological order in Kitaev chain model while there is only Landau symmetry broken order in the Jordan-Wigner dual spin model. We explore the algebra of the Majorana fermions of the Kitaev chain model, and we find that these two models do not have the same symmetries. The fermionic model

has extra symmetries which are important for the topological order. We particularly identify some symmetry operators which commute with the Hamiltonian and anti-commute with parity operator and hence lead to the doubling of the spectrum in Kitaev chain model. We have also explored the implication of these fermionic symmetries for the Majorana fermion braid group representations. In future, we would like to extend our work to parafermion systems and show that same formalism can be applied there also to explain the topological order in parafermion models. Similarly we would like to extend our formalism to two dimensional model like toric code model and Kitaev spin model and show that Z_2 topological order can be explained based on our formalism.

In chapter **6** we explore the interplay between Kondo physics and Z_2 topological order in topological superconductors. The motivation of this study comes from the recent surge in the interest of Majorana fermions as the promising candidates for topological quantum computing. So their detection in unambiguous ways and their stability in realistic situations where interactions are also present becomes inevitable. In this chapter, we have considered a setup in which quantum dot is coupled to normal lead on one side and to topological superconductor(TSC) on another side. We calculated the effective Hamiltonian for the system corresponding to the Kondo regime. The effective Hamiltonian is called Majorana-Kondo model and has extra terms coming from the coupling to the TSC. Employing the flow equation renormalization method, we calculated the flow equations for the parameters of the Majorana-Kondo model. We find that particle-hole asymmetry is the relevant perturbation for the Majorana-Kondo model which is one of the signatures of the Majorana fermions. It is known from the renormalization group study of the Kondo model that particle-hole asymmetry is not a relevant perturbation for the Kondo fixed point. In the Majorana-Kondo model, there is an emergent Zeeman field which suppresses the transverse spin fluctuations and hence in the strong Ma-

jorana coupling regime, the physics is governed by Majorana couplings rather than Kondo coupling. From the numerical solutions of the flow equations of Majorana-Kondo model, we find that Kondo divergence gets suppressed as we increase the coupling strength to TSC.

Flow equation renormalization method gives us access to dynamic spin susceptibility, and hence we explored the signatures of Majorana fermions in this quantity. These signatures can be probed in experiments on quantum dots, and hence our studies offer another way for the detection of Majorana fermions in quantum dots. Though we found that Majorana fermions have strong renormalization effects on the Kondo fixed point, however, we were not able to confirm the existence of Andreev fixed point which was found in one research group based on perturbative renormalization and other related methods. In future, we would like to do a more detailed study of other parameter regimes of the model to find out whether flow equations of Majorana-Kondo model lead to instability of the Kondo fixed point and Andreev fixed point determines the low energy physics of Majorana-Kondo model.

Appendices

Appendix A

Commutators

Appendix A

Commutators for Flow Equations for Majorana-Kondo model

In this appendix we have evaluated all the commutators needed to calculate the flow equations for the coupling constants and spin dynamics of Majorana-Kondo model. The generator for the Majorana-Kondo model is:

$$\begin{aligned}\eta =&\frac{1}{2}\sum_{pq}(\epsilon_p-\epsilon_q)(J^{\uparrow}(p,q):c^{\dagger}_{p\uparrow}c_{q\uparrow}:-J^{\downarrow}(p,q):c^{\dagger}_{p\downarrow}c_{q\downarrow}:)S^z+\\ &(\epsilon_p-\epsilon_q+h)J_{\perp}(p,q)(:c^{\dagger}_{p\uparrow}c_{q\downarrow}:S^{-}-:c^{\dagger}_{q\downarrow}c_{p\uparrow}:S^{+})+\\ &\epsilon_p J_1(p)(i\gamma)(c^{\dagger}_{p\uparrow}-c_{p\uparrow})+\epsilon_p J_2(p)(i\gamma)(c^{\dagger}_{p\uparrow}-c_{p\uparrow})S^z+\\ &(\epsilon_p+h)J_3(p)(i\gamma)(c^{\dagger}_{\downarrow}S^{\dagger}-c_{p\downarrow}S_{-})\end{aligned} \tag{A.1}$$

For convenience we have divided the generator in following way:

$$\eta=\eta^{\parallel}_K+\eta^{\perp}_K+\eta^1_M+\eta^2_M+\eta^3_M \tag{A.2}$$

$$[\eta_K^{\parallel}, H_0] = -\sum_{pq}(\epsilon_p - \epsilon_q)^2(J^{\uparrow}(p,q) : c_{p\uparrow}^{\dagger}c_{q\uparrow} - J^{\downarrow}(p,q) : c_{p\downarrow}^{\dagger}c_{q\downarrow} :)S^z \tag{A.3}$$

$$[\eta_K^{\perp}, H_0] = -\sum_{pq}(\epsilon_p - \epsilon_q + h)^2 \left(: c_{p\uparrow}^{\dagger}c_{q\downarrow} : S^- + : c_{q\downarrow}^{\dagger}c_{p\uparrow} : S^+\right) \tag{A.4}$$

$$\left[\eta_{\perp}, H_K^{\perp}\right] =$$

$$\sum_{pq}\sum_{rs}(2(\epsilon_s - h) - \epsilon_p + \epsilon_q)J_{\perp}(p,s)J_{\perp}(q,s)(1 - 2n(s)) : c_{p\uparrow}^{\dagger}c_{q\uparrow} : S^z$$

$$- (2(\epsilon_s + h) - (\epsilon_p - \epsilon_q))J_{\perp}(s,p)J_{\perp}(r,q)(1 - 2n(r))(: c_{p\downarrow}^{\dagger}c_{q\downarrow} : S^z)$$

$$- (\epsilon_p - \epsilon_q + h)(n(p) + n(q) - 2n(p)n(q))J_{\perp}^2(p,q)S^z) \tag{A.5}$$

$$\left[\eta_K^{\parallel}, \sum_k J_1(k)(i\gamma)(c_{k\uparrow} + c_{k\uparrow}^{\dagger})\right]$$

$$= \sum_{pq}(\epsilon_p - \epsilon_q)J^{\uparrow}(p,q)J_1(q)(i\gamma)(c_{p\uparrow} + c_{p\uparrow}^{\dagger})S^z \tag{A.6}$$

$$\left[\eta_K^{\parallel}, \sum_k iJ_2(k)(: \gamma c_{k\uparrow} : + : \gamma c_{k\uparrow}^{\dagger} :)S^z\right]$$

$$= \frac{1}{4}\sum_{pq}(\epsilon_p - \epsilon_q)J^{\uparrow}(p,q)J_2(q)(i\gamma)(c_{p\uparrow} + c_{p\uparrow}^{\dagger}) \tag{A.7}$$

$$\left[\eta_K^{\parallel}, \sum_k J_3(k)(i\gamma)(c_{k\downarrow}^{+}S^{\dagger} + c_{k\downarrow}S^-\right]$$

$$= -\frac{1}{2}\sum_{pq}(\epsilon_p - \epsilon_q)J^{\downarrow}(p,q)J_3(q)(i\gamma)(1 - 2n(q)(c_{p\downarrow}^{\dagger}S^{\dagger} + c_{p\downarrow}S^-) \tag{A.8}$$

$$\left[\eta_K^{\perp}, \sum_k J_1(k)(i\gamma)(c_{k\uparrow} + c_{k\uparrow}^{\dagger})\right]$$

$$= -\sum_{pq}(\epsilon_q - \epsilon_p + h)J^{\perp}(q,p)J_1(q)(i\gamma)(c_{p\downarrow}S^- + c_{p\downarrow}^{\dagger}S^+) \tag{A.9}$$

$$\left[\eta_K^{\perp}, \sum_k J_2(k)(i\gamma)(c_{k\uparrow} + c_{k\uparrow}^{\dagger})S^z\right]$$

$$= \frac{1}{2}\sum_{pq}(\epsilon_q - \epsilon_p + h)J^{\perp}(q,p)J_2(q)(1 - 2n(q))(i\gamma)(c_{p\downarrow}S^- + c_{p\downarrow}^{\dagger}S^{\dagger}) \tag{A.10}$$

$$\left[\eta_K^{\perp}, \sum_k J_3(k)(i\gamma)c_{k\downarrow}^{\dagger}S^{\dagger} + c_{k\downarrow}S^{-})\right] \tag{A.11}$$

$$= -\sum_{pq}(\epsilon_p - \epsilon_q + h)J_3(q)J^{\perp}(p,q)(i\gamma)(c_{p\uparrow}^{\dagger} + c_{p\uparrow})S^z(1-2n(q)) +$$

$$+\frac{1}{2}\sum_{pq}(\epsilon_p - \epsilon_q + h)J_3(q)J^{\perp}(p,q)(i\gamma)(c_{p\uparrow}^{\dagger} + c_{p\uparrow}) \tag{A.12}$$

$$\left[\sum_p \epsilon_p J_1(p)(i\gamma)(c_{p\uparrow}^{\dagger} - c_{p\uparrow}), \sum_{q\sigma}\epsilon_q c_{q\sigma}^{\dagger}c_{q\sigma}\right] = -\sum_p J_1(p)\epsilon_p^2(i\gamma)(c_{p\uparrow}^{\dagger} + c_{p\uparrow}) \tag{A.13}$$

$$\left[\sum_p \epsilon_p J_2(p)(i\gamma)(c_{p\uparrow}^{\dagger} - c_{p\uparrow})S^z, \sum_{q\sigma}\epsilon_q c_{q\sigma}^{\dagger}c_{q\sigma}\right] = -\sum_p J_2(p)\epsilon_p^2(i\gamma)(c_{p\uparrow}^{\dagger} + c_{p\uparrow})S^z \tag{A.14}$$

$$\left[\sum_p (\epsilon_p + h)J_2(p)(i\gamma)(c_{p\downarrow}^{\dagger}S^{+} - c_{p\downarrow}S^{-}), \sum_{q\sigma}\epsilon_q c_{q\sigma}^{\dagger}c_{q\sigma}\right]$$

$$= -\sum_p J_2(p)\epsilon_p(\epsilon + h)(i\gamma)(c_{p\downarrow}^{\dagger}S^{+} + c_{p\downarrow}S^{-}) \tag{A.15}$$

$$\left[\sum_p (\epsilon_p + h)J_2(p)(i\gamma)(c_{p\downarrow}^{\dagger}S^{+} - c_{p\downarrow}S^{-}), -hS^z\right]$$

$$= \sum_p J_2(p)(\epsilon_p + h)h(i\gamma)(c_{p\downarrow}^{\dagger} + c_{p\downarrow})S^z \tag{A.16}$$

$$\left[\sum_k J_1(k)\epsilon_k(i\gamma)(c_{k\uparrow}^{\dagger} - c_{k\uparrow}), \sum_{pq} J^{\parallel}(p,q)c_{p\uparrow}^{\dagger}c_{p\uparrow}S^z\right]$$

$$= -\sum_{pq}\epsilon_p J_1(q)J^{\uparrow}(p,q)(i\gamma)(c_{p\uparrow}^{\dagger} + c_{p\uparrow})S^z \tag{A.17}$$

$$\left[\sum_k \epsilon_k J_1(k)(i\gamma)(c_{k\uparrow}^{\dagger} - c_{k\uparrow}), \sum_{pq} J^{\perp}(p,q)(c_{p\uparrow}^{\dagger}c_{q\downarrow}S^{-} + c_{q\downarrow}^{\dagger}c_{p\uparrow}S^{+}\right]$$

$$= -\sum_{pq} J_1(q)J^{\perp}(q,p)\epsilon_q(i\gamma)(c_{p\downarrow}^{\dagger}S^{+} + c_{p\downarrow}S^{-}) \tag{A.18}$$

$$\left[\sum_k \epsilon_k J_2(k)(i\gamma)(c^\dagger_{k\uparrow} - c_{k\uparrow})S^z, \sum_{pq} J^\uparrow(p,q) : c^\dagger_{p\uparrow} c_{q\uparrow} : S^z\right]$$
$$= -\frac{1}{4}\sum_p \epsilon_q J_2(q) J^\uparrow(p,q)(i\gamma)(c^\dagger_{p\uparrow} + c_{p\uparrow}) \tag{A.19}$$

$$\left[\sum_k \epsilon_k J_1(k)(i\gamma)(c^\dagger_{k\uparrow} - c_{k\uparrow}, \sum_{pq} J^\perp(p,q)(: c^\dagger_{p\uparrow} c_{q\downarrow} : S^- + : c^\dagger_{q\downarrow} c_{p\uparrow} : S^+\right]$$
$$= -\sum_k \epsilon_p J_1(p) J^\perp(p,q)(i\gamma)(c_{q\downarrow} S^- + c^\dagger_{q\downarrow} S^+) \tag{A.20}$$

$$\left[\sum_k \epsilon_k J_2(k)(i\gamma)(c^\dagger_{k\uparrow} - c_{k\uparrow})S^z, \sum_{pq} J^\perp(p,q)(: c^\dagger_{p\uparrow} c_{q\downarrow} : S^- + : c^\dagger_{q\downarrow} c_{p\uparrow} : S^+)\right]$$
$$= -\frac{1}{2}\sum_{pq} \epsilon_p J_2(p) J^\perp(p,q)(i\gamma)(c^\dagger_{q\downarrow} S^+ + c_{q\downarrow} S^-)(1 - 2n(p)) \tag{A.21}$$

$$\left[\sum_k (\epsilon_k + h) J_2(k)(i\gamma)(c^\dagger_{k\downarrow} S^+ - c_{k\downarrow} S^-), -\sum_{pq} J^\downarrow(p,q) : c^\dagger_{p\downarrow} c_{q\downarrow} : S^z)\right]$$
$$= -\frac{1}{2}\sum_{pq} (\epsilon_q + h) J_2(q) J^\downarrow(p,q)(i\gamma)(c^\dagger_{p\downarrow} S^+ + c_{p\downarrow} S^-)(1 - 2n(q)) \tag{A.22}$$

$$\left[\sum_k (\epsilon_k + h) J_2(k)(i\gamma)(c^\dagger_{k\downarrow} S^+ - c_{k\downarrow} S^-), \sum_{pq} J^\perp(p,q)(: c^\dagger_{p\uparrow} c_{q\downarrow} : S^- + : c^\dagger_{q\downarrow} c_{p\uparrow} : S^+\right]$$
$$= \sum_{pq} (\epsilon_q + h) J_2(q) J^\perp(p,q)(i\gamma)(c^\dagger_{p\uparrow} + c_{p\uparrow})(1 - 2n(q)) S^z$$
$$- \frac{1}{2}\sum_{pq} (\epsilon_q + h) J_2(q) J^\perp(p,q)(i\gamma)(c^\dagger_{p\uparrow} + c_{p\uparrow}) \tag{A.23}$$

$$\left[\sum_p (\epsilon_p + h) J_2(p)(i\gamma)(c^\dagger_{p\downarrow} S^+ - c_{p\downarrow} S^-), \sum_q (\epsilon_q + h) J_2(q)(i\gamma)(c^\dagger_{q\downarrow} S^+ + c_{q\downarrow} S^-)\right]$$
$$= 2\sum_{pq} (\epsilon_p + h)^2 J_2^2(p) S^z + \sum_p (\epsilon_p + h)^2 J_2^2(p) \tag{A.24}$$

A.1 Commutators for the Spin dynamics

$$[\eta(l), h(l)S^z] = -\sum_{pq}(\epsilon_p - \epsilon_q + h)J^{\perp}(p,q)h(l)(:c^{\dagger}_{p\uparrow}c_{q\downarrow}:S^- + :c^{\dagger}_{q\downarrow}c_{p\uparrow}:S^+)$$

$$-\sum_{p}(\epsilon_p + h)J_3(p)h(l)(i\gamma)(c^{\dagger}_{p\downarrow}S^{\dagger} + c_{p\downarrow}S^-) \tag{A.25}$$

$$\left[\sum_{r}\epsilon_r J_1(r)(i\gamma)(c^{\dagger}_{r\uparrow} - c_{r\uparrow}), \sum_{pq}\gamma_{pq}(l)(:c^{\dagger}_{p\uparrow}c_{q\downarrow}:S^- + :c^{\dagger}_{q\downarrow}c_{p\uparrow}:S^+)\right]$$

$$= -\sum_{pr}\epsilon_r J_1(r)\gamma_{rp}(l)(i\gamma)(c^{\dagger}_{p\downarrow}S^+ + c_{p\downarrow}S^-) \tag{A.26}$$

$$\left[\sum_{r}\epsilon_r J_2(r)(i\gamma)(c^{\dagger}_{r\uparrow} - c_{r\uparrow})S^z, \sum_{pq}\gamma_{pq}(l)(:c^{\dagger}_{p\uparrow}c_{q\downarrow}:S^- + (:c^{\dagger}_{q\downarrow}c_{p\uparrow}:S^+)\right]$$

$$= \frac{1}{2}\sum_{r}\epsilon_r J_2(r)\gamma_{rp}(l)(i\gamma)(1-2n(r))(c^{\dagger}_{\downarrow}S^+ + c_{p\downarrow}S^-) \tag{A.27}$$

$$\left[\sum_{pqr}(\epsilon_r + h)J_3(r)(i\gamma)(c^{\dagger}_{r\downarrow}S^+ - c_{r\downarrow}S^-, \sum_{pq}\gamma_{pq}(l)(:c^{\dagger}_{p\uparrow}c_{q\downarrow}:S^- + :c^{\dagger}_{q\downarrow}c_{p\uparrow}:S^+\right] \tag{A.28}$$

$$= \sum_{pqr}(\epsilon_r + h)J_3(r)\gamma_{pr}(l)(1-2n(r))(i\gamma)(c^{\dagger}_{p\uparrow} + c_{p\uparrow})S^z) \tag{A.29}$$

$$\left[\sum_{pq}(\epsilon_p - \epsilon_q + h)J^{\perp}(p,q)(:c^{\dagger}_{p\uparrow}c_{q\downarrow}:S^- - :c^{\dagger}_{q\downarrow}c_{p\uparrow}:S^+), \sum_{r}\zeta_r(l)(i\gamma)(c_{r\uparrow} + c^{\dagger}_{r\uparrow})S^z\right]$$

$$= \frac{1}{2}\sum_{r}(\epsilon_r - \epsilon_q + h)J^{\perp}(r,q)\zeta_r(l)(1-2n(r))(c_{q\downarrow}S^- + c^{\dagger}_{q\downarrow}S^+) \tag{A.30}$$

$$\left[\sum_{r}(\epsilon_r + h)J_3(r)(i\gamma)(c^{\dagger}_{r\downarrow}S^+ - c_{r\downarrow}S^-), \sum_{p}\eta_p(l)(i\gamma)(c^{\dagger}_{p\downarrow}S^+ + c_{p\downarrow}S^-)\right]$$

$$= \sum_{r}(\epsilon_r + h)\eta_p(l)J_3(r)(2S^z(1-2n(p)) + (\epsilon_r + h)\eta_p(l)J_3(r)) \tag{A.31}$$